PERFORMANCE AND DESIGN OF A METHANOL GEL FUELED PASSIVE DIRECT METHANOL FUEL CELL

A THESIS SUBMITTED IN PARTIAL FULFILLMENT OF THE REQUIREMENTS FOR THE DEGREE OF:

Chemical Engineering

Worcester Polytechnic Institute

by

Casey Rivera

Diego Lugo

Approved by _____

Professor Ravindra Datta, Advisor

Program Authorized

to Offer Degree _____

Date _____

Table of Contents

Table of Figures

Table of Tables

NOTATION

Variable	Description
ΔG^o	Gibbs free energy (standard)
ΔH^o	enthalpy (standard)
V^o0	Standard thermodynamic potential
V^omax	Standard maximum potential
ρPt	Platinum Density
ρRu	Ruthenium Density
$d_{M,A}$	Anode catalyst metal crystalline diameter
$d_{M,C}$	Cathode catalyst metal crystalline diameter
ϕ_I	available metal surface involved in electrocatalysis in contact with ionomer
$i^*_{A,0,ref}$	exchange current density, anode, reference
$i^*_{C,0,ref}$	exchange current density, cathode, reference
$c_{me,ref}$	concentration of methanol, reference (Standard)
C_w	concentration of water diluted methanol solutions
T_{ref}	temperature, reference
$p_{O2,0,ref}$	partial pressure of oxygen, reference
α_A	transfer coefficient, cathode
ν_{Ae-}	electron stoichiometric number, anode
α_C	transfer coefficient, anode
ν_{Ce-}	electron stoichiometric number, cathode
ν_{Ae-}	stoichiometric coefficient of electrons in MOR
$\nu_{A,Me}$	stoichiometric coefficient of methanol in MOR
$E_{A,\varphi 0}$	effective activation energy for MOR
$E_{C,\varphi 0}$	effective activation energy for ORR
K_{Me}	equilibrium constant
L_D	anode gas diffusion layer thickness
L_B	Nafion® 117 membrane thickness
L_E	cathode gas diffusion layer thickness
ε_E	void fraction of gas diffusion layer, cathode (porosity)

ε_D	void fraction of gas diffusion layer, anode (porosity)
κ_{O2}	partition coefficient of oxygen
$\kappa_{Me,D}$	partition coefficient of methanol through ADL
$\kappa_{Me,B}$	partition coefficient of methanol through CDL
ξ	electro-osmotic drag coefficient of water
E_μ	activation energy for water viscosity
λ	water molecules per sulfonic group in Nafion®
δ	ratio of mutual to matrix diffusion coefficients
q_w	volume fraction of water formation at cathode
$D_{Me,W}$	diffusion of methanol in water
$D^e_{Me,D}$	diffusion of methanol in anode GDL
$D_{O2,W}$	diffusion of oxygen in water
$D_{O2,E}$	diffusion of oxygen
p_w	water vapor pressure in cathode
R_I	MEA interfacial resistance
F	Faraday's constant
R	gas constant
μ	Viscosity of Water
V	Cell Voltage
V_o	DMFC Cell Potential theoretical
η_A	overpotential, anode
η_B	Ohmic overpotential
η_C	overpotential, cathode
η_I	Interfacial resistance
$x_{Me,b}$	mole fraction of methanol in PEM
$\kappa_{W,B}$	partition coefficient of methanol through CDL
$i_{A,0}$	exchange current density, anode
$i_{A,L}$	limiting exchange current density, anode
$i_{C,0}$	exchange current density, cathode
$i_{C,L}$	limiting exchange current density, cathode
$i_{X,O2}$	crossover current density, oxygen

$i_{X,Me}$	crossover current density, methanol
$i_{X,Me,L}$	limiting crossover current density
γ_{MA}	electrocatalyst roughness, anode
$_{\gamma MC}$	electrocatalyst roughness, cathode
$\rho_{M,A}$	Pt-Ru Alloy density
$k^*_{Me,D}$	rate constant for reaction
$C_{O2,0,ref}$	concentration of oxygen, reference
$C_{Me,0}$	initial concentration of methanol
$C_{O2,0}$	concentration in CCL under equilib
$C_{Me,b}$	concentration of methanol in PEM
$C_{W,b}$	concentration of water in PEM
$C_{O2,b}$	concentration of oxygen in PEM
$m_{M,A}$	catalyst leading
$m_{M,C}$	catalyst leading
ω_{Ru}	mass fraction of RU
θ_{COS}	adsorbed carbon monoxide sites
$\theta_{COS,ref}$	adsorbed carbon monoxide sites, reference
$C_{Me,A}(a)$	Concentration Profile
$D^e_{O2,E}$	diffusion of oxygen in cathode
$D^e_{Me,B}$	diffusion of methanol in PEM
$D^e_{O2,B}$	diffusion of oxygen in PEM
$P^e_{Me,D}$	Effective Methanol Permeance
$P^e_{O2,E}$	Effective Oxygen Permeance
$P_{O2,B}$	Oxygen permeance
ε_B	void fraction of gas diffusion layer, anode (porosity)
K_a	dissociation equilibrium constant for acid sites
ε_{Bo}	percolation threshold
σ_B	effective PEM conductivity
β	degree of dissociation

ABSTRACT

In this project the performance of multiple variations of a Passive Direct Methanol Fuel Cell (PDMFC) were tested. The experiments ranged from using different Membrane Electrode Arrays (MEAs), to changing the material or shape of the current collectors. In addition to hardware variations, the main focus of this paper is experimenting with MeOH gel as a fuel as compared to a liquid methanol feed. The results show promise for the methanol gel. A mathematical model designed to theoretically reproduce the performance of a methanol fuel cell was adapted for the passive DMFC. There were many tests conducted on the cell both before and after the finalized stack design was completed. These tests were conducted to determine the best performance based on the configuration of the available hardware for the fuel cell stack. The parts changed on the cell ranged from the current collectors, to removing the GDLs, changing the fuel type and arrangement, and types of screws used.

Keywords: Passive Direct Methanol Fuel Cell, DMFC, PDFMC, MEA, Methanol Gel Fuel

ACKNOWLEDGEMENTS

We would like to thank Professor Ravindra Datta for being our advisor, providing us with assistance whenever we needed it, and for giving us the opportunity to work with him. We would also like to thank everyone who helped with materials, such as Jack Ferraro, Doug White, and Neil Whitehouse who helped us manufacture any parts that were necessary and that were beyond our expertise. We would like to thank Matt Kellas for assistance with 3D modeling of the theoretical stack design

We would also like to thank our graduate student advisors, Neal Rosenthal, Matt Perrone, Nick Deveau, Dan Knox, Jason Morgan, Drew Martino and Pei Shan Yen who helped us in lab with the equipment and day to day questions. We also would like to thank the other MQP group working in the fuel cell lab with us, Matt Suarez, Kaitlyn Spetka, and Samantha Do, for cross referencing projects with us, and allowing us to work with you to combine efforts for success.

Last but not least, we would like to thank our friends and family for always giving us the support we needed while completing this MQP.

CHAPTER 1: EXECUTIVE SUMMARY

Fuel cells have been researched for some time now, which is leading to better development and higher efficiency. In order to increase efficiency for some small scale applications, it is necessary to remove any devices that require energy that aid the cell, such as fans and pumps for the fuel. This research is concerned with the development of Passive Direct Methanol Fuel Cells (PDMFC).

PDMFCs work independently from ancillary devices; this is why they are called passive. These fuel cells are usually comprised of a chamber where the fuel is placed and is allowed to freely flow by diffusion towards the MEAs. The MEAs vary in position and direction by stack, so the components of a fuel cell that can vary and be experimented on are many. The size and shape of the stack is probably the most important factor in its efficiency and portability. Depending on what type of fuel the cell uses (Liquid or Gel); the orientation of the cell could also have an effect on the performance.

Chapter 2 gives an in-depth background on the history of fuel cells, as well as today's applications. The design of the fuel cell is discussed in more detail in Chapter 3. Some of the parts that are more interchangeable on the cell include the MEAs, the current collectors and other small pieces of hardware. The focus of this project was to optimize the current collectors by testing various materials and channel geometry.

There are several issues when experimenting with the PDMFC; including hardware problems. These can come from leakage as well as short circuiting of screws and poor insulation in wires. These happen while manufacturing, fabricating and assembling the cell.

Another problem with a MeOH gel PDMFC was found to be diffusion limitation of methanol and how it diffused towards MEAs based on their position. The current stack that was used in the experiment uses 2 rows of MEAs, six lining the top of the fuel cell and 6 lining the bottom of the fuel cell. Although the methanol molecular weight is similar to that of air, it tended to diffuse in an upward direction. This caused the MEAs place on the upper row to be favored, leading to faster degradation, and the bottom to become fuel starved.

Another problem that will be discussed in the detailed background is methanol cross-over that occurs at the MEA. This is when unreacted methanol diffuses through the MEA causing it to increase the over potential of the oxygen reduction reaction (ORR) at the cathode as well as limit the oxygen diffusion from the outside of the cell.

There are many advantages to methanol fuel cells. One of these is that fuel cells are not limited by the dynamic efficiency of a Carnot Cycle like other internal combustion engines. Most importantly, methanol is an inexpensive, readily available liquid fuel, unlike hydrogen. Another advantage is the lack of moving parts in PDMFCs. This leads to higher efficiency, long lifetimes and high durability as well as being silent when in use. Unlike other forms of energy storage, the fuel cell will keep producing energy as long as it is fed fuel. However, the cost of fuel cells is an issue because of the use of precious metal catalysts and the Nafion® membrane.

Direct methanol fuel cells provide a great option for future use in a world where sustainability is much needed. The long lasting nature of DMFC provides great promise towards the idea long lasting energy systems that will replace batteries. The leading research in DMFC is to provide long lasting power to applications of portable needs. Passive DMFCs could be used to power cell phones and laptops as well as any other portable micro power system. [1]

CHAPTER 2: BACKGROUND

As the demand for energy increases in the world, many are seeking alternative sources of energy. Although the demand for energy is not the only reason for seeking new sources, there is also a growing concern for the well-being of the globe. It is believed that current major sources of energy, like coal, are the leading causes of pollution. The latest research in this topic is in using sources of energy with less contribution to pollution and higher energy efficiency.

Research is now looking towards other options such as renewable energy, or energy comes from natural, renewable resources such as sunlight, wind, rain, tides, and geothermal heat. Between the years 2004 and 2009, worldwide renewable energy capacity grew at rates of 10–60 percent annually for many technologies.[2] This has led to a growing need for knowledge of these energies and how to improve them. For wind power and many other renewable technologies, growth accelerated in 2009 relative to the previous four years. [2]

There are also many countries experimenting with biofuels. These were used in early days of vehicle history, however they were overrun by petroleum and gas, obtained simply by companies drilling a hole in the ground and extracting fuel that was cheap. [2]

However, in recent years other alternative energy generation technologies have been explored, such as the fuel cell. A fuel cell is a device that converts the chemical energy from a fuel into electricity through a chemical reaction involving oxygen or another oxidizing agent. The most common type of fuel for such a fuel cell is hydrogen; however, natural gases and methanol are also utilized in some fuel cells.

Hydrogen is agreed as the most useful fuel because it results in high power and only water is produced in operating the fuel cell. Hydrogen is very difficult to store, as well as difficult and costly to compress. Hydrogen also has lower energy content than natural gas when pressurized in

tanks. At present time, there is no way of making cheap hydrogen. Recently, energy has demanded an equal or larger amount of another form of energy to produce it. Currently, hydrogen is mostly made from natural gas. However, this process is only 65% efficient when storage losses are considered, which results in a loss in efficiency compared to directly using the natural gas. [3]

The Direct Methanol Fuel Cell (DMFC) uses a fuel which, compared to hydrogen, is easier to handle and to distribute. It is also allows a fairly simple system design compared to those utilizing liquid fuels to produce hydrogen by steam reforming or partial oxidation. The hydrogen produced is used to feed a standard polymer electrolyte membrane fuel cell (PEMFC). [4] The DMFC relies upon the oxidation of methanol on a catalyst layer to form carbon dioxide and, protons and electrons. Water is consumed at the anode and produced at the cathode. Protons are transported across the proton exchange membrane, usually made of Nafion, to the cathode where they react with oxygen to produce water. Electrons are transported through an external circuit from anode to cathode, providing power to connected devices. [3]

Fuel cells are in the fifth significant cycle of attempts to turn them into commercial reality [4]. In the past the attempts often failed to the point where few companies continued development. The major reasons for this occurring are the high cost of production and the small power output of fuel cells.

Fuel cells are still a few years away from commercialization on a large scale. It is very difficult to tell which fuel and which technology will be predominant in the future. There are some problems to be solved, yet in all these types of fuel cells. If those can be solved then, those will become the predominant fuel cells in the future.

2.1 Types of Fuel Cells

There are many different kinds of fuel cells; they are usually classified by the kind of electrolyte used. The electrolyte determines the kind of chemical reaction, the kind of catalyst, temperature range, and fuel required amongst other factors. Based on the characteristics and efficiency, it is determined for which application the fuel cell is going to be used. Fuel cells are currently under development, each type with its own advantages and limitations. The following are different kinds of fuel cells.

2.1.1 Polymer Electrolyte Membrane (PEM) Fuel Cells

Also called proton exchange membrane fuel cells, PEMFCs have the advantages that they can deliver high density power, can be very small and work on lower amounts of fuel. PEMFCs use a solid polymer as an electrolyte and porous carbon electrodes containing a platinum catalyst. They require only hydrogen, oxygen from the air, and water to operate.

PEM fuel cells operate at relatively low temperatures, from room temperature to 80C. The advantages of starting up at low temperatures are that the cell needs less time to start up, and that the cell can operate with less wear to the components around it. However, it is important to note that the PEM must contain a catalyst composed of platinum, which adds cost to the production of this cell. Just like the direct methanol fuel cell, the PEM fuel cell suffers from the same problem with the CO bonding to the platinum catalyst. To counteract this, the same second catalyst is used, ruthenium.

PEM fuel cells are used primarily for transportation applications and some stationary applications. Due to their fast startup time, low sensitivity to orientation, and favorable power-to-weight ratio, PEM fuel cells are particularly suitable for use in passenger vehicles, such as cars and buses. [5]

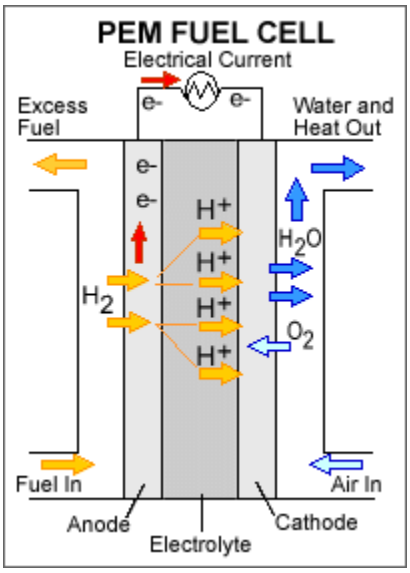

Figure 1: Proton Exchange Membrane Schematic [5]

2.1.2 Alkaline Fuel Cells

Alkaline fuel cells (AFC) were some of the first fuels cell ever commercially developed. They were first widely used on spacecraft missions in space. These fuel cells use a solution of potassium hydroxide in water as the electrolyte and can use a variety of non-precious metals as a catalyst at the anode and cathode. They operate at temperatures between 100°C and 250°C. However, newer AFC designs operate at lower temperatures of roughly 23°C to 70°C. AFCs' high performance is due to the rate at which chemical reactions take place in the cell.

The downside for this type of fuel cell is how easily it can be poisoned by CO_2. The smallest amount of carbon dioxide can make the cell's efficiency suffer by reacting with this alkaline

electrolyte. Due to this, the fuel needed for this cell, oxygen and hydrogen, need to be purified. The purification process is very costly and adds rapidly to the cost of production of hydrogen. [5]

2.1.1.1 NAFION® as the Proton Exchange Membrane (PEM)

The PEM used during this process was Nafion® 117. As the industry standard for PEMs this material is an ion conductor made and developed by DuPont. The structure is shown by Figure 2. Nafion® is one of the best chemicals to use for this purpose because it has a perflourinated backbone that gives it a significant increase in strength and hydrophobicity. One of the reasons Nafion® is a great ionomer is because of the tetrafluoroethylene backbone that allows the addition of perfluorovinyl ether groups terminated with sulfonate groups onto it.

The sulfonic acid group is an exceptional ion-conducting moiety because its conjugate base is highly resonance stabilized. If R–SO3H loses a proton, H+, the negative charge is distributed over three oxygen atoms providing high stability.

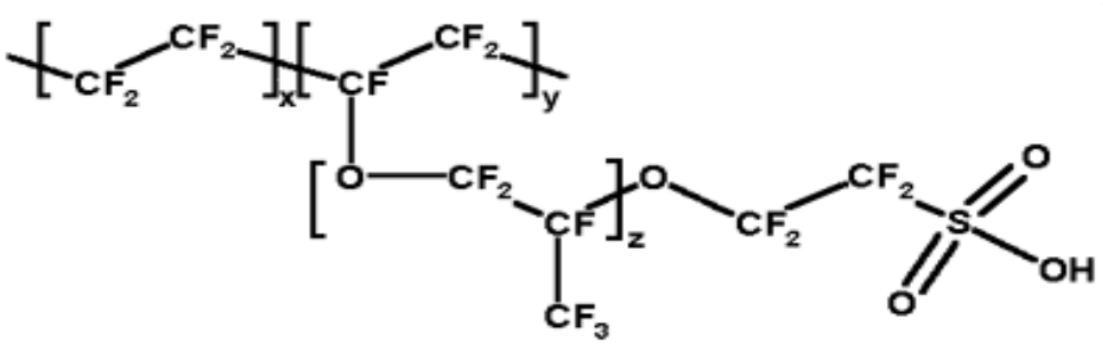

Figure 2: Nafion Chemical Formula

Since sulfonic acid sites in Nafion® are highly acidic they contribute hydrophilicity to an otherwise hydrophobic organic macromolecule. Thus, they promote the formation of ion clusters in Nafion®. When the cell takes in enough water, the ion clusters will start to expand allowing them to take over. These clusters expand to a point that ionic channels start to form in the

Nafion®. This however, is a downside for a DMFC because it leads to higher methanol crossover.

There is a limit as to how much Nafion® one can use while making an MEA. This is due to the fact that if too much Nafion® is used the mechanical strength of the polymer would be jeopardized. A highly hydrophilic membrane can be overly sensitive to water. There is also a downside to using too much water when activating the membrane. Because the Nafion® ion clusters expand with water, the more large scale repetition of experiments will lead to deterioration of the Nafion®. It will also cause cracks in the catalyst layer as well as tears in the membrane, which would lead to the cell being useless.

2.1.3 Phosphoric Acid Fuel Cells

The phosphoric acid fuel cell was one of the first fuel cells to be used commercially and it is in the more advance stages of development. Phosphoric acid fuel cells use liquid phosphoric acid as an electrolyte, which is contained in a Teflon bonded silicon carbide matrix. This kind of fuel cell also uses porous carbon electrodes as well as platinum as a catalyst, and operates at a temperature of around 170C.

Phosphoric acid fuel cells are very tolerant when it comes to impurities in hydrogen. Unlike direct methanol fuel cells, phosphoric acid cells do not get poisoned by carbon monoxide in the platinum catalyst of the anode side. Because of this, efficiency of the cell does not decrease due to poisoning, and the cell runs at 85% overall efficiency. This cell generates both heat and electricity. When generating electricity alone, though, they are only 40% efficient.

One of the few downsides of phosphoric acid fuel cells is the weight and volume they need to operate; the size to output ratio is relatively high. Because of this, fuel cells are typically large

and heavy. In addition, the cell requires a platinum catalyst like other cells, and raises the prices of the cell significantly. [5]

2.1.4 Molten Carbonate Fuel Cells

Molten carbonate fuel cells have developed to a stage where applications are feasible. These fuel cells run at very high temperatures, they use an electrolyte composed of a molten carbonate salt mixture suspended in a porous, chemically inert, ceramic lithium aluminum oxide matrix. Due to the extremely high temperatures the cell runs at, about 650°C, non-precious metals can be used as a catalyst instead of the platinum that is used in direct methanol fuel cells, and so the cost is lower.

There is a gain in efficiency over the lower temperature fuel cells. Molten carbonate cells when using a turbine are 65% efficient, which is better than the 40% efficiency of the phosphoric acid fuel cell plants. The efficiency of the molten carbonate fuel cells increases further when the heat is captured from the cell, making the efficiency 85 percent.

One of the major advantages to molten carbonate fuel cells is, unlike other fuel cells, these fuel cells do not require a hydrogen feed. This is because the cell runs at such high temperatures that the cell converts the primary fuel into hydrogen within the cell. This also greatly reduces the cost of the cell.

Molten carbonate fuel cells are not prone to carbon monoxide or carbon dioxide poisoning. They can even use carbon oxides as fuel, making them more attractive for fueling with gases made from coal. Assuming they can be made resistant to impurities such as sulfur and particulates that result from converting coal into hydrogen. It is possible that molten carbonate fuel cells can be used to convert coal to hydrogen and be able to run the cell simultaneously. [5]

2.1.5 Regenerative Fuel Cells

Regenerative fuel cells produce electricity from hydrogen and oxygen and generate heat and water as byproducts, just like other fuel cells. However, regenerative fuel cell systems can also use electricity from solar power or some other source to decompose water into oxygen and hydrogen fuel, a process called "electrolysis." This is a comparatively young fuel cell technology being developed by NASA and others. [5]

2.2 Direct Methanol Fuel Cells (DMFC)

2.2.1 Conventional Direct Methanol Fuel Cells

A direct methanol fuel cell (DMFC) is composed of a multiple layer configuration where there is an anode bipolar plate, a cathode bipolar plate, a membrane electrode assembly consisting of an anode and cathode gas diffusion layer (GDL), an anode and a cathode layer, and a proton exchange membrane (PEM). This assembly can be seen in Figure 3. The bipolar plates also serve as current collectors. The purpose of the GDLs having pores is to allow the flow of oxygen in and carbon dioxide out and water [6]. The size and shapes of the perforations and pores are important to the performance of the methanol fuel cell.

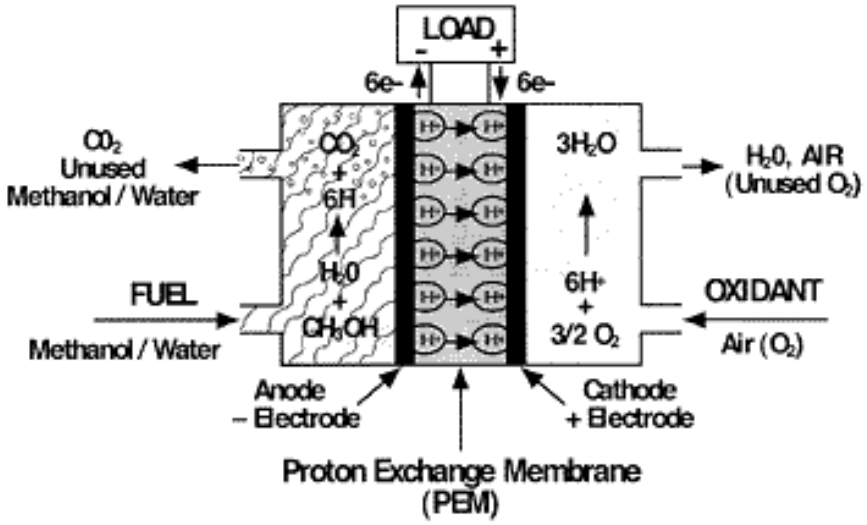

Figure 3: Direct Methanol Fuel Cell Schematic [8]

The main difference between passive and regular methanol fuel cells is that in a passive system there are no extra pumps or fans to promote fuel flow. This requires less energy and cost to run a passive fuel cell. However, the performance is lower due to transportation limitations.

The next component of the methanol fuel cell is a gas diffusion layer, or GDL. This layer is composed of carbon paper or carbon cloth that is conductive and distributes the anode and cathode fuels and products. This allows the flow in the fuel cells as well as transports the electrons to the plates. Another characteristic of the GDL is that it helps with is the heat generated by the fuel cell. There are several ways to improve the performance of the cell by treating the GDL. For example, it can be wet-proofed with polytetraflouroethylene or by using a hydrophilic anode backing layer.

The catalyst used in the MEA to promote the half-cells reactions is usually made of platinum and ruthenium alloy at the anode and platinum at the cathode [3]. There is a certain amount of improvement that can come from adding more catalyst; however this reaches a maximum where

performance begins to level off. Adding more catalyst would also greatly increase the cost of the cell.

Two of the biggest issues with the direct methanol fuel cell are that a pure platinum catalyst at the anode side cannot sufficiently activate the methanol or the water, and it also cannot remove CO from poisoning the cell. For the anode reaction seen in Table 1, a bi-functional catalyst composed of platinum and ruthenium is needed because each performs a different function. As the methanol begins to activate by coming in contact with the platinum, it reduces to carbon monoxide, protons and electrons.

Table 1: Methanol Fuel Cell Electrode Reaction

	Equation
Anode	$CH_3OH + H_2O \rightarrow 6\ H^+ + 6\ e^- + CO_2$ Methanol Oxidation reaction (MOR)
Cathode	$\frac{3}{2}O_2 + 6\ H^+ + 6\ e^- \rightarrow 3\ H_2O$ Oxygen Reduction Reaction (ORR)
Overall Reaction	$CH_3OH + \frac{3}{2}O_2 \rightarrow 2\ H_2O + CO_2$ Redox reaction

The carbon monoxide created by the anode reaction is a major cause of problems since it strongly binds to the catalyst reducing the effectiveness of the fuel cell. This is where the ruthenium acts to decompose water into hydroxide, another proton and another electron. The hydroxide created can then react with the carbon monoxide that is bonding to the catalyst

surface; this would lead to the production of carbon dioxide, along with another proton and electron. [9]

This leads to the anode half reaction to generate a total of six protons and six electrons per molecule of methanol (Table 1). This is in contrast to the two protons and electrons that are produced in a PEMFC. It is noted that the electrons travel through an external circuit, which creates power from the cell. However, the protons created in the half cell reaction travel through the Nafion® membrane via diffusion. [3]

At the cathode, an oxygen reduction reaction takes place between permeated protons and electrons that have gone through the outer loop and returned to the cathode. By combining the first two reactions for the anode and cathode, the reactions provide the overall methanol reaction that occurs in the methanol fuel cell, as seen in Table 1. However, methanol also crosses over through the anode across the membrane to the cathode, and undergoes MOR at the cathode as well. This attributes to fuel and efficiency loss.

2.2.2 Passive Direct Methanol Fuel Cells (PDMFC)

Direct methanol fuel cells, like other fuel cells, require heat exchangers, pumps and fans to promote better efficiency and to keep the cell running. If these were to be eliminated, it would reduce the cost of the cell as well as the size, making it suitable for small scale portable applications. The additional equipment greatly reduces the power density of the fuel cell, since they require power to run on as well. If these were removed, this would increase the power density that the fuel cell outputs. This is the rationale for PDMFC; they do not use other equipment and are thus “passive”.

PDMFC works with the methanol gel being inserted in the anode chamber of the cell. After this, the ambient diffusion allows the methanol to reach the anode without any use of fans or heat

exchangers. On the other side, oxygen diffuses into the cathode naturally. However, passive transports by diffusion rather than by concentration or flow increase. This transport increases resistance and reduces performance.

The design and fabrication of air breathing, pump less direct methanol fuel cells for portable applications was developed more in detail by Shimizu et al. [1]. A small PDMFC was developed, and its performance was evaluated at 36 cm^2. This cell took oxygen from the surrounding and had methanol stored in a built-in reservoir. The cell ran efficiently with liquid methanol concentrations of .5 to 4 M. it reported a current density of 11 mW/cm^2 and reached current densities as high as 36 mA/cm^2.

The simple set up that PDMFCs require makes them suitable for small scale application such as cellphones, PDAs or camping equipment. However, because PDMFCs do not use any ancillary equipment, their performance is reduced when compared to regular DMFC. The drop in performance from a DMFC to a PDMFC is 45 mW/cm^2 to 13 mW/cm^2; this is a 70% drop in performance. [10]

PDMFC are also more easily poisoned by carbon monoxide due to the lack of flow at the membrane, reducing the efficiency to about 30%. [5] Further, the diffusion of methanol towards the anode requires a much higher concentration of methanol. However, having a passive fuel cell also allows for the water that is created at the cathode not to be removed by the air flow from the ambient. Rather, this water produced diffuses across the membrane and is used in the MOR.

The consequences of methanol cross over in PDMFC was explored by Beck Kyun Kho et al.[6] They showed that the methanol crossing over from the anode to the cathode was due to a concentration gradient, and this lead to a decrease in open current voltage. Since methanol

crossover rate is dependent on the methanol concentration in the reservoir, it is expected that OCV will vary with methanol concentration.

Throughout experimentation with suppression of the methanol crossover, Woo-Jae Kim et al was able to minimize the methanol crossover. [11] This was done by soaking the MeOH fuel in hydrogels rather than using a liquid feed of methanol. It was observed in the experiment that when using hydrogels instead of liquid, the power density increase from 16 to 22 mW/cm^2. Hydrogels suppressed the excess fuel supply from the fuel reservoir to the anode electrode even at high fuel concentrations by reducing the fuel diffusion rate, so that the unconverted MeOH, which crosses over to the cathode electrode, is minimized.

Another issue with the cell is the direction of the cell. The best flow for methanol gel is to have the vessel for the fuel below the MEA allowing the flow of fuel in an upward direction towards the membrane. Guo and Fagri [12] have developed a fuel cell that operates at 1 W and is direction independent. This PDMFC used four cells and used a total active area of 36 cm^2. This design was composed of neat methanol flowing from a separate compartment that would dissolve in water supplied by the membrane in the anode chamber. This particular PDMFC has many features that improve functionality such as a micro methanol flow controller that shuts off methanol supply, a stable vapor fuel supply that is heated, a water management system and air filtering via additional GDLs.

In the same topic of porous plates, Mohammad Ali et al. [13] performed a study on the efficiency operation at high methanol concentrations using porous plates. However, in the experiment a layer was added of CO_2 to increase distance between the current collector and the GDL. The highest power density that this experiment observed was 24 mW/cm2 at room temperature, using a 2 M solution of methanol. Once the porous plate was added, 16 M methanol solution had to be

used to achieve the same power density. The results from this experiment show that adding a layer of CO_2 increases transport resistance.

Other research done for the PDMFC includes a study done by R. Chen and T.S. Zhao, describes the porous current collectors for passive direct methanol fuel cells. In this study, current collectors made from porous metal foam were investigated experimentally. The polarization curves in the experiments showed a much higher and much more stable performance, than the cell did with conventional perforated plate current collectors. [14]

2.2.3 Objectives

The advancements in technology will allow for fuel cells to be used in a more wide range of uses. The objective is to maximize output from the fuel cell stack while at the same time reducing cost. There is also the idea of reducing the size of the fuel cell stack to allow for other, more portable uses, such as cell phones and laptops.

CHAPTER 3: STACK DESIGN AND EXPERIMENTAL

3.1 Stack Design and Construction

A direct methanol fuel cell has many key requirements in order to function properly under passive conditions. Since there is no active components to increase mass transfer to the MEAs, construction of a stack must be carefully done in order to maximize performance. A main consideration for a passive direct methanol fuel cell is that the fuel chamber must be sealed airtight from the surroundings. This is to prevent methanol fuel, either liquid or vapor, from escaping and either reacting on the cathode or leaking out of the fuel cell. This is both a waste of fuel and is considered a safety hazard when using highly concentrated methanol solutions. Another reason for having the cell airtight is to prevent oxygen from entering the anode chamber, due to the oxygen concentration difference of the outside and the inside of the fuel container. When the oxygen enters the cell, it can react on the anode and cause over potential, lowering the overall cell voltage. [15]

A single cell setup was constructed from polycarbonate material to simulate the performance of a stack on a smaller scale. This allowed many experiments to be run much more easily than on the stack itself. Figure 4 and Figure 5 show the single cell setup, as well as its components. The polycarbonate base is hollow, allowing a small amount of either methanol gel or concentrated solution to be put into the cell. The polycarbonate is screwed on to form a complete seal. On the electrode side of the base, a layer of silicon gasket is placed between the anode current collector and the top of the cell. This helps to form a complete seal, preventing leakage. A small amount of vacuum grease is placed between the base plate and cell as well as the silicon layer and the cell. This prevents slippage and maintains perfect sealing.

The next layer is a piece of foam gasket that goes directly on the MEA, with a cutout fit for the active area. This layer prevents any leaks across the non-active area on the Nafion® membrane. A carbon cloth gas diffusion layer (GDL) cut to the size of the active area, $5cm^2$, is placed on the anode side of the MEA. This helps to diffuse the methanol on the platinum catalyst more evenly. Many different materials can be considered as the gas diffusion layer. Carbon cloth helps to both even out the diffusion, maximizing surface area contact, while limiting mass transfer resistance. Catalyst layers can be put on the GDL to improve redox reaction rate, but this increases overall cost. Two commercial sources for the MEAs purchased are IRD (www.ird.dk) and Fuel Cell Store (FCS) (www.fuelcellstore.com/). The catalyst loading for the MEAs was kept consistent between companies, to keep results similar. Table 2 shows the properties for the MEAs. As can be noted, the 5 layer DMFC MEAs do contain GDLs already hot pressed onto the assembly, however further tests were run with extra GDLs to assess effectiveness.

Table 2: MEA Properties

Property	**Value**
Catalyst Loading	4mg/cm2
Catalyst Type	Pt/Ru Anode, Pt Cathode
Active Area Size	$5cm^2$
Nafion® Thickness	117
Layers	5 Layer DMFC MEA, 2GDL, 2Catalayst, 1 Nafion

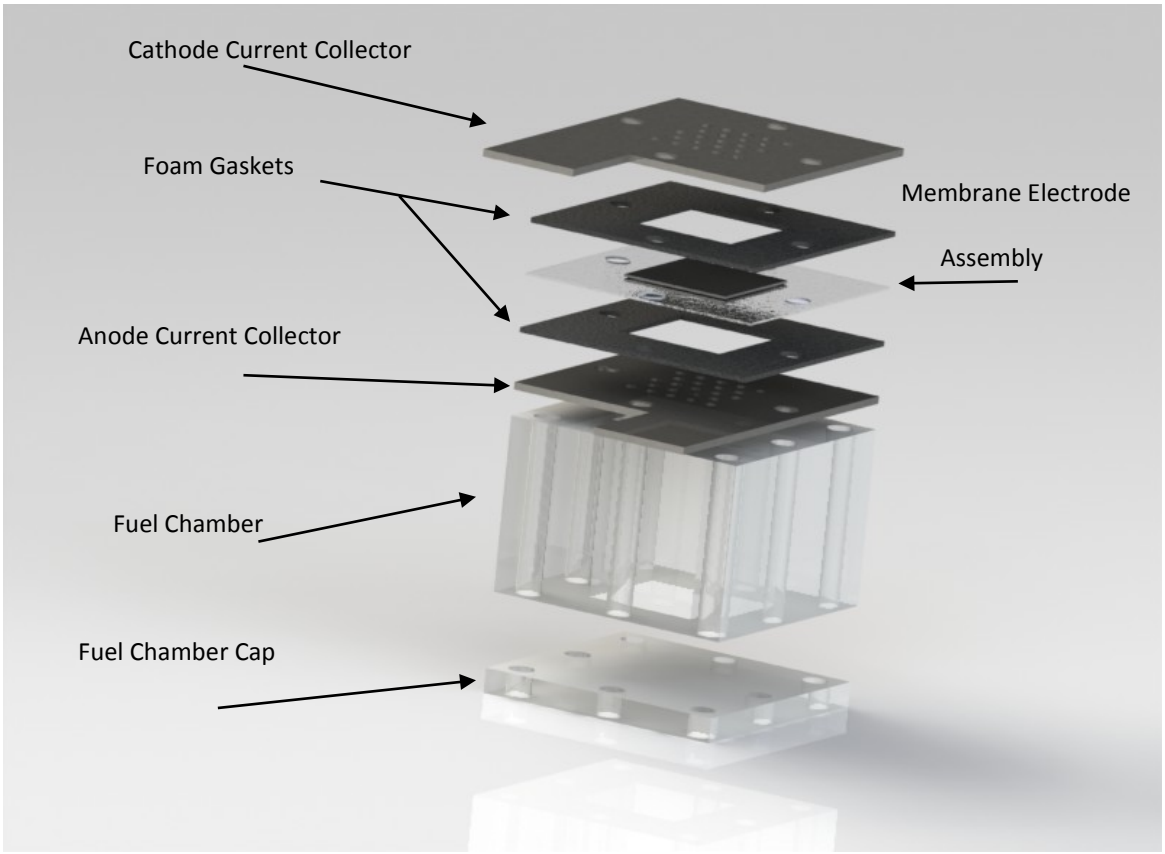

Figure 4: Single Cell Schematic Exploded, 5cm^2 Active Area

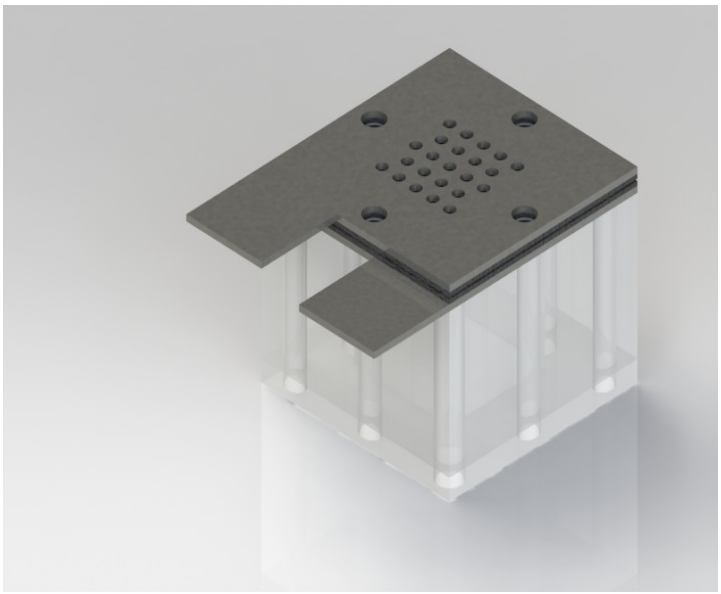

Figure 5: Single Cell Schematic Compacted, 5cm^2 Active Area

The prototype fuel cell that was available for testing, named Prototype 5, was constructed by a former graduate student, Neal Rosenthal [16]. It is a passive direct methanol fuel cell designed to run off of concentrated methanol solution or gel fuel from a Sterno® (MSDS in Appendix 3) fuel can, or similar. One example is shown below in Figure 6 as the Power Heat Brand.

Figure 6: Methanol Chafing Fuel, Power Heat Brand, Similar to Sterno

It contains 12 individual cells with an active area of 5 cm^2, wired in series. It was constructed from a polycarbonate base that is airtight, watertight and non-conductive. The circular fuel chamber was designed so that an entire open can of chafing gel could be placed in the bottom, allowing the fuel to diffuse to the cells passively. The electrode assembly is exactly that of the single cell, with the layers of gaskets and GDL being the same materials and thickness. The stack has a polycarbonate lid with an O-ring that also forms an airtight seal.

While using metal screws could give stronger hold, the metal screws conduct electricity, which can short circuit the cells. This is why the IsoPlast screws were chosen over both nylon and stainless steel. IsoPlast is polyurethane composite that is stronger than nylon, but doesn't conduct electricity. These IsoPlast screws were obtained through SmallParts.com. Nylon screws were tested, but the torque required to compress the assembly proved to be too much for the weak

nylon. Stainless steel screws with an insulated wrapping were also tested, but completely insulating the stainless screws proved to be difficult and time consuming. The stainless steel screws also began to strip the softer polycarbonate base, weakening the screw even more than before. Ceramic screws were looked at as an alternative, but proved to be far too expensive for the project. A compromise between torque, conductivity, and cost must be made, so the IsoPlast Material was made. Figure 7 shows a cutaway view of the stack, while Figure 8 shows the complete stack.

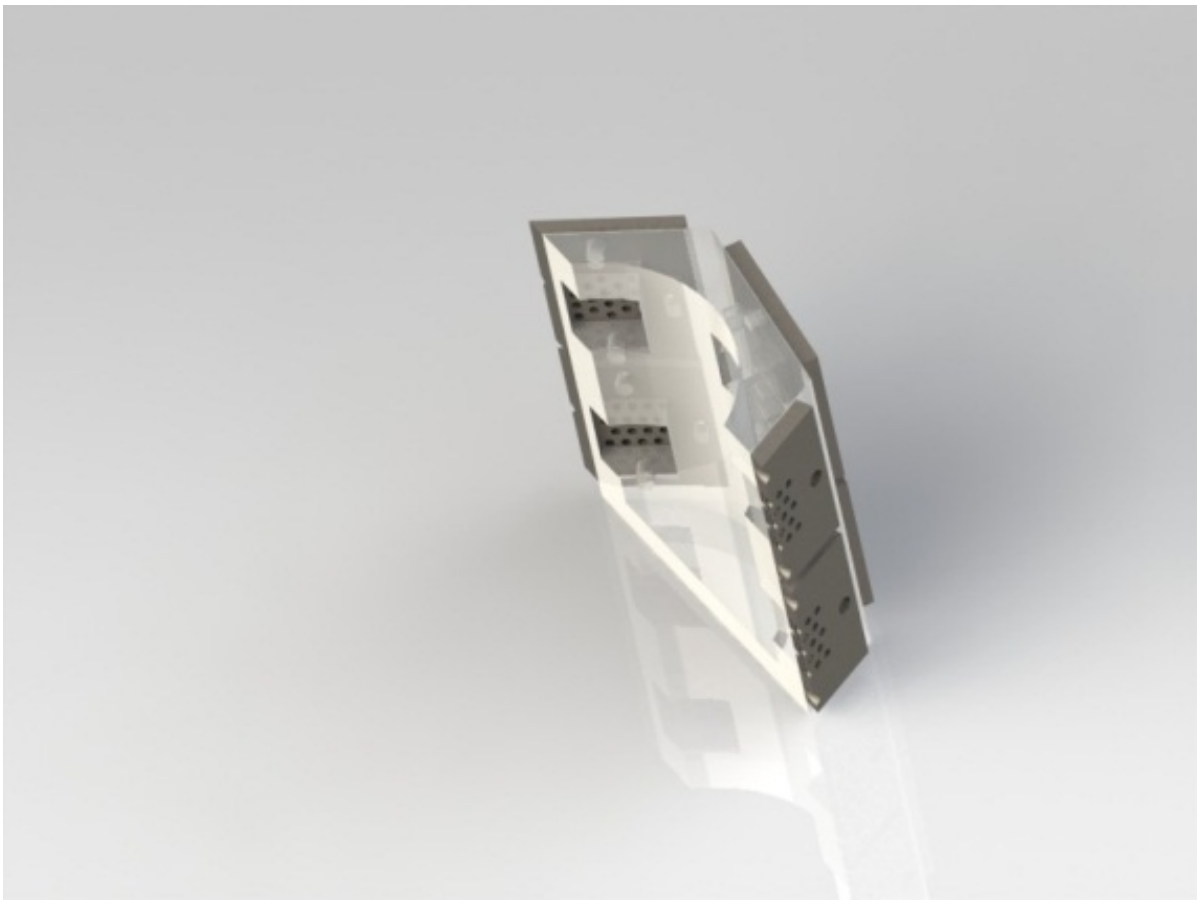

Figure 7: Cutaway Stack View, 5cm^2 Active Area, 12 Cells in Series

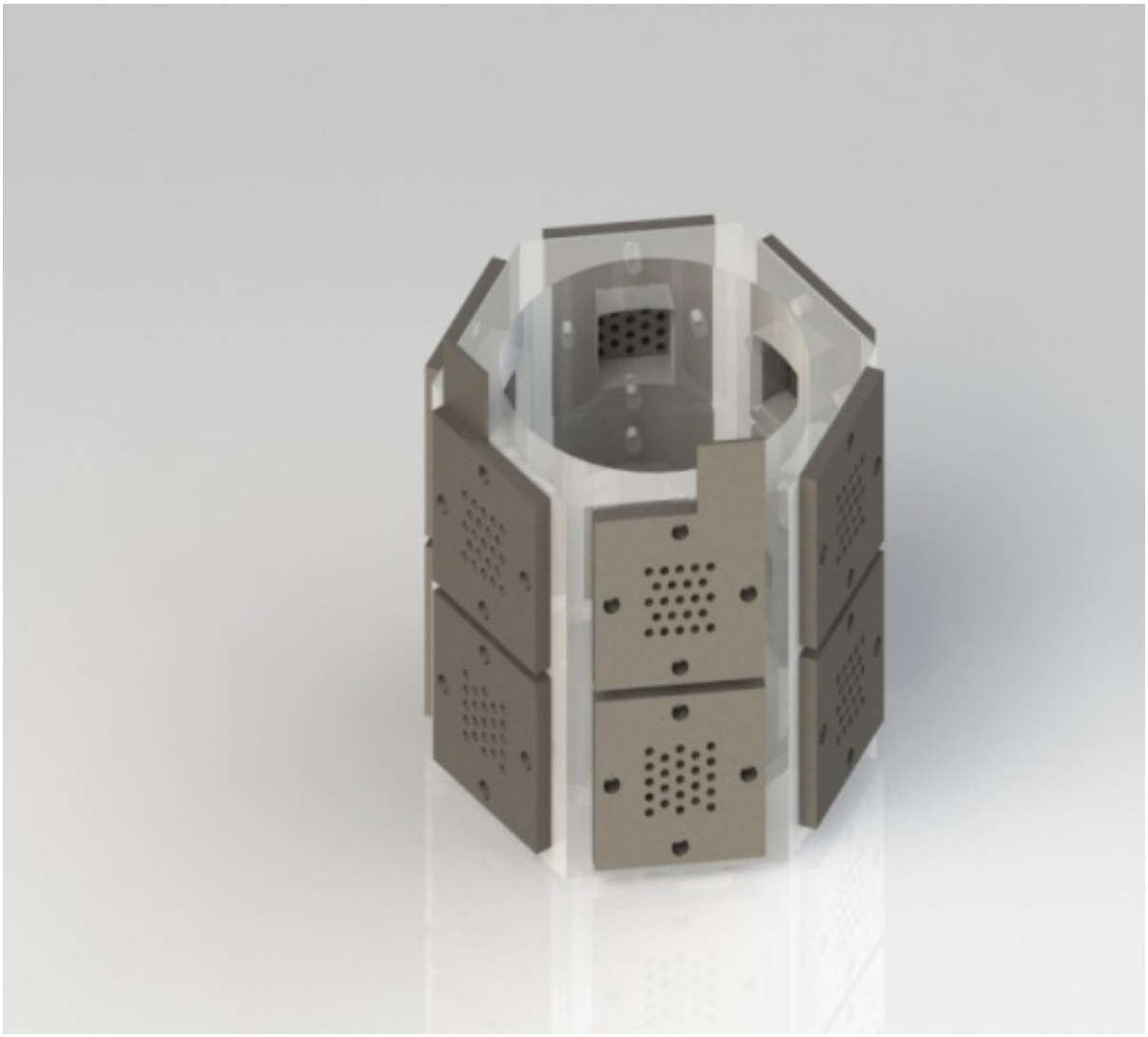

Figure 8: Complete Stack View, 5cm^2 Active Area, 12 Cells in Series

3.1.1 Current Collector Optimization

The current collectors on the single cell were experimentally tested in various configurations. The main goal of the experiments was to determine the ideal collector arrangement by comparing the different collectors and the amount of space open for diffusion. The tests on a single cell were run using 5g of methanol gel, in passive conditions (ambient temperatures and atmospheric pressure). The standard current collector arrangement was a perforated, solid stainless steel plate 1mm thick, which are also outfitted on the 12-cell stack. During our tests this was used as the control, to allow it to be possible to see the relative performance from the current setup. All of

the current collectors had a 5cm^2 active area. The tests were all run with Nafion®-117 MEAs from IRD fuel cell store. They had catalyst loading of 4 mg/cm^2 Pt/Ru on the anode and 4mg/cm^2 Pt on the cathode. The data was collected experimentally using the FuelCell program, conducting a voltage sweep every 5 minutes, from 0V to the open current voltage in increments of .05V. Pictures of the different current collectors are as follows:

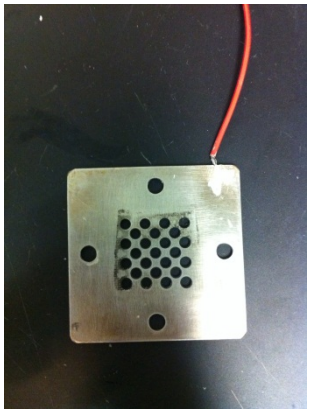

Figure 9: Perforated Current Collector

[Control]: Solid Stainless Steel, 25 holes, 34% open space)

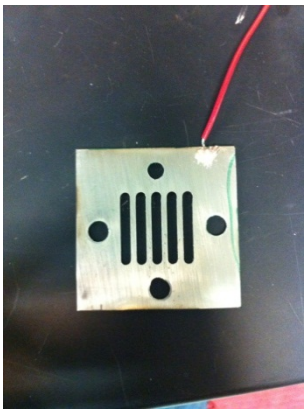

Figure 10: Channeled Current Collector

Solid Stainless Steel, (5 channels, 69% open space)

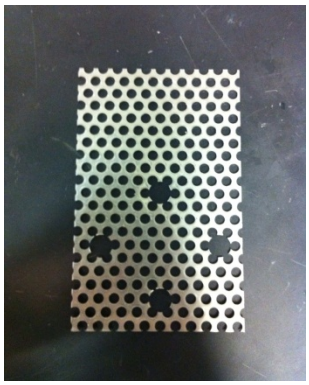

Figure 11: Wire Mesh Current Collector

Solid Stainless, 34% open space

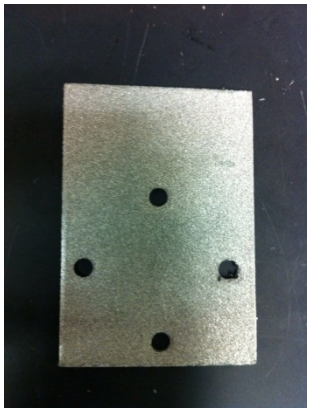

Figure 12: Porous Current Collector

Porous Stainless Steel, No open area

MottCorp: .078” thick, Media Grade 40, 316LSS

3.2 Experimental Setup

3.2.1 Testing Methodologies:

The fuel cell lab setup is optimized to collect data from the passive setup using the FuelCell 7 computer program. The computer program has an automatic load box controller that will monitor voltage power and current connected to the positive and negative leads. (This is shown in Figure 13)

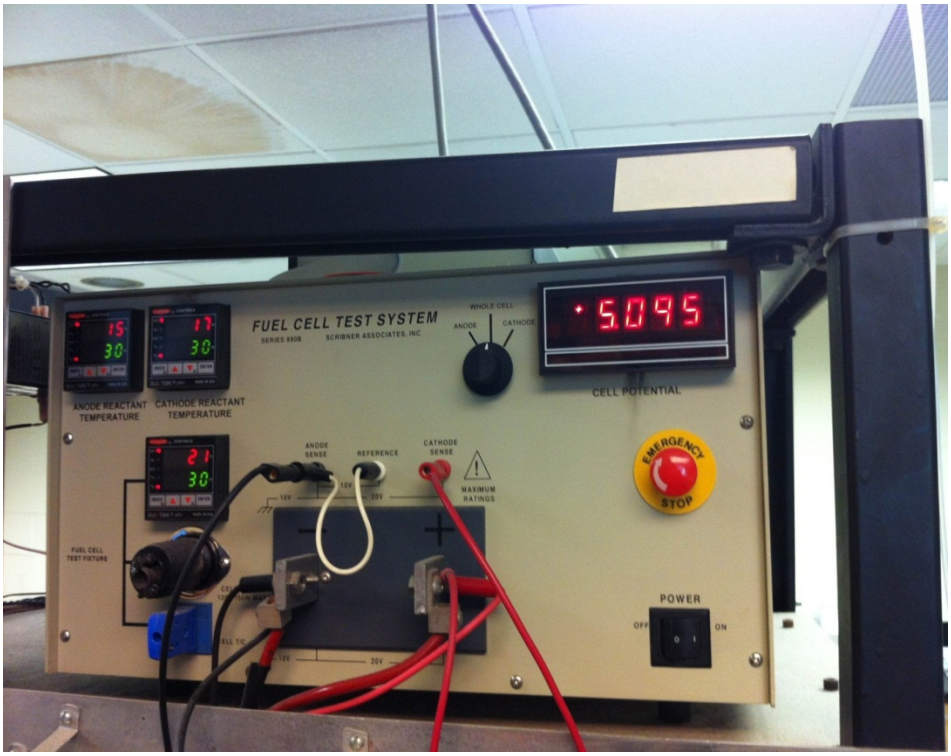

Figure 13: FuelCell Load Box and Display for Test Station

The FuelCell program allows different programs to be preloaded into the setup that are completely customizable and stackable. This allows programs to be run in a sequential order as determined by the user. The program queue used by our experiments consisted of multiple tests to perform a range of data collection quickly and easily, as well as to guarantee consistent conditions in the stack. Figure 14 shows the program layout, as well as the test queue.

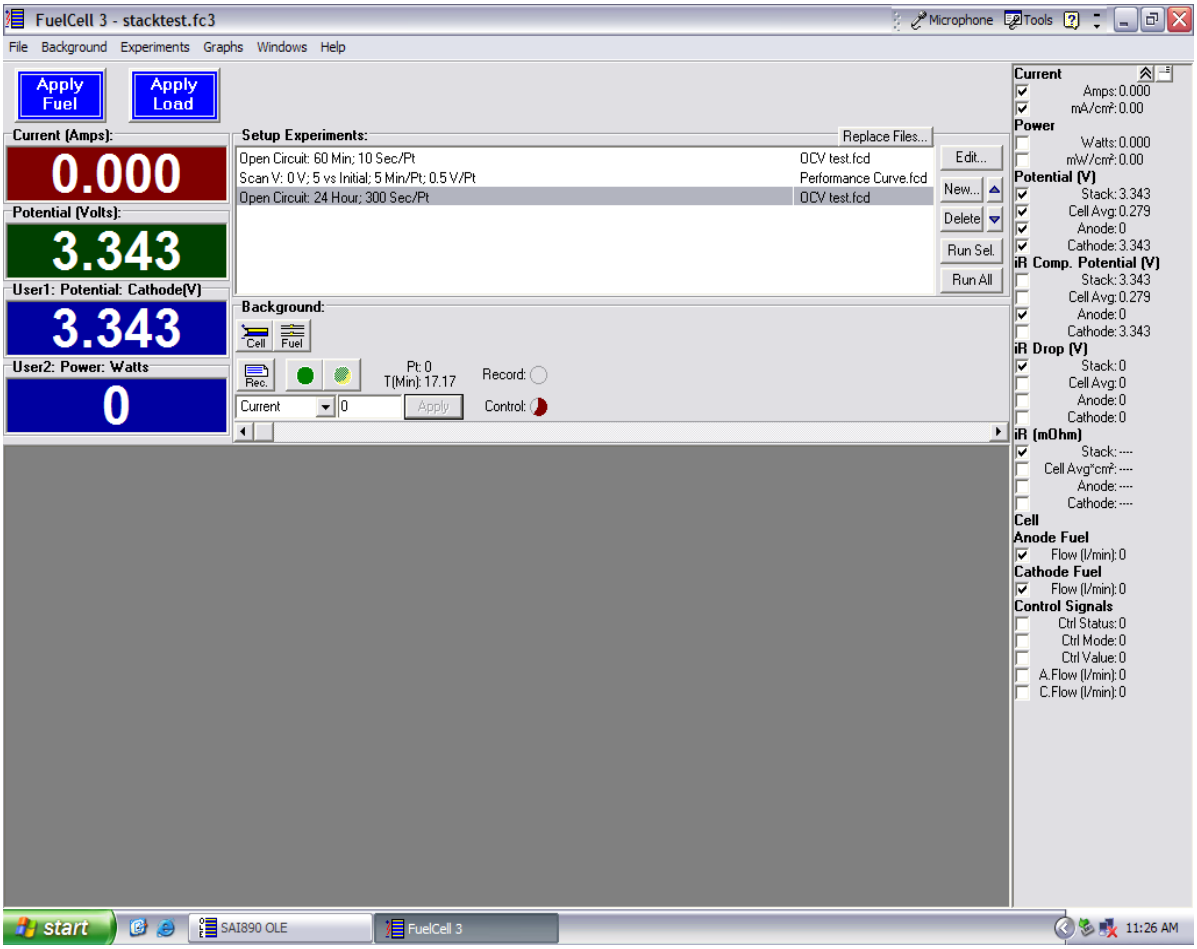

Figure 14: FuelCell7 Program Queue for Typical Experimental Run on Stack Layout

3.2.1.1 OCV Test

The first program was a test to hold the voltage at open circuit voltage (OCV) conditions for a set amount of time, about an hour to ensure steady state is met, taking points at a predetermined interval. The input for the program is shown in Figure 15.

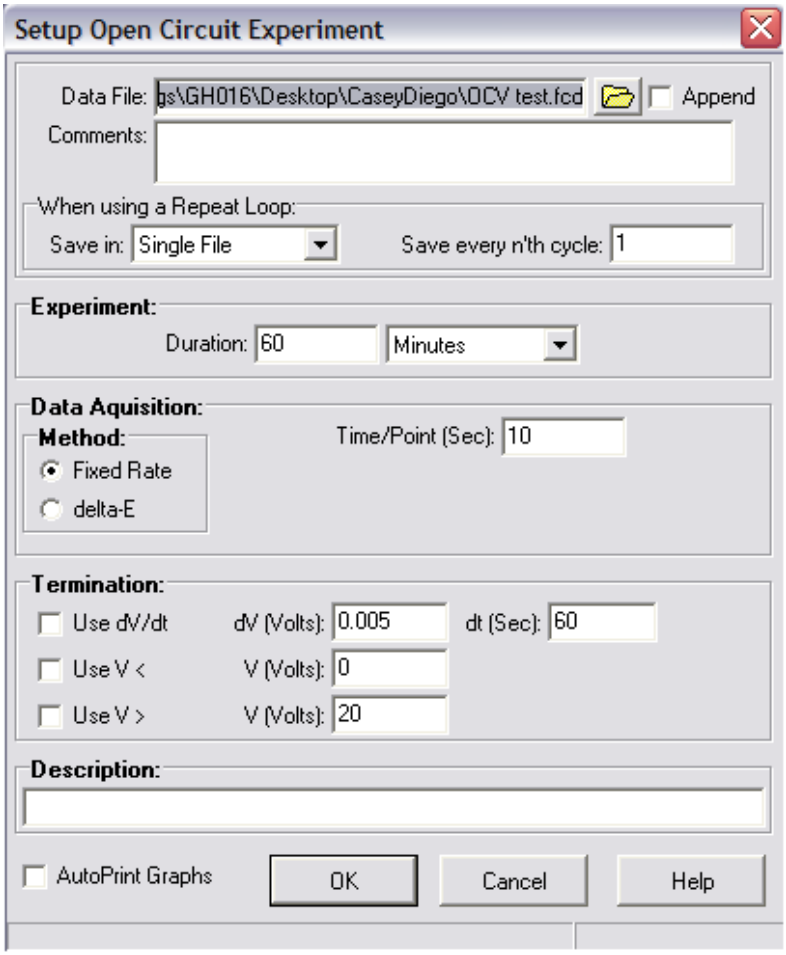

Figure 15: Input Used to Run OCV Tests on Fuel Cell

3.2.1.2 Voltage Scan Test

The second program in the queue is a voltage scan test that starts the voltage at zero and adjusts it by a set amount, usually (+.5V for the stack, or .05V for the single cell) until the unit has reached OCV. The time interval between these points is 5 minutes, to ensure steady state at each condition has been reached. The input for the voltage scan for a stack test is shown by Figure 16.

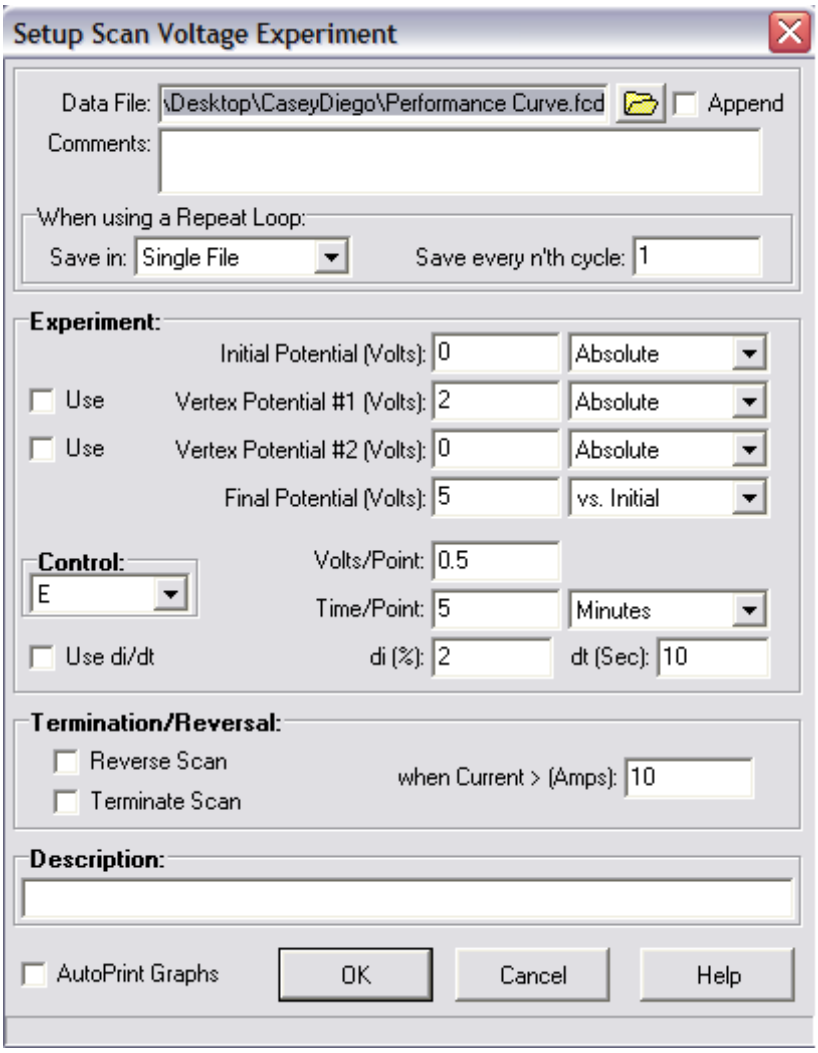

Figure 16: Input Used to Run Voltage Scan Tests on Fuel Cell

3.2.1.3 Long Term Performance Test

Another test that was used for long term performance and judging cell performance over time was an OCV test set for 24 hours. Shown in Figure 17, this allows stability over a long period of time to be analyzed. Running the tests in this order allows the OCV, polarity plots and stability to be determined in one run. This is imperative in collecting consistent data.

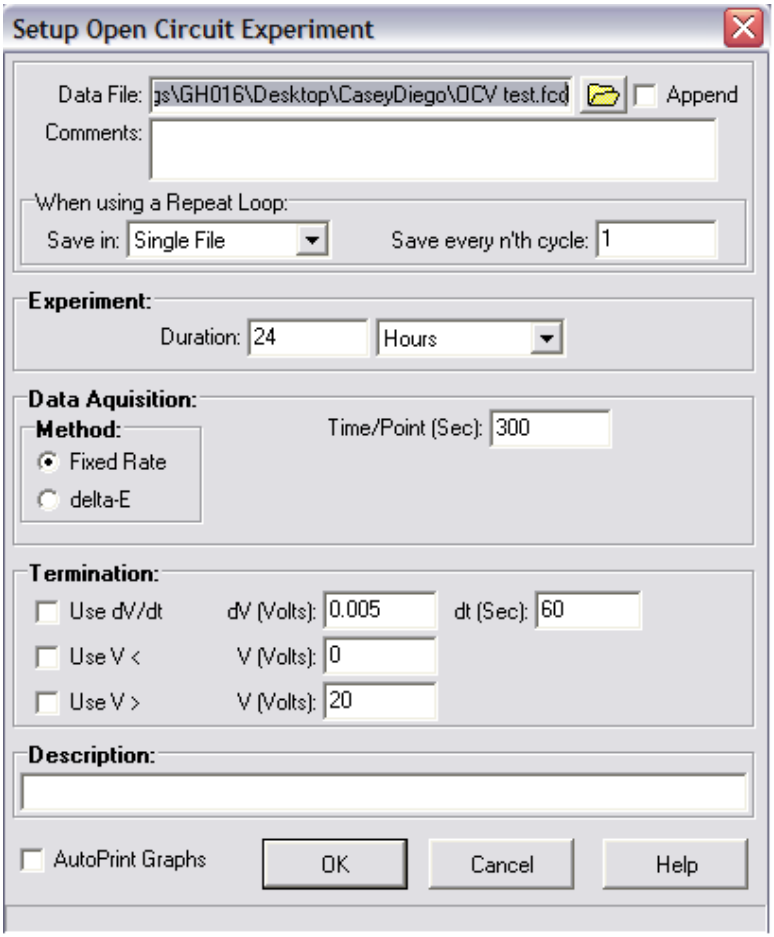

Figure 17: Input Used to Run Long Term Performance Tests on Fuel Cell

With these data collection methodologies, many different tests were able to be run. Experiments were conducted by adjusting one variable and keeping all other parameters constant. By using the single cell unit, it was possible to run small scale tests that were easier to setup that would be eventually translated to the larger stack. This, however, was only accurate for concentrated liquid methanol solutions. The diffusion rate of using the gel had too much variation from the single cell to the stack, as discussed above.

To test the performance of gel fuel, a control must be set. The determined control stack setup was the twelve cell stack as described above, with the perforated current collectors on the anode and cathode sides.

Once the stack design was finalized, long term tests with the 12-cell stack were run with ancillary devices, such as fans, lamps, and radios to judge fuel usage and performance stability over a long period of time. This was to estimate actual PDMFC application potential.

3.2.2 Single Cell Tests

3.2.2.1 EXPERIMENT 1: Different Methanol Concentrations

To understand the basic functionality of a fuel cell, the single cell setup was experimented on. The small scale of the single cell, along with the ease of building, allowed multiple tests to be run fairly quickly. Since the performance of a single cell is much lower than that of a stack, these experiments were conducted only to compare experimental cell builds and fuel concentrations.

Using a liquid solution of methanol ranging from 1M to 4M, experiments were run to compare how varying concentration would affect the performance of the cell. From Guo [12], it is assumed that by increasing the concentration the performance would increase as well. This was expected to be shown in the tests ran as stated. Guo [12] recommends using a range of 1-5M solutions of methanol, because for any higher concentrations, the performance will become hindered due to increased crossover from the higher concentration. The control current collector arrangement was used on the single cell when the tests were conducted.

Table 3: Experiment 1, Different Methanol Concentrations

Fuel Type:	Concentrated Methanol 1M-4M
Current Collectors:	Perforated Cathode, Perforated Anode
Testing Purpose:	To Compare Concentration versus Performance

3.2.2.2 EXPERIMENT 2: Different Current Collectors

Another variation that was tested on the single cell was the construction of the current collectors using different materials. Since the current collectors essentially control the diffusion rate in a passive DMFC along with the GDL, the media from which they are made can affect performance greatly. The different materials that were tested were solid stainless steel and porous stainless steel. The solid stainless steel was cut into different patterns as described above to control diffusion of methanol and oxygen through it. The porous stainless was not cut because of the porous properties it inherently has.

Table 4: Experiment 2, Different Current Collectors

Fuel Type:	Methanol Gel
Current Collectors:	Varying
Testing Purpose:	To Determine Optimized Current Collector Design

3.2.2.3 EXPERIMENT 3: Varying Temperature Tests

The varying temperature test consisted of setting up the single cell with varying temperatures. To do this a heating lamp was used to change the temperature of the cell. The temperature of the heating lamp could not be changed. It would heat at a certain set temperature and depending on the distance the temperature would change and remain constant for the duration of the test.

Thus, the lamp would be set closer to the cell for higher temperatures, and the test that were run were at 30 C and 50 C. These tests were run with the purpose of determining the effect of temperature using the methanol gel, as well as if the performance of the fuel cell would improve at higher or lower temperatures.

Table 5: Experiment 3, Varying Temperature

Fuel Type:	Methanol gel
Current Collectors:	Perforated Cathode, Perforated Anode
Testing Purpose:	To compare the performance at different temperatures.

3.2.3 12-Cell Stack Tests

3.2.3.1 EXPERIMENT 4: Control Stack (default)

After experiments with the single cell tests were conducted, the results and conclusions were then translated onto the fuel cell stack design and performance. By using the stack, a better representation to the actual performance of a practical passive DMFC can be observed. To easily analyze and compare the effects of any changes in the stack design and operation, a control unit was set up before any tests were run. The control unit was designed and constructed by Rosenthal [16]. The stack described consists of twelve cells wired in series, using the control (perforated) current collector arrangement.

Table 6: Experiment 4, Control Stack

Fuel Type:	Methanol Gel
Current Collectors:	Perforated Cathode, Perforated Anode
Testing Purpose:	To establish a control data set

3.2.3.2 EXPERIMENT 5: Initial Condition Study and Steady State

In order to better understand the various transport processes that occur within a passive fuel cell, an initial conditions experiment was run to determine voltage based on time immediately following fuel injection. The voltage trends described in Rosenthal's thesis [16] explain the time dependent diffusion of the fuel reaching the MEA, the saturation time, and steady state

equilibrium point. By analyzing diffusion rates in relation to the time of fuel injection, the diffusion rates can be better optimized based on stack design, fuel amount, fuel concentration, and current collector materials. One of the downsides to having a passive fuel cell is that in order for the cell to reach steady state maximum OCV, a considerable amount of time must pass for the fuel to fully saturate the stack via diffusion. An in depth look at these trends is observed in the first hour after fuel being loaded into the cell. The control current collector arrangement was used.

Table 7: Experiment 5, Initial Condition Study

Fuel Type:	Methanol Gel
Current Collectors:	Perforated Cathode, Perforated Anode
Testing Purpose:	To analyze cell "warm up time"

3.2.3.3 EXPERIMENT 6: Gas Diffusion Layer Removal

To be able to understand the performance of the cell and how the MEA was set up, tests were run on the cell by removing the gas diffusion layers. These tests were set up by first removing the gas diffusion layers from both the cathode and the anode. After this test, the same fuel and setup were used with the difference of using a GDL only on the anode side, followed by using a GDL on both sides. This test would help in understanding how using different materials for current collectors can impact differences in mass transfer and diffusion, leading to changes needed to be made to the MEA.

Table 8: Experiment 6, Gas Diffusion Layer Removal

Fuel Type:	Methanol Gel
Current Collectors:	Porous Cathode, Perforated Anode

Testing Purpose:	To Compare Concentration versus Performance

3.2.3.4 EXPERIMENT 7: Individual MEA Performance

In order to ensure the stack is functioning properly, an easily observable method of judging the individual performance of each MEA in the stack was conducted. This was carried out by using a voltmeter to measure the potential across the individual bipolar plates. By taking these measurements, the quality of the individual MEAs can be determined. This allows any repairs or replacements to be easily determined without individually running each MEA on the single cell setup. This also allows the entire voltage drop across the stack to be determined by comparing added individual voltages to the actual read voltage from the leads. Having this trouble shooting method can also help to judge performance based on location in the fuel cell stack, which can vary due to diffusion path lengths of the fuel.

During the progress of this project, a few different types of MEA were tested to see which one gave the best performance. MEAs were ordered from both IRD and Fuel Cell Store. During the course of experimentation, tests were run to compare the performance of the two companies. This was done to give future groups a recommendation for purchases. In Figure 18, it is shown how each MEA was assembled.

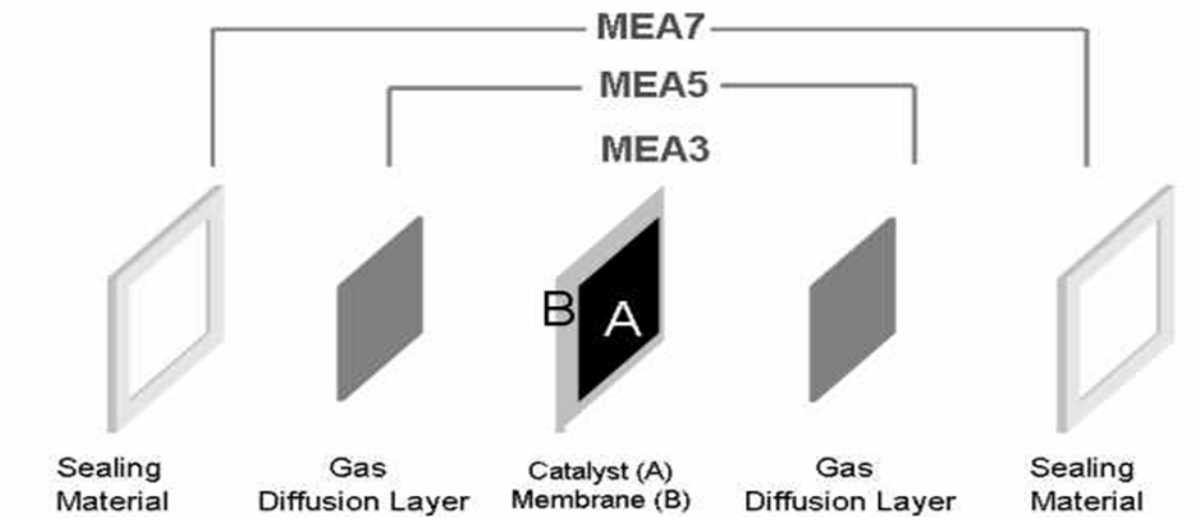

Figure 18: Membrane Electrode Assembly Schematic

Table 9: Experiment 7, Individual MEA Performance

Fuel Type:	Methanol Gel
Current Collectors:	Control (Perforated Perforated)
Testing Purpose:	To compare MEA performance on an individual scale

3.2.3.5 EXPERIMENT 8: Using Porous Plate on Cathode with Perforated Plates

When using the porous stainless steel as a current collector, the lack of rigidity of the material tends to cause additional internal resistance due to the resulting compression forces on the MEA not being even or strong. This is important when constructing the assembly to ensure even pressure on the entire MEA and provide a strong seal. Using the porous current collectors, this becomes difficult to do without additional reinforcement. A perforated solid stainless steel piece, thus, was placed on top of the porous current collector to add rigidity and structure. This also allowed the screws to be tighter and the porous bipolar plate to be compressed evenly. The tests were then run to determine any difference the reinforcement made.

Table 10: Experiment 8, Porous Plate Cathode with Perforated Plate

Fuel Type:	Methanol Gel
Current Collectors:	Porous Cathode, Perforated Anode
Testing Purpose:	To test the importance of MEA rigidity

3.2.4 Miscellaneous Tests

3.2.4.1 EXPERIMENT 9: Mass Transfer / Diffusion test

The methanol gel that was used in most of these tests has different transport properties than the concentrated solutions that are traditionally used. Because of this, the diffusion properties must be experimentally found. This is important because to understand relative performance and these transport values are needed for the theoretical model. By calculating the diffusion rate of gel for a controlled surface area, it can also be scaled up to allow for estimation on the minimum surface area of gel to achieve a required current load. The experimental diffusion rate is also necessary to do mass transfer calculations, such as the flux, mass transfer coefficient of the gel, and the diffusion time. The diffusion experiment was conducted by placing 25g of methanol gel into a 50mL beaker. The mass of the beaker was tarred off and the mass of the gel was measured every 5 minutes for an hour. The difference in gel over the amount of time was assumed to be the diffusion rate of the methanol from the gel medium.

3.2.4.2 EXPERIMENT 10: Active Fan Test

A test was conducted using a fan powered by the fuel cell stack as an indicator or practical utility and also to attempt to monitor the effects of increasing oxygen flow to the cathode sides of the MEA. The fan was wired into the load box in parallel, but no current was being applied by the load box. The system was allowed to reach OCV conditions before the fan's duty was switched on. The fan had two different settings, a high and a low setting. Both were tried, and then the

high setting was left to run for a continuous amount of time to judge how long the amount of fuel would last. 30g of methanol gel was used as the control fuel amount. Figure 19 shows the setup as it is reaching OCV conditions.

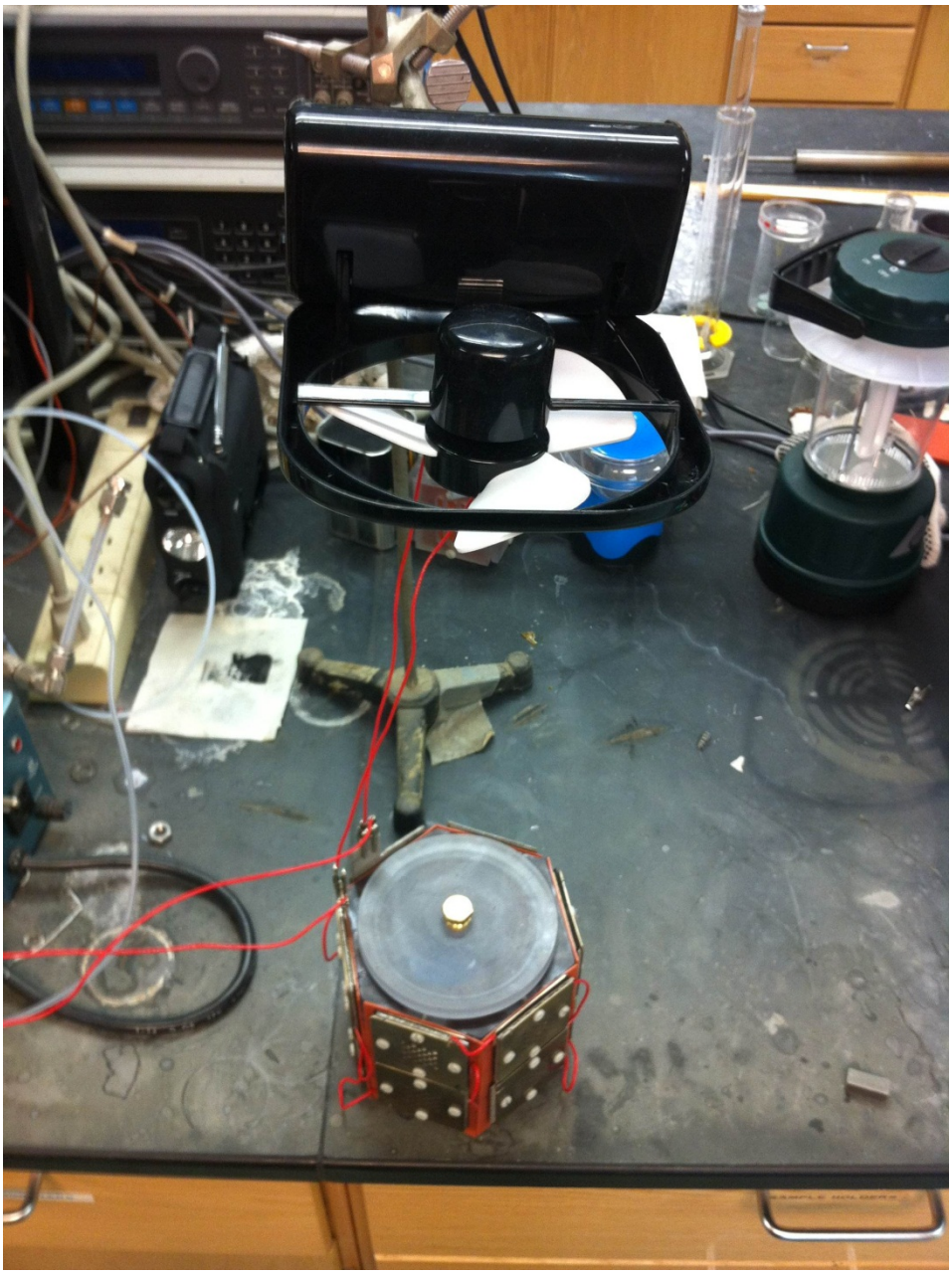

Figure 19: Fan Powered by the Fuel Cell Stack as an Ancillary Utility

3.2.5 Membrane Activation

3.2.5.1 Initial MEA Activation

MEAs must be activated to promote enough hydration to optimize performance. It is necessary to activate the anode catalyst because of the slow reaction kinetics of the methanol oxidation reaction at the anode. The activation of the MEA consisted of a pulse treatment over several hours. At first a steady feed of oxygen at 70 mL/min was put in the cathode and a 1 mL/min of .5 Molar methanol solutions was put in the anode. Every 30 min the voltage was pulsed by .05 volts ranging from the open current voltage (OCV) of the MEA at the time, usually around .75 V, to 1.5 V. Once this procedure was complete, the set up would run for another 4 hours without any changes in the voltage or feed. It is important to note that the cell and the methanol feed were both heated to 60℃.

3.2.5.2 Full Stack Activation

Whole stack activation is also possible in the case that time is short, or activating large quantities of MEAs at one time is not a feasible procedure. To activate a whole stack of cells at once, a 50mL beaker of pure methanol was placed in the stack and left to diffuse for an extended period of time, generally about five days. The Fuel Cell program was also set to limit the max voltage on the cell to 2.5V. This was done by adjusting the current load to maintain constant voltage. By pulling a current, this makes sure that the cells were constantly under a load. The pure methanol vapors allowed a stronger, more long lasting fuel source than the gel, ensuring top performance for the activation period. This methodology can also be used to reactivate cells that haven't been run in a period of time. This is to rehydrate the cells, and to allow for proton conduction.

3.2.6 Troubleshooting

When testing the fuel cell stack, problems occasionally arose that limited performance of the fuel cell. Because passive fuel cells operate simply based on existing conditions, have no active

controllers and have no fuel regulators, troubleshooting and detection of problems becomes a much different issue than with active fuel cells. The main considerations when building the stack and putting it together is to prevent leakage of oxygen as well as methanol crossover as much as possible. One way that methanol can crossover and cause cathode overpotential is to leak out of the cell and react on the cathode side of the MEA. Ways of sealing the cell and preventing leakage of oxygen or methanol are by using the vacuum grease on the silicon, which provides an airtight and watertight seal, using gasket foam in between the MEA and the current collector to prevent leakage through the Nafion®, and using solid stainless current collectors, especially on the anode side, to prevent diffusion through the edges.

Another cause of poor performance could be high resistance in the individual cells. Since the fuel cell stack contains cells connected in series, all of the parts must be functioning well for maximum performance. Some of the causes of electrical resistance are in the individual MEA units, due to conductivity between the current collectors over the Nafion® membrane. The resistance can be caused by the layers of the MEA not being screwed together tight enough. The tighter the unit can be fastened, the lower the interfacial resistance in the cell, which will increase performance proportionally.

Another factor of electrical resistance in the cell is the use of alligator clips for dynamic connections to the fuel cell. Since connections from the fuel cell to the test station need to be removable, alligator clips are used. They allow for easy connections, but create resistance at the point of interface. Figure 20 shows how the electrical conductivity is focused on the teeth of the clip. Alternate connection methods could decrease electrical resistance throughout the stack. Since soldering the fuel cell directly to the test station is not possible, the alligator clips were the best use of the present materials.

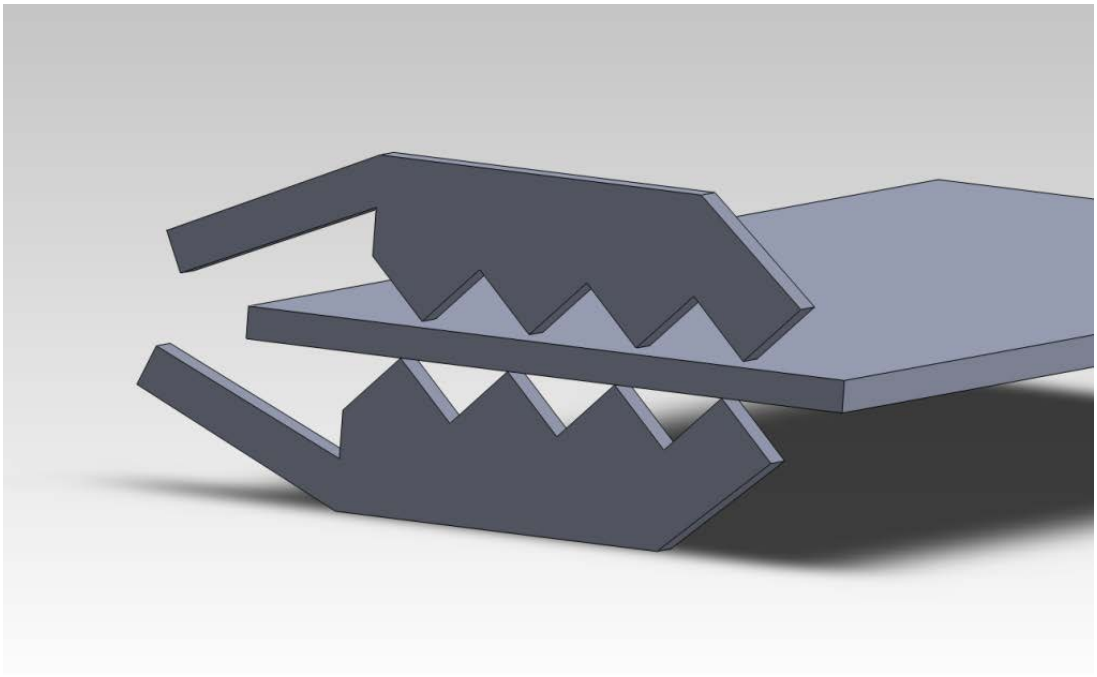

Figure 20: Understanding Alligator Clip Resistance

CHAPTER 4: MODELING AND THEORY

4.1 Background

In the absence of proper fuel cell testing equipment, alternatives to investigating the performance of a fuel cell operating at specified conditions are available using mathematical models. These models use implicit equations, predetermined parameters, and input conditions to predict the OCV, voltage at specified current, i.e. polarization and power output. Since it is a quick, but relatively accurate method of calculating performance, initiative and effort can be saved by combining experiments with the theoretical modeling. Using the mathematical model for DMFC by combining as described by Rosenthal et al [10], an adaptation for passive DMFC could be developed. The work done by Rosenthal is for a DMFC operating with active fuel transports. By adjusting the mass transfer sections, as well as fuel concentrations the proposed model is applied to PDMFC, as discussed below.

4.2 Modeling:

4.2.1 Overall Equations

The mathematical model takes into consideration key functions of the transport parameters and thermodynamic behavior of a direct methanol fuel cell assembly, as well as the kinetics of the methanol oxidation and oxygen reduction reactions. The overall equation, Equation 1, being used to describe the cell voltage is a summary of all the key overpotentials being subtracted by the thermodynamic potential.

$$V = V_0 - \eta_A + \eta_C - \eta_B - \eta_I \tag{1}$$

As tabulated in the parameter list, V is the voltage; V_0 is the thermodynamically calculated max voltage, while η_A η_B η_C and η_I are the overpotentials calculated in the Anode, PEM, Cathode, and Interface, respectively. The interfacial resistance has been assumed to be zero, and as such is not included in the model, although for PDMFC this may not be true dependent on fabrication and torque. It is included to show its relative importance to the overall performance. The thermodynamic maximum voltage is given as Equation 2:

$$V_0 = 1.214 - 1.4\times10^{-4}(T-298) + \frac{RT}{6F}\ln\left\{\frac{a_{\mathrm{Me}}}{a_{\mathrm{H_2O}}}\left(\frac{p_{\mathrm{O_2}}^{3/2}}{p_{\mathrm{CO_2}}}\right)\right\} \quad (2)$$

The overpotentials are derived by Rosenthal et al [10] below, and are summarized. Equation 3 is the overpotential at the anode, and Equation 4 is the overpotential at the cathode. They are dependent on certain limiting current densities, as well as the crossover current densities The anode overpotential is affected by both methanol and oxygen crossover. The cathode polarization is simplified under the assumption that the effect of oxygen crossover is negligible. These are further described below.

$$\eta_A = \frac{RT}{\alpha_A^{\bullet}\nu_{A,\mathrm{e}^-}^{\bullet}F}\sinh^{-1}\left[\frac{1}{2}\left\{\frac{(i+i_{X,\mathrm{O_2}})/i_{A,0}}{1-(i+i_{X,\mathrm{O_2}})/i_{A,L}}\right\}\left\{1+\frac{1}{i_{A,L}}\left(i_{X,\mathrm{Me},L}+3\left(\frac{\kappa_{\mathrm{Me},B}}{\kappa_{\mathrm{W},B}}\right)x_{\mathrm{Me},b}\xi i\right)\right\}\right] \quad (3)$$

$$\eta_C = \frac{RT}{\alpha_C^{\bullet}\nu_{C,\mathrm{e}^-}^{\bullet}F}\sinh^{-1}\left\{\frac{1}{2}\left(\frac{(i+i_{X,\mathrm{Me}})/i_{C,0}}{1-(i+i_{X,\mathrm{Me}})/i_{C,L}}\right)\right\} \quad (4)$$

$$\eta_B = \left(\frac{L_B}{\sigma_B}\right)i \quad (5)$$

$$\eta_I = iR_i \quad (6)$$

4.2.2 Catalyst Loadings:

To begin the modeling, an in depth look at the catalyst loading is necessary. Since the catalyst on the anode contains a mixture of both Platinum and Ruthenium, the density is given from the mass fraction of Ruthenium, ω_{Ru}, and the densities for both metals, Equation 7. The values are given by the parameter table.

$$\rho_{M,A} = (1-\omega_{\mathrm{Ru}})\rho_{\mathrm{Pt}} + \omega_{\mathrm{Ru}}\rho_{\mathrm{Ru}} \tag{7}$$

The electrocatalyst surface roughness is estimated from Equation 8, which describes the amount of catalyst surface area on either side of the MEA catalysts.

$$\gamma_M = \varphi_I m_M \frac{6}{\rho_M d_M} \tag{8}$$

Since carbon monoxide is formed at the catalyst sites, knowing the roughness allows the calculation for CO suffocation, θ_{COS}, which is the fraction of catalyst sites covered in CO. This is shown in Equation 9.

$$\theta_{\mathrm{CO\bullet S}} = \frac{K_{\mathrm{Me}} c_{\mathrm{Me},0}}{1 + K_{\mathrm{Me}} c_{\mathrm{Me},0}} \tag{9}$$

The adsorption equilibrium constant for CO on Platinum is given by Equation 10.

$$K_{\mathrm{Me}} = 1.41\times10^{-8} \exp\left(\frac{130{,}000\ \mathrm{J\ mol^{-1}}}{RT}\right) \tag{10}$$

4.2.3 Transport Parameters

To better understand the concentration profile of methanol and oxygen at various locations throughout the cell, the transport parameters were derived from basic definitions. Some of the diffusion coefficient equations are listed below. The diffusivity of methanol in water is described as Equation 11, which is a major consideration for the interactions of the cell.

$$D_{\mathrm{Me},W} = 2.1\times10^{-5} \exp\left\{-\frac{20{,}460}{R}\left(\frac{1}{T} - \frac{1}{313}\right)\right\} \tag{11}$$

The equation for the effective diffusion coefficient of oxygen in the cathode GDL is shown by Equation 12. Since oxygen has low solubility properties in water, it is mainly considered in the gas phase.

$$D^{e}_{\mathrm{O}_2,E} = \varepsilon_E^{1.5}(1-q_{\mathrm{W}})^{1.5} D_{\mathrm{O}_2,E} \tag{12}$$

Similarly to the oxygen diffusion in the cathode GDL, the diffusion coefficient for methanol in the anode GDL is given in Equation 13. The main difference, however, is the bubbles of CO_2 produced are taken into consideration, as shown by q_{CO_2}, which is the volume fraction of bubbles, and the liquid gas partition coefficient, κ_{MeCO_2}.

$$D^{e}_{\mathrm{Me},D} = \varepsilon_D^{1.5}\left\{(1-q_{\mathrm{CO}_2})^{1.5} D_{\mathrm{Me},W} + (q_{\mathrm{CO}_2})^{1.5} \kappa_{\mathrm{Me,CO}_2} D_{\mathrm{Me,CO}_2}\right\} \tag{13}$$

Since there is not much available information on how this varies as the current and temperature are varied, a simplified fitted equation is used in this model. This allows a more convenient calculation to be done, without complex equations.

$$D^{e}_{\mathrm{Me},D} = 9.75\times10^{-1}\exp\left(-\frac{30{,}975}{RT}\right) \tag{14}$$

The diffusion coefficient of methanol in the PEM can be calculated from Equation 15.

$$D^{e}_{\mathrm{Me},B} = \varepsilon_B^{1.5} D_{\mathrm{Me,W}} \tag{15}$$

The main difference between a passive and an active fuel as far as the model is concerned is the transport rate at which the fuel in the anode chamber reaches the anode. Since the active fuel cell has pumps to continuously move the methanol solution to the anode, one can expect the mass transfer for the active cell to be much higher. Both estimations for the mass transfer coefficient are given below, in Equations 16 and 17, for the active and passive cells, respectively. D_i is the diffusion medium and d is the diffusion length from the fuel to the active area of the MEA.

$$k_i = 2.696 \frac{D_i}{d}\left(1 + 0.139 \frac{d^2/\tau_i}{D_i}\right)^{0.81} \tag{16}$$

$$k_i = 2.696(D_i / d) \tag{17}$$

Equation 17 provides and estimation for the mass transfer coefficient for the vapor feed at passive conditions.

4.2.4 Resistance Associated with the PEM

Since the overall resistance over the PEM is proportional to its thickness and conductivity, equations are provided to help calculate them. The overall simplified equation for the conductivity is given by Equation 18.

$$\sigma_B = (\varepsilon_B - \varepsilon_{B,0})^{1.5}\left(\frac{349.8}{1+\delta}\right)\exp\left\{-\frac{E_\mu}{R}\left(\frac{1}{T} - \frac{1}{298}\right)\right\}\left(\frac{1}{18\lambda}\right)\beta \tag{18}$$

Equation 19 and 20 are the degree of acid dissociation sites and acid dissociation equilibrium constant, respectively.

$$\beta = \frac{(\lambda+1) - \sqrt{(\lambda+1)^2 - 4\lambda(1-1/K_a)}}{2(1-1/K_a)} \tag{19}$$

$$K_a = \exp\left[\frac{-52,300}{R}\left(\frac{1}{T} - \frac{1}{298}\right)\right] \tag{20}$$

4.2.5 Characteristic Current Densities

To calculate the overpotentials, an expression of the crossover current with respect to actual current measured and temperature is required. To accurately calculate electrode overpotentials and the crossover currents, the exchange current, as shown with a subscript *0*, and the limiting current, subscript *L*, are taken into consideration. The crossover current of methanol is given by Equation 24. It is related to the limiting current density, which is the largest possible crossover current density (at OCV). This is shown by Equation 23. The GDL limiting equations for cathode and anode are given by Equation 21 and 22, respectively. Equation 25 goes on to further describe the crossover current of oxygen similarly. Equation 26 and 27 provide the exchange current density of the cathode and anode, respectively.

$$i_{C,L} \equiv 4FP^e_{\mathrm{O_2},E} c_{\mathrm{O_2},b} \tag{21}$$

$$i_{A,L} \equiv \left(\frac{\nu_{A,\mathrm{e^-}}}{-\nu_{A,\mathrm{Me}}}\right) FP^e_{\mathrm{Me},D} c_{\mathrm{Me},b} \tag{22}$$

$$i_{X,\mathrm{Me},L} \equiv \left\{\frac{D^e_{\mathrm{Me},B}}{L_B}\left(\frac{\nu_{A,\mathrm{e^-}}}{-\nu_{A,\mathrm{Me}}}\right)F\right\} \kappa_{\mathrm{Me},B} c_{\mathrm{Me},b} \tag{23}$$

$$i_{X,\mathrm{Me}} = \frac{\left\{ i_{X,\mathrm{Me},L} + 3\left(\frac{\kappa_{\mathrm{Me},B}}{\kappa_{\mathrm{W},B}}\right) x_{\mathrm{Me},b}\xi(i) \right\}\left(1 - \frac{i}{i_{A,L}}\right)}{\left[1 + \frac{1}{i_{A,L}}\left\{ i_{X,\mathrm{Me},L} + 3\left(\frac{\kappa_{\mathrm{Me},B}}{\kappa_{\mathrm{W},B}}\right) x_{\mathrm{Me},b}\xi(i) \right\}\right]} \tag{24}$$

$$i_{X,\mathrm{O}_2} = \left\{ P_{\mathrm{O}_2,D} + \left(\frac{1}{P^e_{\mathrm{O}_2,E}} + \frac{1}{P_{\mathrm{O}_2,B}} \right)^{-1} \right\} 4Fc_{\mathrm{O}_2,b} \approx (P_{\mathrm{O}_2,D} + P_{\mathrm{O}_2,B}) 4Fc_{\mathrm{O}_2,b} \tag{25}$$

$$i_{C,0} = \gamma_{M,C}\left(\frac{c_{\mathrm{O}_2,0}}{c_{\mathrm{O}_2,ref}}\right) \exp\left[-\frac{E_{C,\Phi_0}}{R}\left(\frac{1}{T} - \frac{1}{T_{ref}}\right)\right] i^*_{C,0,ref} \tag{26}$$

$$i_{A,0} = \gamma_{M,A}\frac{c_{\mathrm{Me},0}}{c_{\mathrm{Me},ref}}\left(\frac{1-\theta_{\mathrm{CO\bullet S}}}{1-\theta_{\mathrm{CO\bullet S},ref}}\right) \exp\left[-\frac{E_{A,\Phi_0}}{R}\left(\frac{1}{T} - \frac{1}{T_{ref}}\right)\right] i^*_{A,0,ref} \tag{27}$$

4.2.6 Final Polarization Equations

As provided by Rosenthal et al [10], the final model equations are as follows. The OCV equation, Equation 28, assumes a current of 0 and is derived from the overall voltage equation. The basic voltage equation from Equation 1, expanded by the addition of Equation 2, 3, 4, 5 and 6 results in the final polarization model, Equation 29. This allows the voltage versus current density to be calculated for the DMFC at various parameters. Once the voltage has been calculated, a simple multiplication by the current density provides the relation to the power, as shown by Equation 30. This is useful also for verifying the performance of the DMFC. From these two equations and experimental data for conventional active DMFCs given by Chiu et al [17] plots were made to prove the accuracy of the model by Rosenthal et al [10].

$$OCV = V_0 - \frac{RT}{\alpha_A^{\bullet} \nu_{A,e^-}^{\bullet} F} \sinh^{-1}\left\{\frac{1}{2}\left(\frac{i_{X,O_2}/i_{A,0}}{1-i_{X,O_2}/i_{A,L}}\right)\left(1+\frac{i_{X,Me,L}}{i_{A,L}}\right)\right\} + \frac{RT}{\alpha_C^{\bullet} \nu_{C,e^-}^{\bullet} F} \sinh^{-1}\left\{\frac{1}{2}\left(\frac{i_{X,Me,0}/i_{C,0}}{1-i_{X,Me,0}/i_{C,L}}\right)\right\} \quad (28)$$

$$V = V_0 - \frac{RT}{\alpha_A^{\bullet} \nu_{A,e^-}^{\bullet} F} \sinh^{-1}\left[\frac{1}{2}\left\{\frac{(i+i_{X,O_2})/i_{A,0}}{1-(i+i_{X,O_2})/i_{A,L}}\right\}\left\{1+\frac{1}{i_{A,L}}\left(i_{X,Me,L}+3\left(\frac{\kappa_{Me,B}}{\kappa_{W,B}}\right)x_{Me,b}\xi i\right)\right\}\right] + \frac{RT}{\alpha_C^{\bullet} \nu_{C,e^-}^{\bullet} F} \sinh^{-1}\left\{\frac{1}{2}\left(\frac{(i+i_{X,Me})/i_{C,0}}{1-(i+i_{X,Me})/i_{C,L}}\right)\right\} - \frac{iL_B}{\sigma_B} - i(R_I) \quad (29)$$

$$P = iV_0 - \frac{iRT}{\alpha_A^{\bullet} \nu_{A,e^-}^{\bullet} F} \sinh^{-1}\left[\frac{1}{2}\left\{\frac{(i+i_{X,O_2})/i_{A,0}}{1-(i+i_{X,O_2})/i_{A,L}}\right\}\left\{1+\frac{1}{i_{A,L}}\left(i_{X,Me,L}+3\left(\frac{\kappa_{Me,B}}{\kappa_{W,B}}\right)x_{Me,b}\xi i\right)\right\}\right] + \frac{iRT}{\alpha_C^{\bullet} \nu_{C,e^-}^{\bullet} F} \sinh^{-1}\left\{\frac{1}{2}\left(\frac{(i+i_{X,Me})/i_{C,0}}{1-(i+i_{X,Me})/i_{C,L}}\right)\right\} - \frac{i^2 L_B}{\sigma_B} - i^2(R_I) \quad (30)$$

CHAPTER 5: RESULTS AND DISCUSSION

5.1 Single Cell Tests

5.1.1 EXPERIMENT 1: Liquid Methanol Solution Tests

The methanol solution tests with varying concentration were run on a single cell to determine the best operating concentration of the cell. It is seen by Figure 21 that the cell operated better as the molarity of the methanol solution increased. It was apparent that the more fuel there was, the better the cell would operate.

However, there is a point where too much methanol did saturate the cell and methanol crossover started to affect performance in the single cell. From the results it was concluded that the performance of the 3M was better at higher current densities. Accordingly, the OCV at lower concentrations was higher. Thus, results are consistent with those in active DMFC.

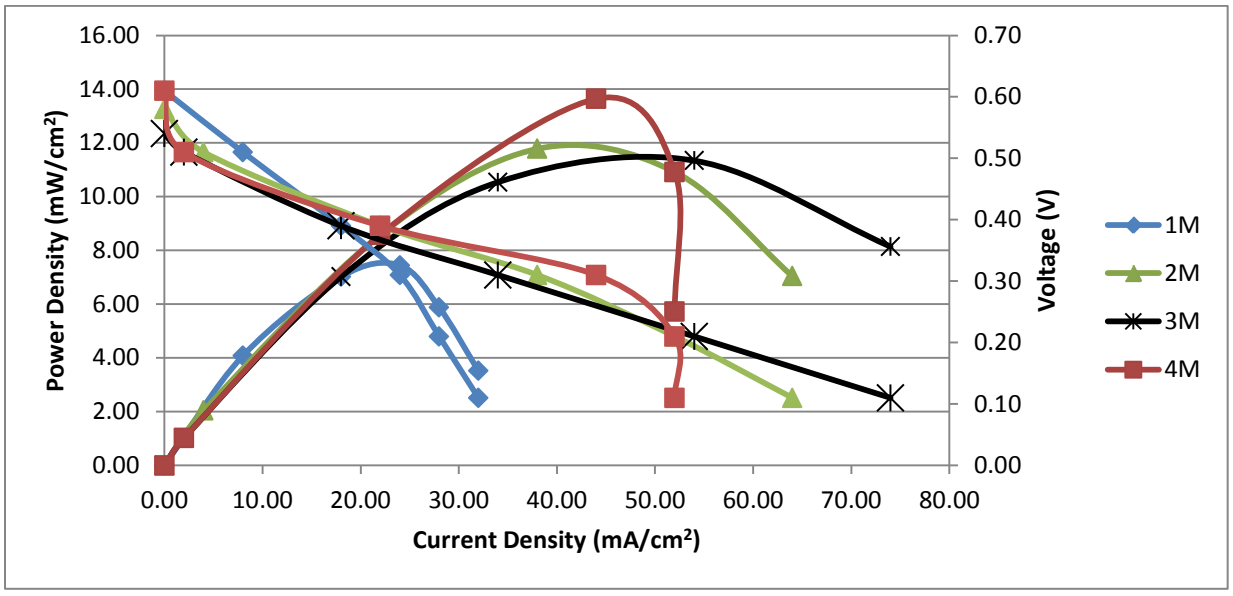

Figure 21: Liquid MeOH Solution with Diff. Concentrations (Single Cell PDMFC, IRD MEA)

5.1.2 EXPERIMENT 2: Current Collector Optimization

5.1.2.1 Cathode Current Collector Testing:

Keeping the perforated control collector on the anode side, the cathode collector was varied between the four different units. The performance is shown in Figure 22.

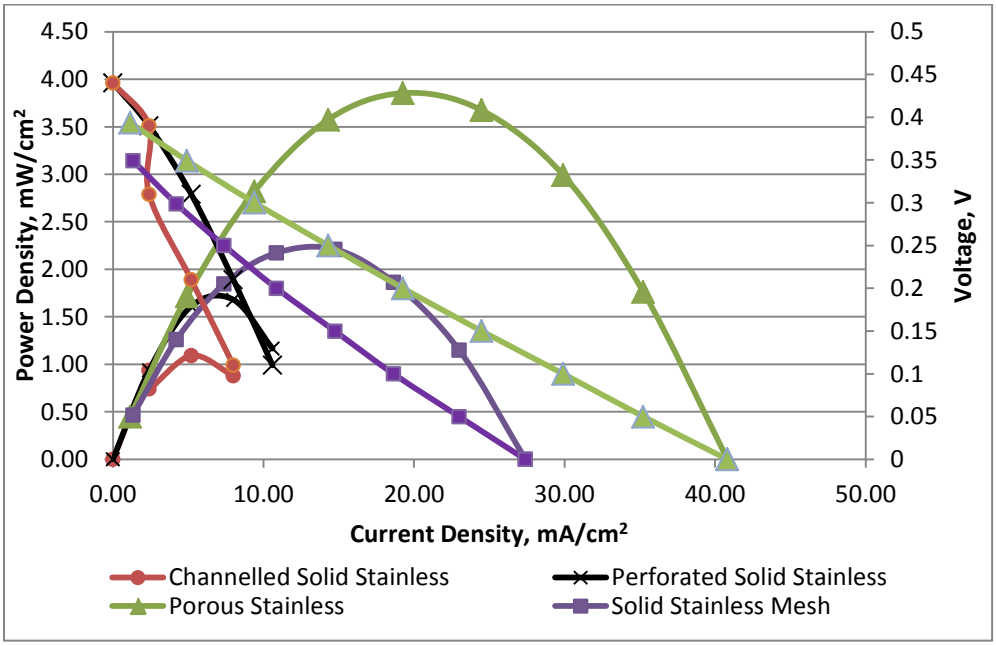

Figure 22: Effects of Cathode C.C. on Performance (Single Cell PDMFC, MeOH Gel)

Looking at the polarity plots for the cathode current collector as a variable, there are two areas of focus that should be noted. At open circuit potential, i.e. with a current of 0A, the highest values were for the channeled and perforated control current collectors. Even though they had the highest OCV, as soon as a small load was put on the cell, the voltage dropped at a much faster rate than the other two collectors. The best performance was seen with the porous current collector, with the perforated current collectors on the anode inside. The power density was much higher, as well as the voltage was higher at higher current density. From these results, it appears that the best current collector for the cathode is the porous stainless steel one.

5.1.2.2 Anode Current Collector Testing:

Keeping the perforated control collector on the cathode side, the anode collector was varied the same way as the previous tests. The performance plots are shown in Figure 23.

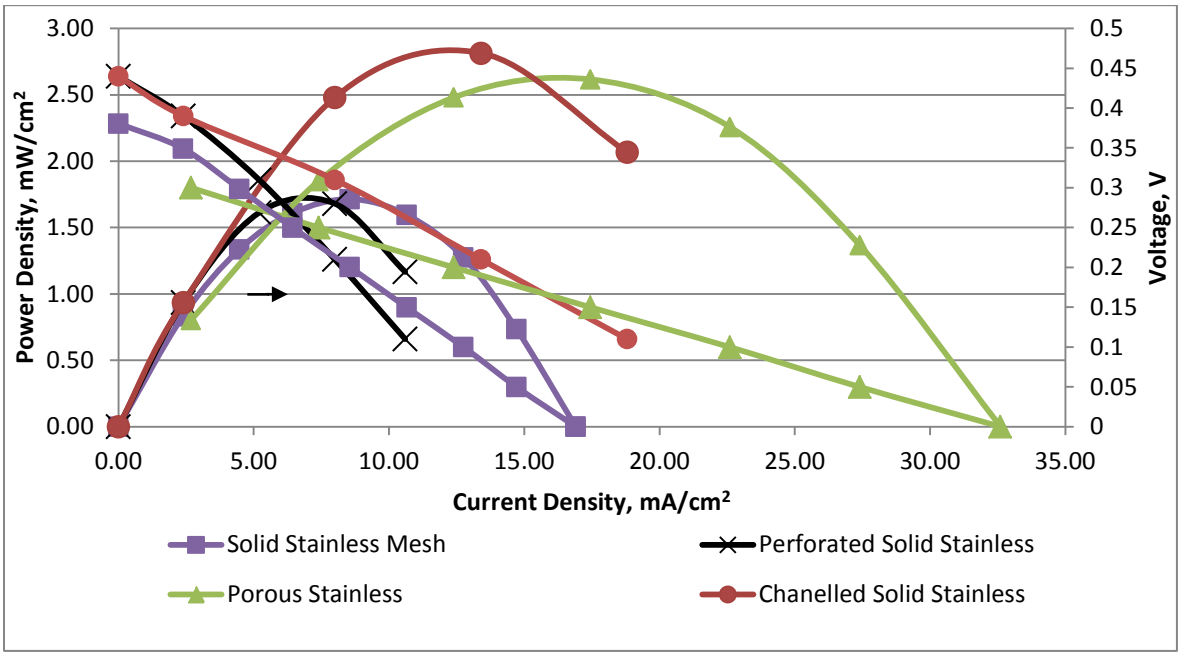

Figure 23: Effects of Anode C.C. on Performance (Single Cell PDMFC. MeOH Gel)

Keeping the cathode current collector constant and varying the anode, performance curves were compared. The channeled and perforated collectors had the highest OCV. Further, on the anode the channeled collector gave better performance than on the cathode. In fact, the channeled collector gave the highest power density output, peaking around 2.75mW at 12.5mA/cm^2, but this was at lower current densities. At higher current densities, however, the porous collector was able to outperform it, peaking around 2.55mW at 17.5mA/cm^2. This could be due to the amount of crossover occurring with different current collectors. Since the channeled collector allows the fuel easier access to the anode catalyst due to more open area, it also allows more methanol crossover to occur relative in lower performance at high concentrations. The porous collector slows crossover more so than the channeled, but it also slows fuel from reaching the active area

which limits the overall performance. Further, use of a porous current collector as an anode allows diffusion of O_2 from ambience into the anode chamber through its edges.

5.1.2.3 Conclusions and Recommendations for Current Collectors:

After testing various configurations, the results shows that having a porous stainless steel current collector on both bipolar locations will give the best overall performance. Although the porous cathode and channeled anode individually gave a higher overall power curve, the porous-porous combination was able to give much higher current densities. As such, both results are shown together for comparison in Figure 24, which provides the performance of the control design versus the optimized current collector design being proposed. It is evident that the control has a higher OCV, but it drops below the performance of the optimized cell at higher current densities. The two layouts give similar performance up until 5mA/cm^2, but for current densities higher than that, the optimized layout of porous anode and porous cathode exceeds the both the performance of the control as well as the porous anode and channeled cathode plate combination. These conclusions are for the single cell, however, and results described from the stack will show that this “optimized” layout is not the best for larger scale. When these results were scaled to the stack, lower performance was obtained. This is discussed in the Final Stack Tests section later in the chapter.

Since porous stainless steel is more expensive than the solid stainless steel, it can be considered to not be worth the cost for a small increase in performance. The material itself is also not as rigid and can be brittle if not handled properly. These porous plates are prone to bending and warping. This does not provide even pressure on the MEA, which increases internal cell contact resistance. The porous stainless material can give better performance if handled correctly, but if proper care is not taken, the performance drops significantly. Due to this, solid stainless plates were used on the stack.

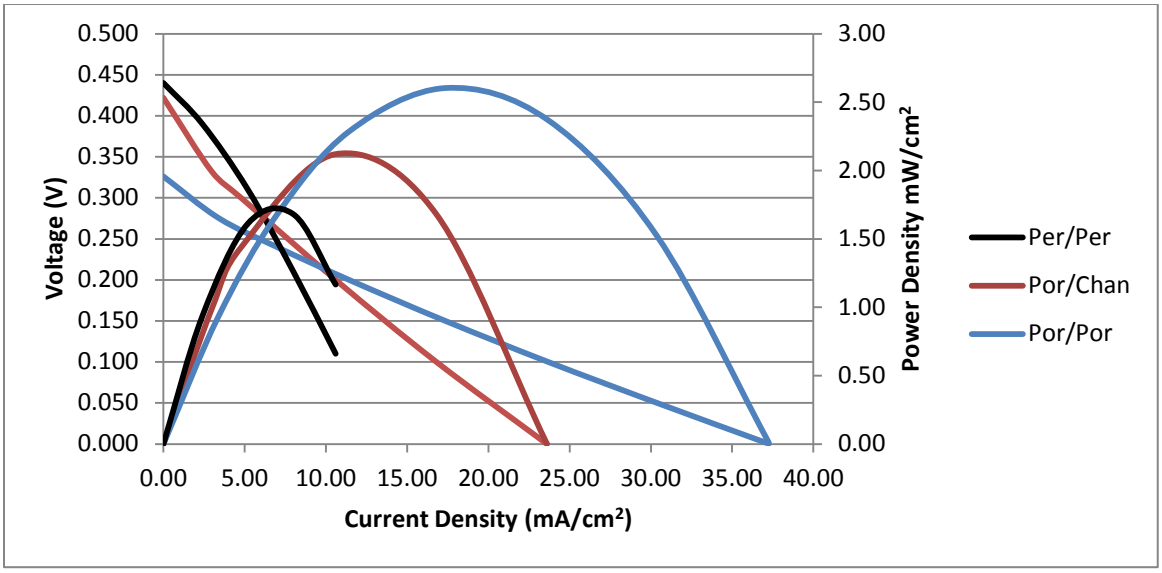

Figure 24: Optimized Current Collector Layout Results (Single Cell, IRD MEA, MeOH Gel)

5.1.3 EXPERIMENT 3: Temperature Variation Tests

An interesting experiment on the single cell unit was a series of temperature tests to see how temperature affected the performance of the cell. There were two main tests run: one was at 30°C and the other was at 50°C. The results in Figure 25 show that the temperature test run at 30 degrees Celsius was significantly better for the MeOH Gel.

The expected results were just the reverse. It was expected to see better diffusion and reaction kinetics with higher temperatures. However, there was some issue with the gel when it reached higher temperatures. The gel would disintegrate and have no effect on the fuel cell output. Therefore the best temperatures with MeOH gel appeared to be at or around room temperature. It is possible that other issues were involved as well, such as the drying out of the Nafion® membranes.

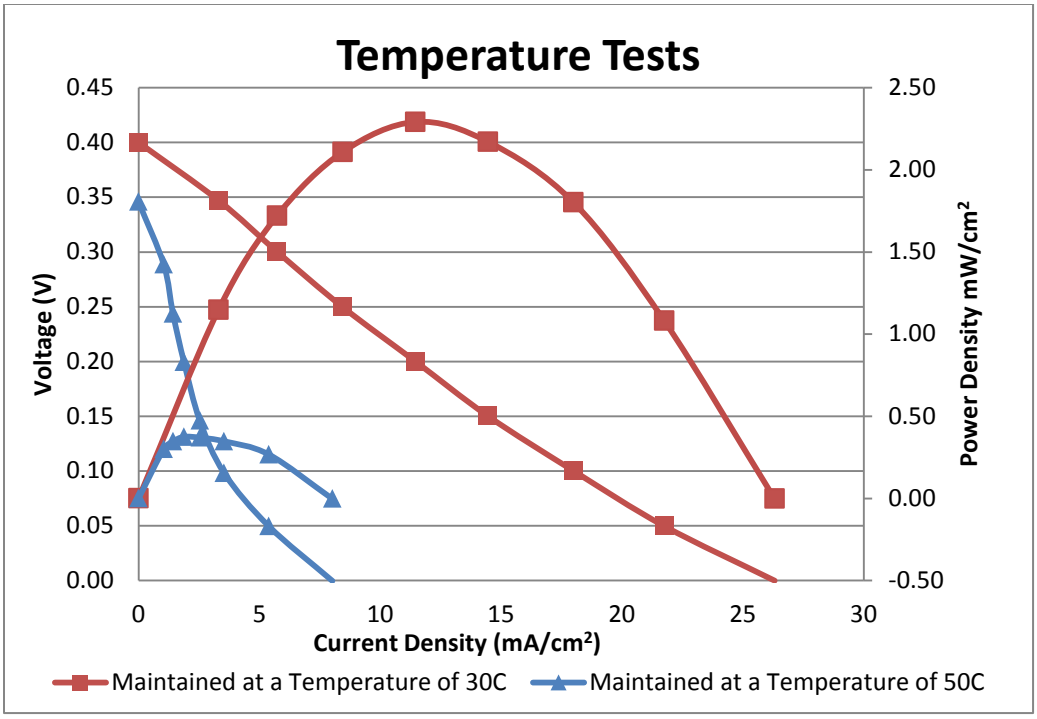

Figure 25: Temperature Test Results (Single Cell, IRD MEA, MeOH Gel)

5.2 Stack Tests

5.2.1 EXPERIMENT 4: Control Stack Tests

The control stack used to compare with all other tests is the DMFC stack with perforated plates for both anode and cathode using MeOH gel as a fuel. This was used to compare other tests ran on the DMFC stack. From Figure 26, it is possible to see that the OCV of the control stack is right below 5V. The maximum power output for this stack was around 16 Mw with a current density of 9 mA/cm^2.

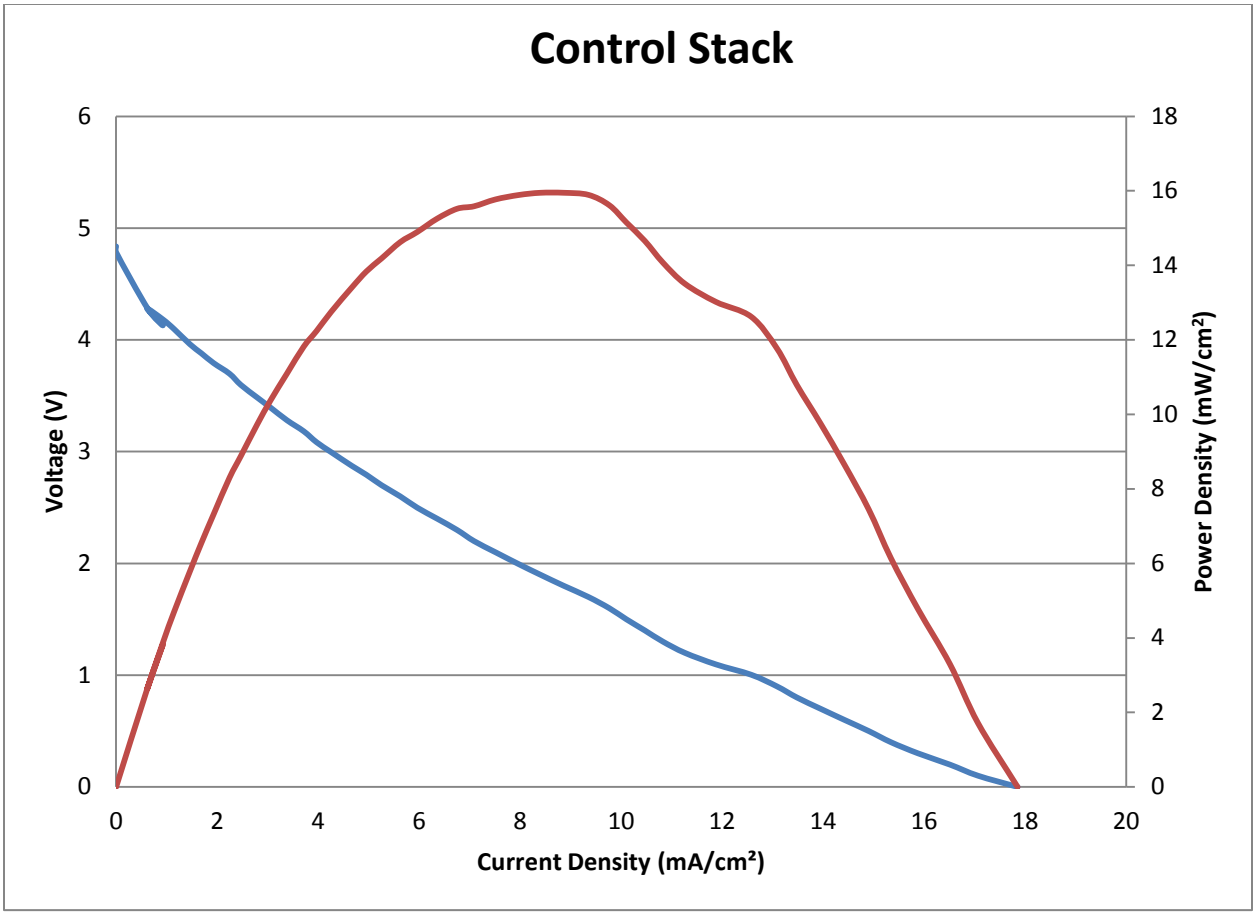

Figure 26: Control Stack (Per, Per with GDL on both sides, MeOH Gel)

5.2.2 EXPERIMENT 5: Initial Transient Conditions and Steady State Tests

In this study, the OCV was monitored as a function of time right after the fuel was placed inside the unit. These tests show the tendencies of the cell before it reaches steady state. Once the test was started, a rapid increase in cell voltage was observed. This lasted for the first 200 seconds of the experiment, and then a sharp dip in voltage would occur. It is believed to be caused by CO suffocation on the anode catalyst as it accumulated on the surface. However, over time an increase in voltage would occur again, perhaps as more methanol reaches the catalyst. At this point in the experiment, the membranes would start to reach full saturation. Therefore, there is a drop as methanol crosses over to the cathode. Once this initial shift in voltages would occur, the cell reached steady state at the OCV shown right above 5V. Figure 27 demonstrates these results.

Something to note from the graph below is how every time the test was run, the cell reached OCV slower. It is safe to say that the continuous use of the cell affects performance. Tests run after a previous test had finished had higher OCV and maximum power under a load. It is believed that this happened because the MEAs deactivate with time when it is not being used.

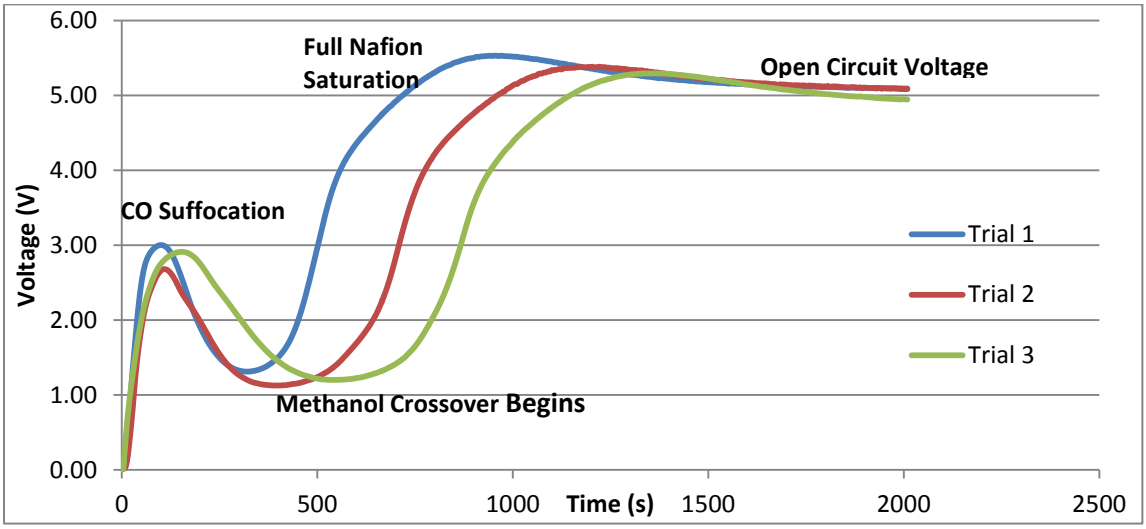

Figure 27: Initial Fuel Injection Results (Stack Setup, 25g MeOH Gel)

5.2.3 EXPERIMENT 6: Gas Diffusion Layer Absence at Cathode

Another test that was run on the stack was to compare the performance of the cell when there was a lack of a gas diffusion layer at the cathode. Thus, the GDL of the cathode side was removed for this test, represented by the purple line in Figure 28, below. There is a noticeable increase in performance with the removal of the GDL at the cathode.

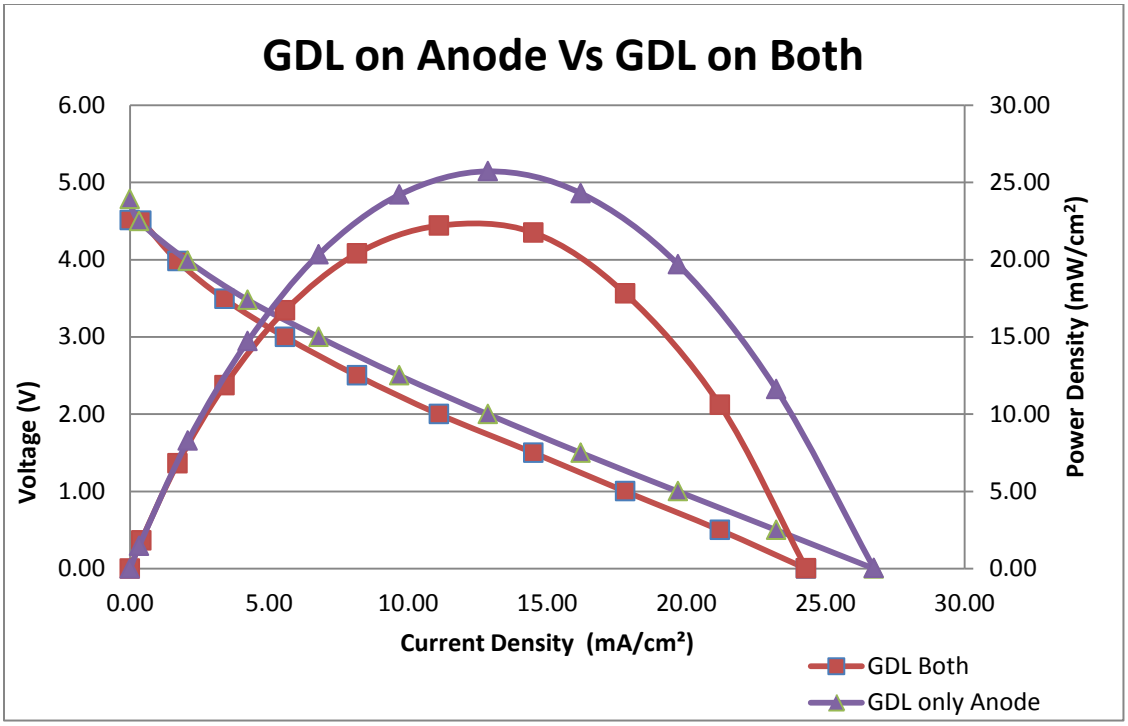

Figure 28: Gas Diffusion Layer Presence Results (Stack Layout, MeOH Gel Fuel)

These tests were run on the cell with porous current collectors on the cathode side and with perforated current collectors on the anode side. The increased performance without the GDL is believed to be because having both the porous current collector and the GDL were slowing down the diffusion of the oxygen to reach the catalyst layer. In this case it was observed that the porous current collector by itself provided better diffusion rates and better dispersion of the oxygen throughout the membrane as compared to the presence of the GDL.

5.2.4 EXPERIMENT 7: Individual Cell Performance in Stack

Another aspect tested on the stack was individual cell voltages. Because two different companies were used to supply MEAs for the stack and every MEA was in a different position with respect to the fuel, it was deemed necessary to take readings on each individual cell performance.

Figure 29 is a plot of the polarization of each individual MEA, i.e. voltage with an increasing current. The MEAs are colored by where they were purchased. Fuel Cell Store MEAs are

colored green and IRD MEAs are colored red. In regards to location of the cell, “t” is the top, and “b” is bottom. The numbers 1-6 denote which side of the hexagonal stack they are located.

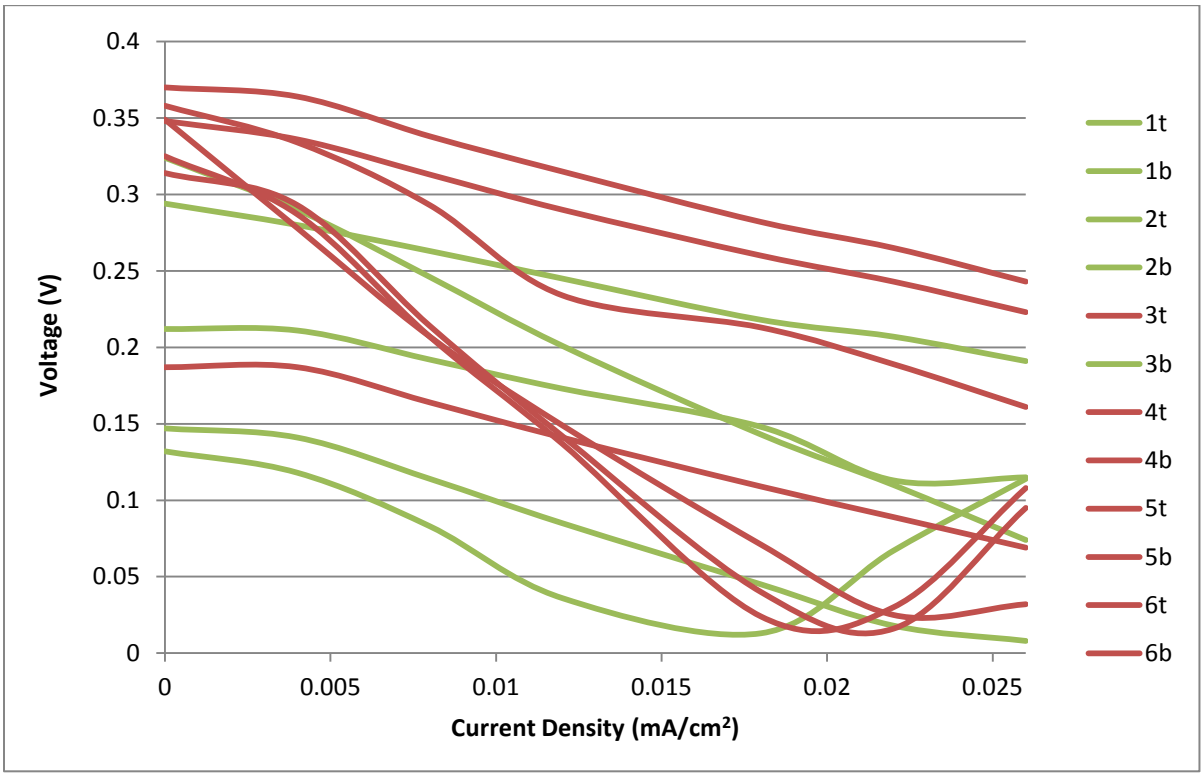

Figure 29: Individual MEA Performance by Manufacturer (Stack Layout, MeOH Gel Fuel)

Another reason that these tests were conducted is because the MEAs were obtained from two different companies. Based on these results, we have determined that there was a significant difference in individual cell performance. This is summarized in Figure 30, highlighting location in the stack rather than manufacturer. The square data points denote bottom cell location, while the triangle denotes top. There was also a noticeable difference in OCV performance for the MEAs depending on manufacturer. In Table 11, it is clear that the OCV ranged from 0.132 to 0.37 volts, with the lower values being for MEAs from The Fuel Cell Store (FCS) and the better performing MEAs from IRD. Table 11 is a color coded summary of each MEA.

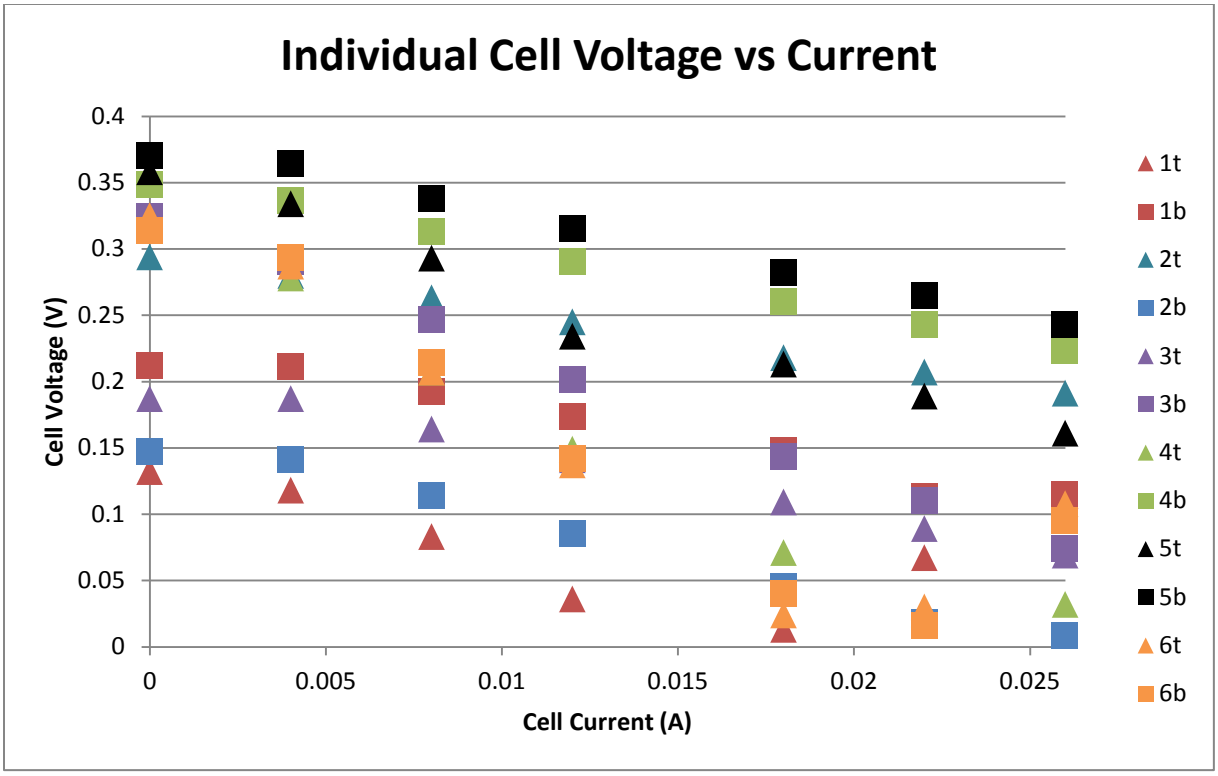

Figure 30: Individual Cell Performance by Stack Location (Stack Layout, MeOH Gel Fuel)

Table 11: Individual Cell OCV Summary

Cell Location	OCV (V)	Manufacturer
1t	0.132	FCS
1b	0.212	FCS
2t	0.294	FCS
2b	0.147	FCS
3t	0.187	FCS
3b	0.324	IRD
4t	0.349	IRD
4b	0.348	IRD
5t	0.358	IRD
5b	0.37	IRD
6t	0.325	IRD
6b	0.314	IRD

5.2.5 EXPERIMENT 8: Porous Current Collector and Reinforcement

Another test that was run on the stack was using perforated current collectors on the anode side and a porous steel plate on the cathode side, but with a reinforcement perforated plate. This was done because when using the porous current collectors alone, it was observed that the porous

steel plate had a tendency to warp due to low rigidity. Once the warping was thus reduced, the performance of the overall cell increased. Figure 31 is a plot that compares a non-reinforced cell, the control stack and the reinforced cell. Both tests were run with MeOH gel. Clearly, the reinforcement provided a significant improvement in the performance.

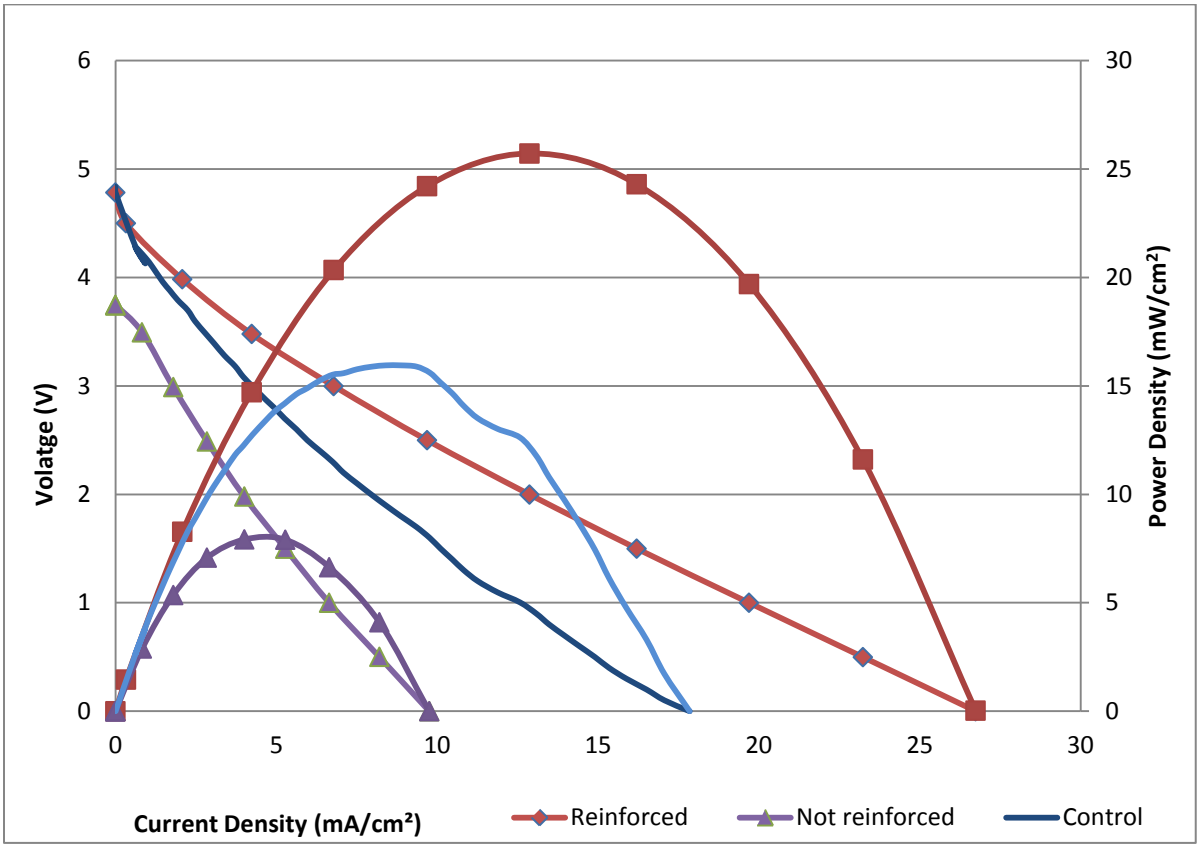

Figure 31: Reinforcement Techniques on Current Collectors (Stack Layout, MeOH Gel Fuel)

The results from these tests were along the lines of what was expected. The improvement in the observed results are largely due to lower leakage of the cell with a reinforcement since a good seal was not achievable without warping the porous current collectors or breaking a screw without it.

The tests were compared also with the control stack. The reinforced stack shows great improvement in performance. These results can be explained by how well the porous cathode

current collectors perform once warping is not an issue. It is important to note that the wiring of the cathode was still attached to the porous current collector as opposed to wiring the cathode to the reinforcement perforated current collector.

5.3 Final Stack Tests

Based on the results of the above described tests run, it is evident that the optimized design of the fuel cell stack with the materials available is a stack with no GDL on the cathode side and a porous stainless steel current collector with perforated stainless steel reinforcement. The reinforced stack also had a perforated anode current collector with a GDL. It is believed that this gives better performance because the open area on the anode side allows more methanol fuel to access the active catalyst on the MEA, increasing fuel transport. The porous current collector, while allowing oxygen to still be able to access the catalyst layer, slows overall mass transfer in and out of the cell, humidifying the membrane. The reason for not having both porous stainless steel current collectors for the cathode and anode is due to the fact that leakage of oxygen from the atmosphere into the fuel chamber due to diffusion through the edge of the porous membrane can occur. This limits performance due to oxygen reacting on the anode side of the MEA, consuming methanol while polarizing the anode. The stack was wired in series and MeOH gel was used as a fuel.

5.3.1 Activation Test and OCV

To test the optimized stack for final results, it was necessary to prepare it by activating the MEAs with pure liquid methanol in a beaker for five days. The experimental procedure followed the one described in section 3.2.5.2, full stack activation. Once this procedure was complete, tests could proceed as normal with the finalized stack for the project. The collected data from this

experiment are shown in Figure 32. The results observed with the final stack show improvement from the control experiments, as expected, despite time elapsed and subsequent deactivation. One of the aspects of the cell stack was to check how it would keep a steady voltage for an extended period of time. Thus, the first test was run with a constant voltage for five days.

Figure 32 shows how steady the voltage of the stack was, holding at 2.5V. When this test was concluded, an OCV test was conducted immediately after without exchanging fuels. This provided an OCV of 4.8 V, as shown in Figure 33, which was maintained for 1 hour. The time units are relative from Figure 32 to Figure 33.

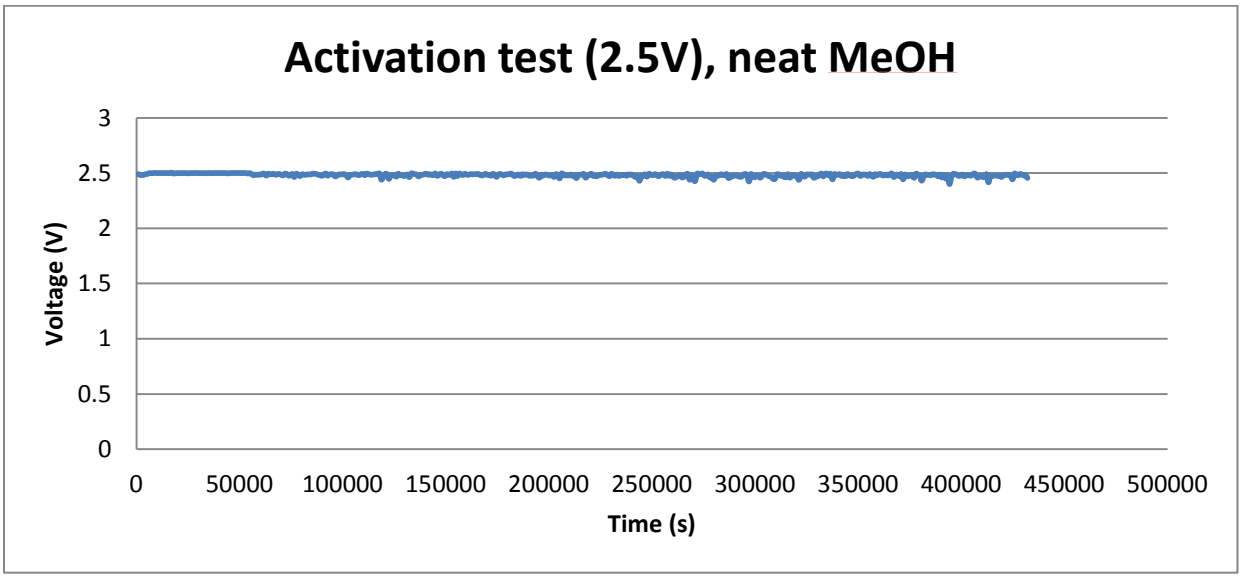

Figure 32: 5 Day Activation Test (Optimized Current Collector Stack Layout, Neat MeOH Fuel)

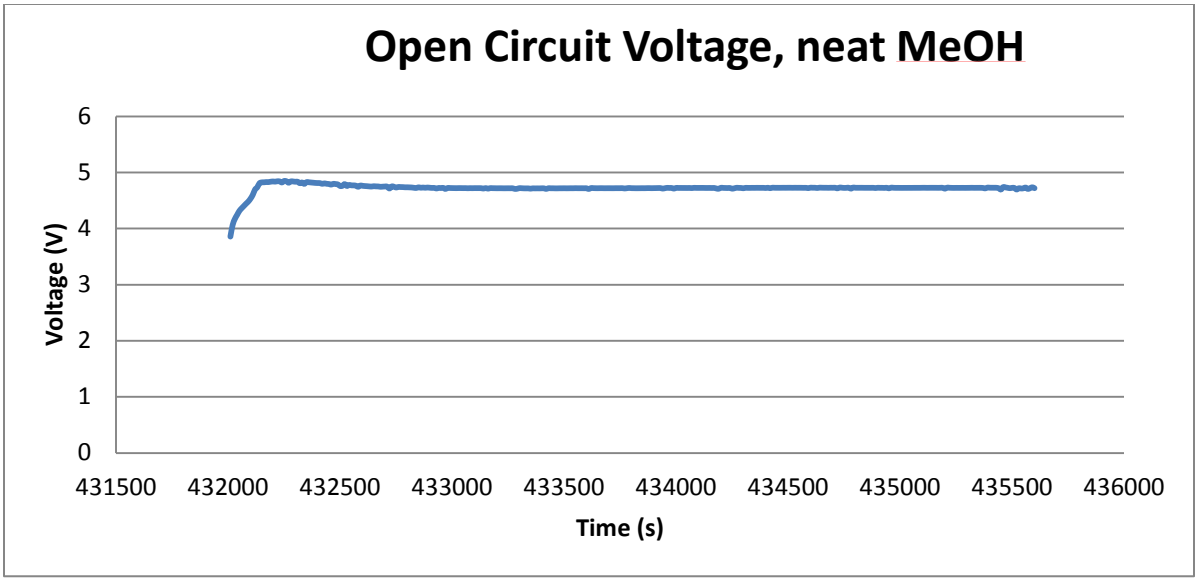

Figure 33: Open Circuit Voltage (Optimized Current Collector Stack Layout, Neat MeOH Fuel)

5.3.2 Fuel Comparison Tests

Once the OVC test and the long term stability test were computed, a performance test was undertaken. The performance with the neat methanol was lower than that of the gel. This was maybe because this work optimized the use of the cell stack when using MeOH gel. Figure 34 compares the performance of the gel versus the performance of the pure methanol. As observed the methanol gel reaches a maximum power output of 21 $mW/cm^{2,}$ however the neat methanol only reaches a maximum power output of 8 mW/cm^2.

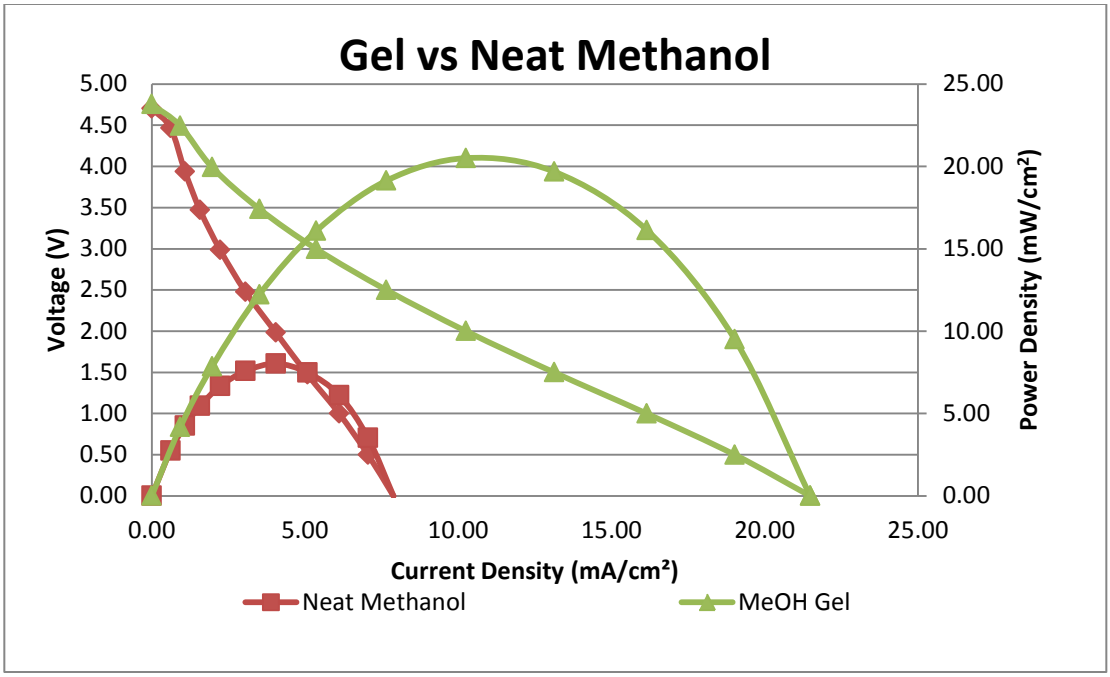

Figure 34: Gel Tests vs. Neat Methanol Tests (Optimized Stack Layout)

Even though the voltage of both tests starts out at the same OCV, the decrease in performance based on fuel was due to the different diffusion rates.

Once the stack was thus activated, different tests were conducted immediately after. These tests were used to compare the performance of the cell with different fuel assemblies. A test was conducted with a random placement of MeOH gel. The next test was conducted using the same amount of gel (30g) as the first test. However, this time the fuel was spread evenly throughout the container that it was placed in, therefore giving it a flat surface area.

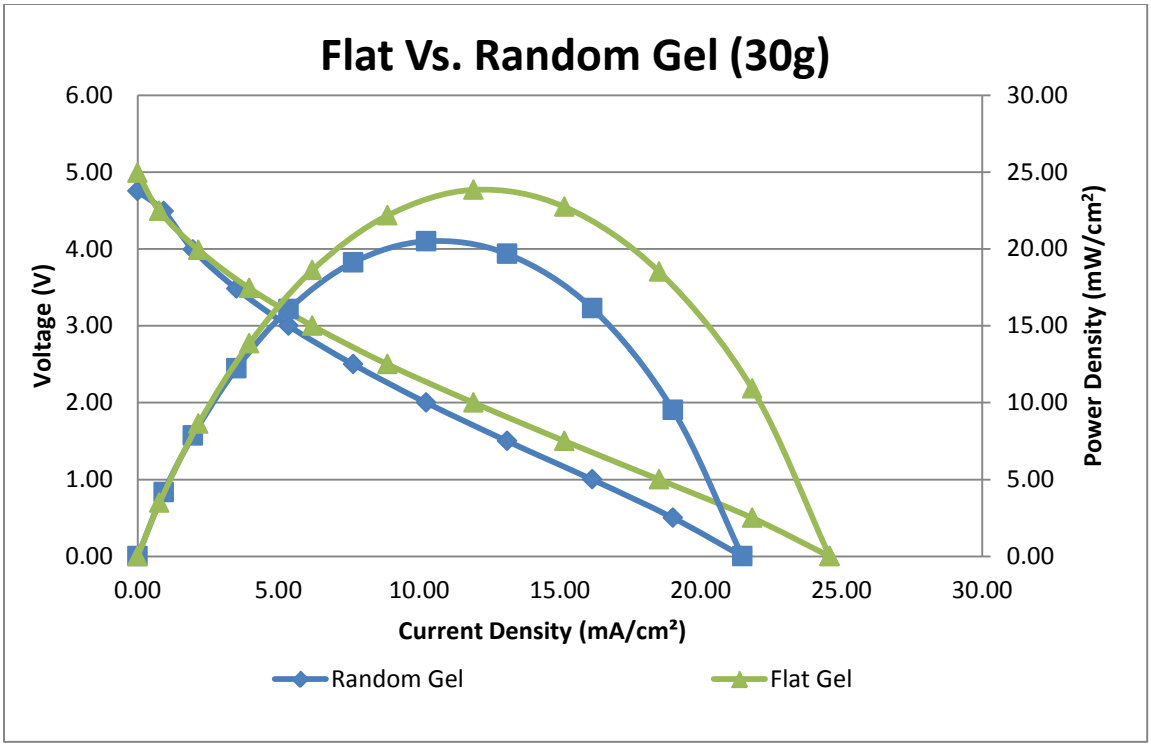

Figure 35: Flat Placed vs. Randomly Placed Gel (Optimized Stack Layout, 30g MeOH Gel Fuel)

The results shown in Figure 35 correspond with the notion that more surface area would lead to better cell stack performance due to enhanced diffusion. Using spread out gel led to more surface area that the methanol could diffuse off into the vapor space inside the anode chamber.

Apart from all the tests that were run with MeOH gel, other tests were conducted with neat methanol. When the methanol was placed directly in a beaker, the performance decreased, as shown in Figure 34. From this result, it was concluded that there needed to be a more effective delivery system for the methanol vapor.

To solve this problem, there was another experiment run with neat methanol with the same beaker used in previous tests, however this time there was a wick that was left in the methanol at one end, and a certain length was left outside the beaker. The lengths varied between 3 cm and 5

cm. The reason a wick was used was because the saturated wick released the methanol vapor into the chamber better than just letting methanol liquid sit in a beaker.

Figure 36: Neat Methanol with Adjustable Wick

The results of this experiment, shown in Figure 37, show that the wick length affects performance positively. The longer the wick that was placed outside the beaker, the better the cell would perform. The reason for this was the wick provided surface area for the methanol to vaporize better. Therefore, the more surface area that the wick provided, the more neat methanol would diffuse into the anode container of the fuel cell stack. Further, the performance with the wick was equivalent to the performance with the methanol gel.

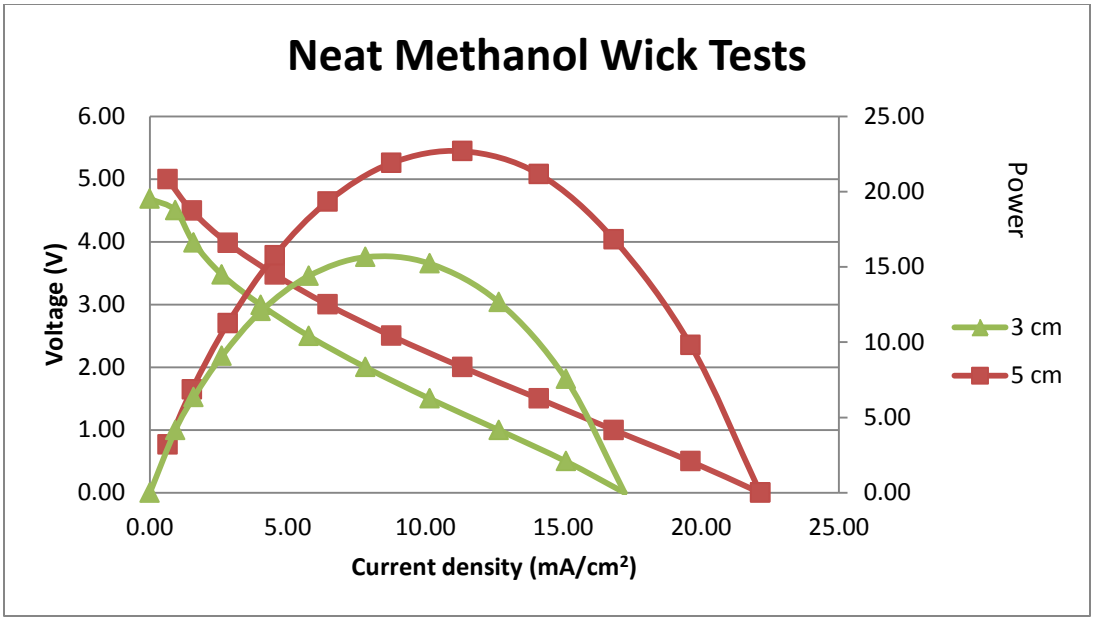

Figure 37: Wick Length Comparison (Optimized Stack Layout, Neat MeOH Fuel)

5.3.3 Test Powering Auxiliary Devices

Another test that was taken on the fuel cell stack once it was finalized was a test to determine how adding a constant load to the fuel cell would make it respond. In this experiment a fan with two different velocity settings was connected to the cell while data was collected on the fluctuations of the voltage of the cell.

As Figure 38 shows with the fan turned off, the cell performs at the highest OCV. Once the fan was turned on and the load was applied to the cell, the drop in the cell voltage can be seen. This same response is seen when increasing the speed of the fan, which requires more power from the cell. This test is useful because it showed how the cell will perform while under an actual load. The cell voltage declined significantly when a current was applied, however the fan did run at the two desired settings. The fan that was used in this experiment is specified for requiring two

size D batteries, at 1.5V each for a total of 3.0V. This proves that the stack can provide enough power to run the fan.

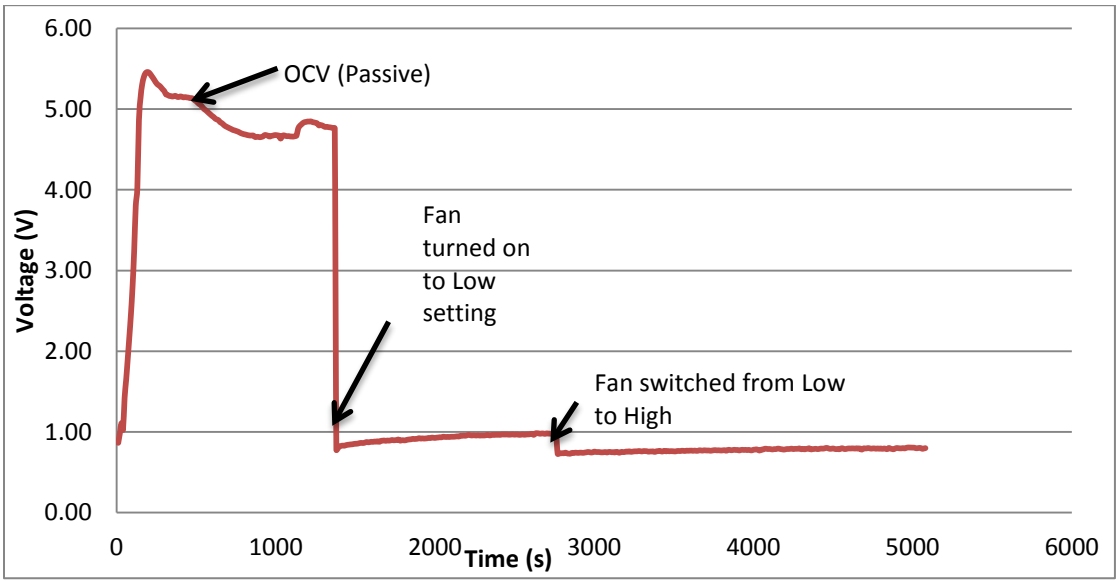

Figure 38: Active vs. Passive (Optimized Stack Layout, 25g MeOH Gel Fuel)

5.4 Miscellaneous Tests

5.4.1 Mass Transfer Calculation

Since the performance appears to be limited by methanol diffusion, experiments and calculations were performed on the mass transfer of vapor form of the methanol liquid or gel to determine the minimum surface area of fuel needed to generate the required current. Using experimentally obtained values for methanol diffusion, an estimated mass transfer rate was determined. A table of experimentally determined values is shown in Table 12, detailing all variables used in the calculations.

Table 12: Various Parameters in Methanol Diffusion and Calculations

Variables			
MW (MeOH)	Mw	32.04	g/mol
R constant	R	8.314	$\frac{m^3 Pa}{molK}$
Temperature	T	298	K
Time	t	65	min
		3900	s
Vapor Pressure Pure	$P^o_{MeOH,\,p}$	138.3	mmHg
		18435	Pa
Vapor Pressure, Gel	$P^o_{MeOH,g}$	97.68	mmHG
		13020	Pa
Area	$A_{,ref}$	12.6	cm^2
50 mL beaker (ref)		0.001257	m^2
Total Mass Difference	Δm	2.1	g
Cell Area	$A_{,\,cell}$	5	cm^2
# cells	n	12	cells
Current Efficiency	ε	50%	
Max Current	i	0.3	Amps
Faraday's	F	96487	Coulombs

Taken over the course of 65 minutes, the change in the mass of methanol gel in a 50mL beaker was measured in a hood at room temperature. This was to give the average mass transfer rate, $\dot{m}$, in grams/second, of the gel at standard conditions. Using the molecular weight of methanol, a transfer rate, $\dot{n}$, in mol/second was estimated.

$$\frac{\Delta m}{\Delta t} = \dot{\mathrm{m}} \tag{1}$$

$$\frac{\dot{\mathrm{m}}}{Mw} = \dot{\mathrm{n}} \tag{2}$$

Once a molar transfer rate was established, the effective mass transfer coefficient for the methanol gel could be determined from the vapor pressure, the area of the beaker and the transfer rate, using the following equation:

$$K, g = \left(\frac{\dot{n}}{A,ref}\right) * \left(\frac{R*T}{P^{o}MeOH,g}\right) \quad (3)$$

The mass transfer coefficient is independent of area of diffusion, so by using it, the area of diffusion can be scaled in relation to a desired methanol mass transfer rate. In order to determine how much methanol vapor from the gel is needed, the current desired and the electrochemical aspects of the reaction must be taken into consideration. Using the following equation, the necessary mass transfer rate of methanol is described.

$$\dot{n}, req = \frac{n*A,cell*i}{6*F*\varepsilon} \quad (4)$$

Once the required mass transfer rate has been calculated, the mass transfer coefficient calculated above can be used to give the required area for desired transfer rate.

$$A, req = \left(\frac{\dot{n},req}{K,g}\right) * \frac{R*T}{(P^{o}MeOH,g)} \quad (5)$$

This value for area required ensures that when the fuel is loaded into the stack, the correct amount to react fully will be available, and that no fuel starvation in the cells will occur. Fuel starvation can severely degrade the cells, causing the MEAs to perform poorly over time. Preventing this will ensure proper performance of the cell stack for a longer period of time. A table of a summary of results is shown in Table 13. Repeating the calculations using the values for the pure methanol similarly provided an estimation of surface area of methanol liquid required.

Table 13: Mass Transfer Calculation Summary

Calculation Summary			
Mass Transfer rate	$\dot{m}_{,ref}$	0.0005	g/s
Molar Transfer rate	$\dot{n}_{,ref}$	1.68E-05	mol/s
mol/s needed for charge:	$\dot{n}_{,req}$	6.22E-05	mol/s
Flux	N	0.1158	g/m^2s
Mass Transfer Coefficient (pure)	$K_{,p}$	0.0018	m/s
Mass Transfer Coefficient (gel)	$K_{,g}$	0.0025	m/s
Surface Area Needed	$A_{,req}$	0.0046	m^2
Gel Fuel		46.5	cm^2

The experimentally calculated mass transfer coefficient as described by the model is found using the depth of the liquid in the beaker. The depth of the liquid in the beaker was measured to be 5 cm. The experimental value of the coefficient was found by first using Equation 11, from the model, to find D_{mew}.

$$D_{\mathrm{Me},W} = 2.1\times10^{-5}\exp\left\{-\frac{20{,}460}{R}\left(\frac{1}{T}-\frac{1}{313}\right)\right\} \tag{11}$$

Once this value was found, the coefficient was calculated using 5 cm as d in Equation 17.

$$k_i = 2.696(D_{Me,W}/d) \tag{17}$$

The experimental value of the coefficient was found to be .0018 m/s, whereas the calculated value from the model for the same coefficient is .001 m/s. The results show from the model and the experimental are close, however the model is for 1.0M concentrated solution, while the

experiment was run using neat methanol. This explains the small discrepancies between the two coefficients, but further proves that the model can be a reliable estimation for certain parameters.

5.5 Modeling Results

Once the DMFC model was run through Mathematica, as dictated by the Appendix 2 Input files and the model as designed by Rosenthal [36], the smooth lines were calculated and graphed. The model was then compared against experimental data collected by Chu [18] with similar operating conditions. The plots below are of voltage against current density in Figure 39, power against current density in Figure 40, and the methanol crossover current density, i_{xMe}, against current density in Figure 41.

Figure 39, voltage against current density, is the first graph of the polarization plots. As shown by the experimental points plotted against the smooth model curves, the model designed by Rosenthal [10] is accurate in calculating the overall observed voltage at certain current densities applied. The concentration was set at 1.0M, and the temperature of the experiment was varied from 303K to 333K in steps of 5K, starting at the bottom curve. These results are expected because the increased temperature allows for increased reaction kinetics. This caused the diffusion of methanol to be increased through the cell, as well as making the MOR/ORR more rapid.

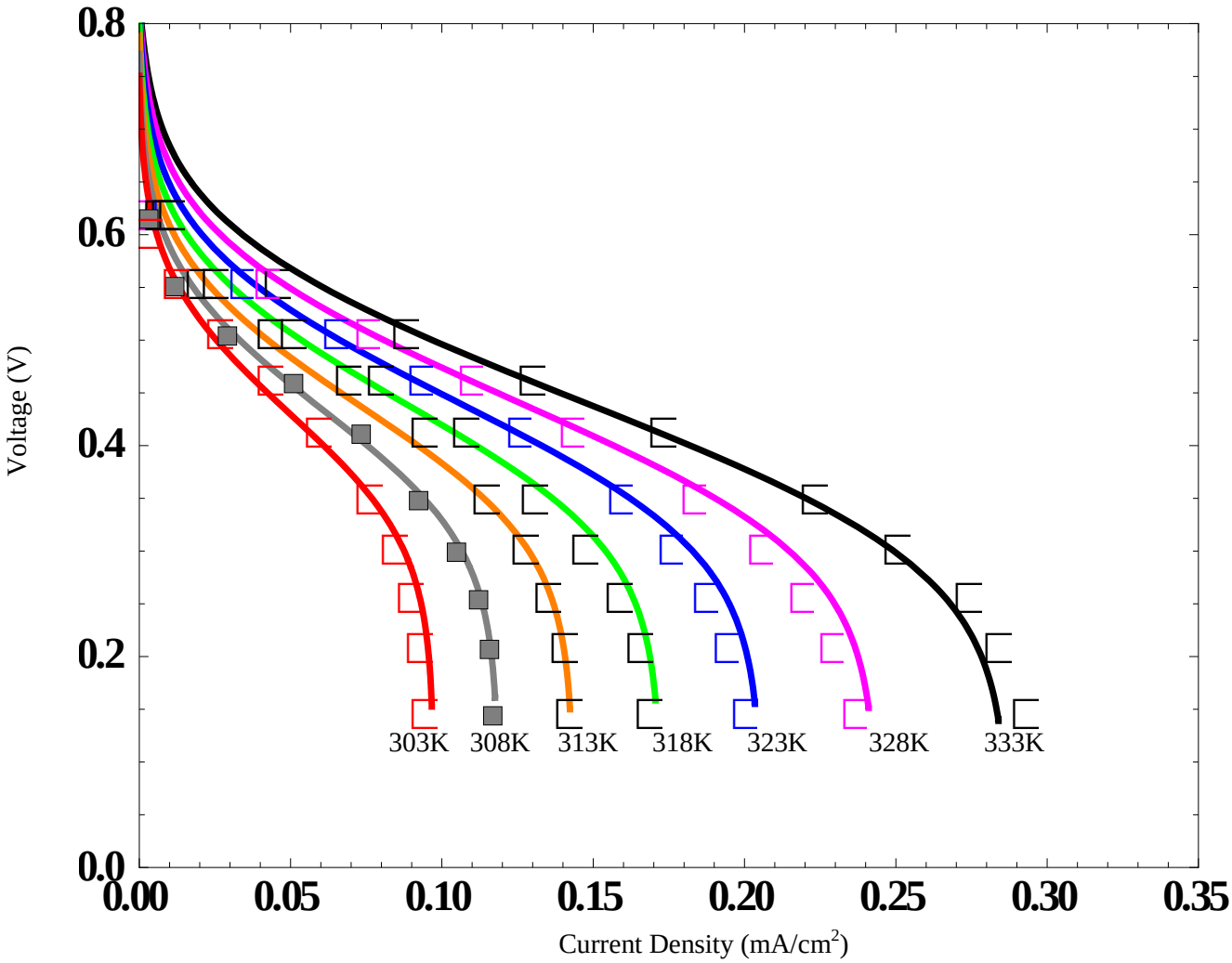

Figure 39: Polarization Plot, 1.0 Molar Solution, variable T. [36]

Figure 40, power density against current density, is the second graph of a combined polarization plot. The same experimental data from Chiu et al [18] was plotted with the proposed model. The concentration was similarly held 1.0M, with the temperature steps being the same as in Figure 39. The trends of these results are expected to be similar to voltage versus current density, because of the definition of power density; $P=iV$.

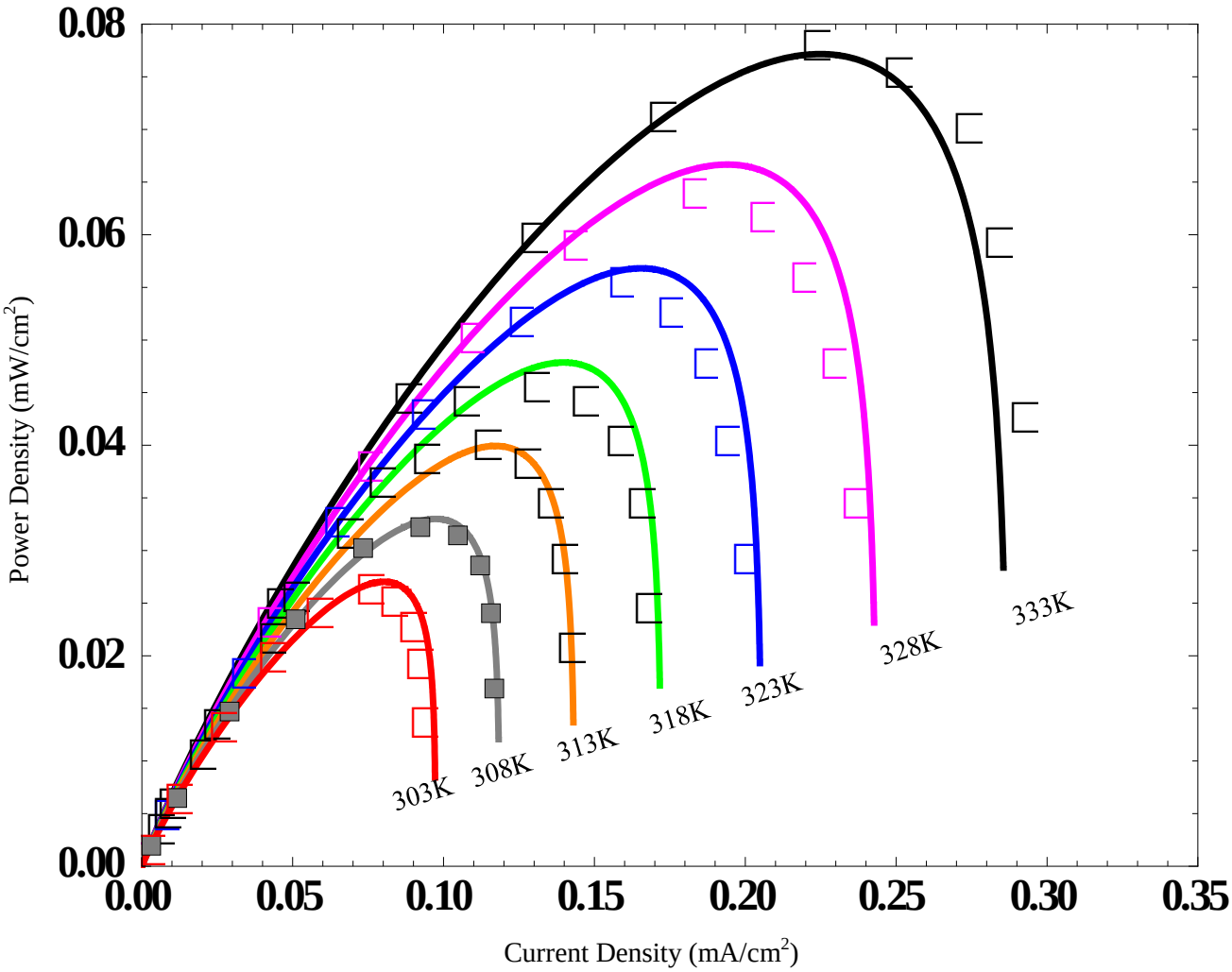

Figure 40: Power Curve, 1.0M, variable T [36]

Figure 41 compares the crossover current density of methanol as compared to the actual measured current density applied. The concentration was set at 1.0M, while the temperature was varied from 303K to 333K, in steps of 10K. These results are expected because as the temperature increases, the rate of methanol crossover also increases. As the methanol crosses over the Nafion® membrane, the crossover reactions of methanol at the cathode create overpotentials. The crossover amount can be controlled by membrane thickness, or operating temperatures and feed concentration.

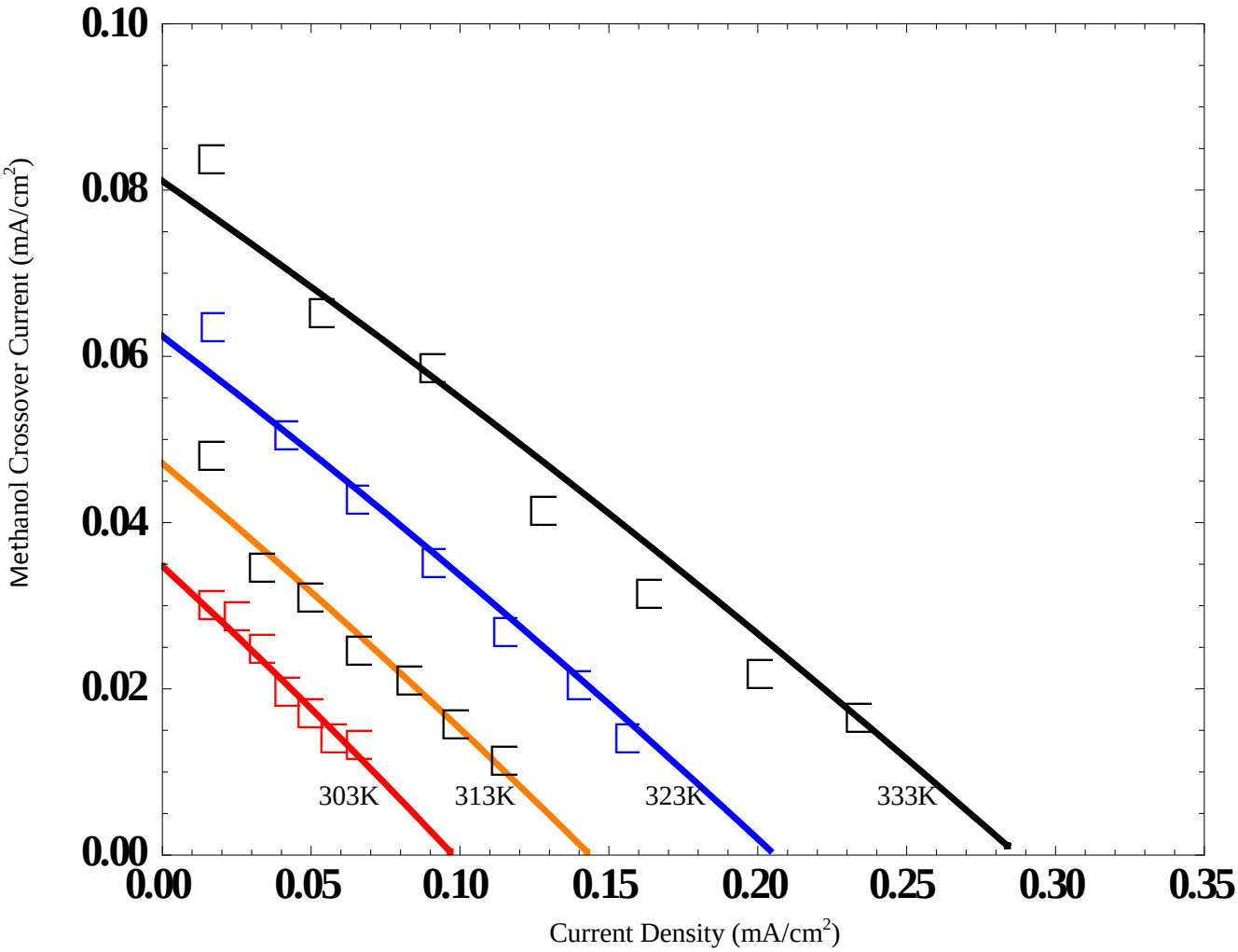

Figure 41: Methanol Crossover Current Density versus Current Density, 1.0M, variable T [36]

Due to the accuracy of the plotted experimental points and the smooth lines of the predicted model, it can be assumed that the model is a reasonable representation of the DMFC performance. Since this report deals with the Passive DMFC functionality, slight changes were made to the model input to reflect the actual performance. The studies made consisted of a variable mass transfer coefficient and a variable bulk methanol concentration. The results were plotted in both power and polarization charts.

The first study is the variation of the mass transfer coefficient, k_{Me}, in relation to overall performance. The bulk concentration of methanol was kept at 1.0M, and the temperature was at

303K, similar to the active modeling, Figures 42 and 43 are the results of the model predictions. As expected, increasing the mass transfer coefficient of the methanol to the MEA proportionally increases the performance. This is one of the main limiting factors in PDMFC performance, as there are no active transport utilities, so mass transfer is highly limited by ambient conditions and concentration differences. As more methanol is able to reach the MEA, the voltage increases in relation to the current density being applied.

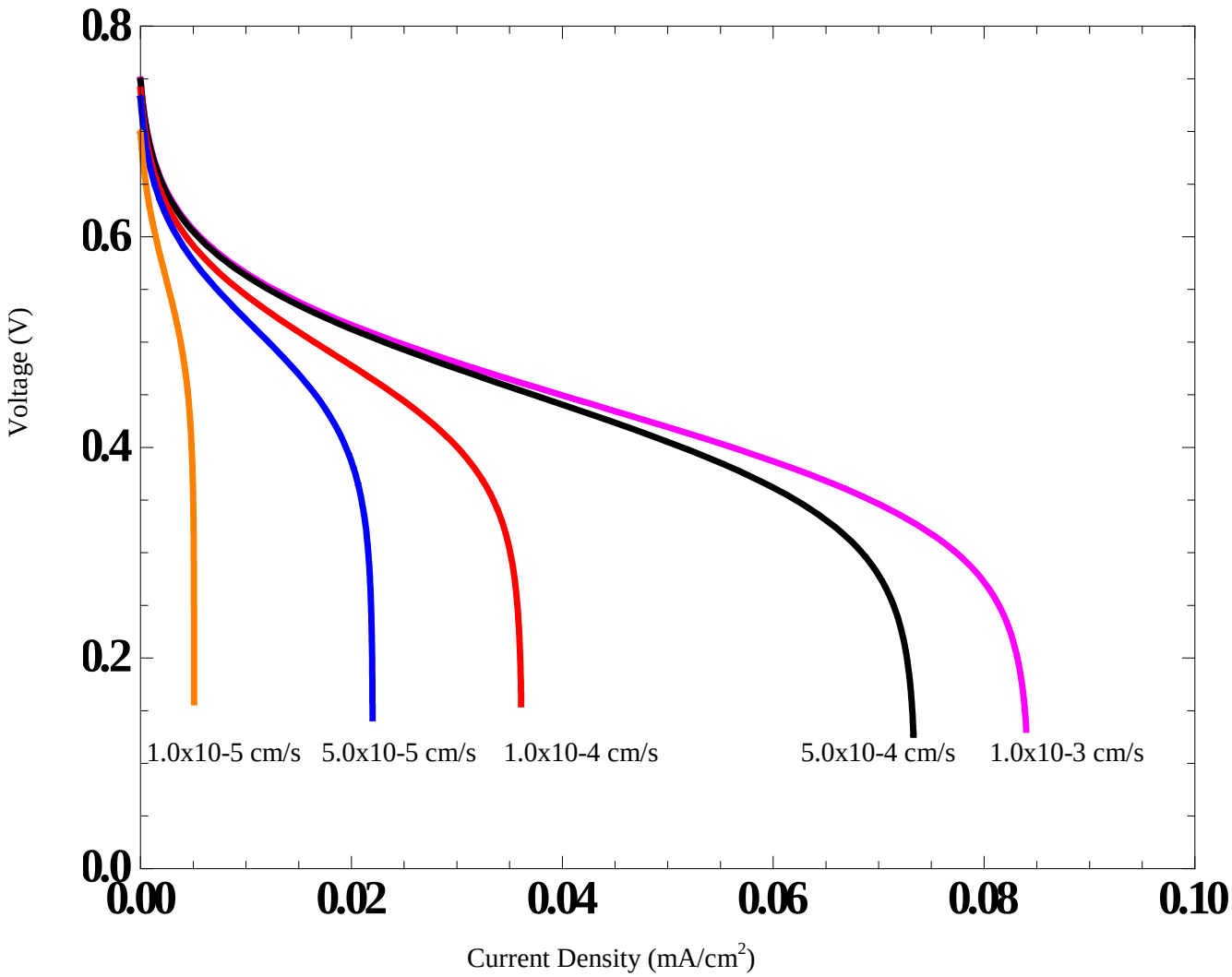

Figure 42: Mass Transfer Coefficient Variable in PDMFC Polarization (303K, 1.0M)

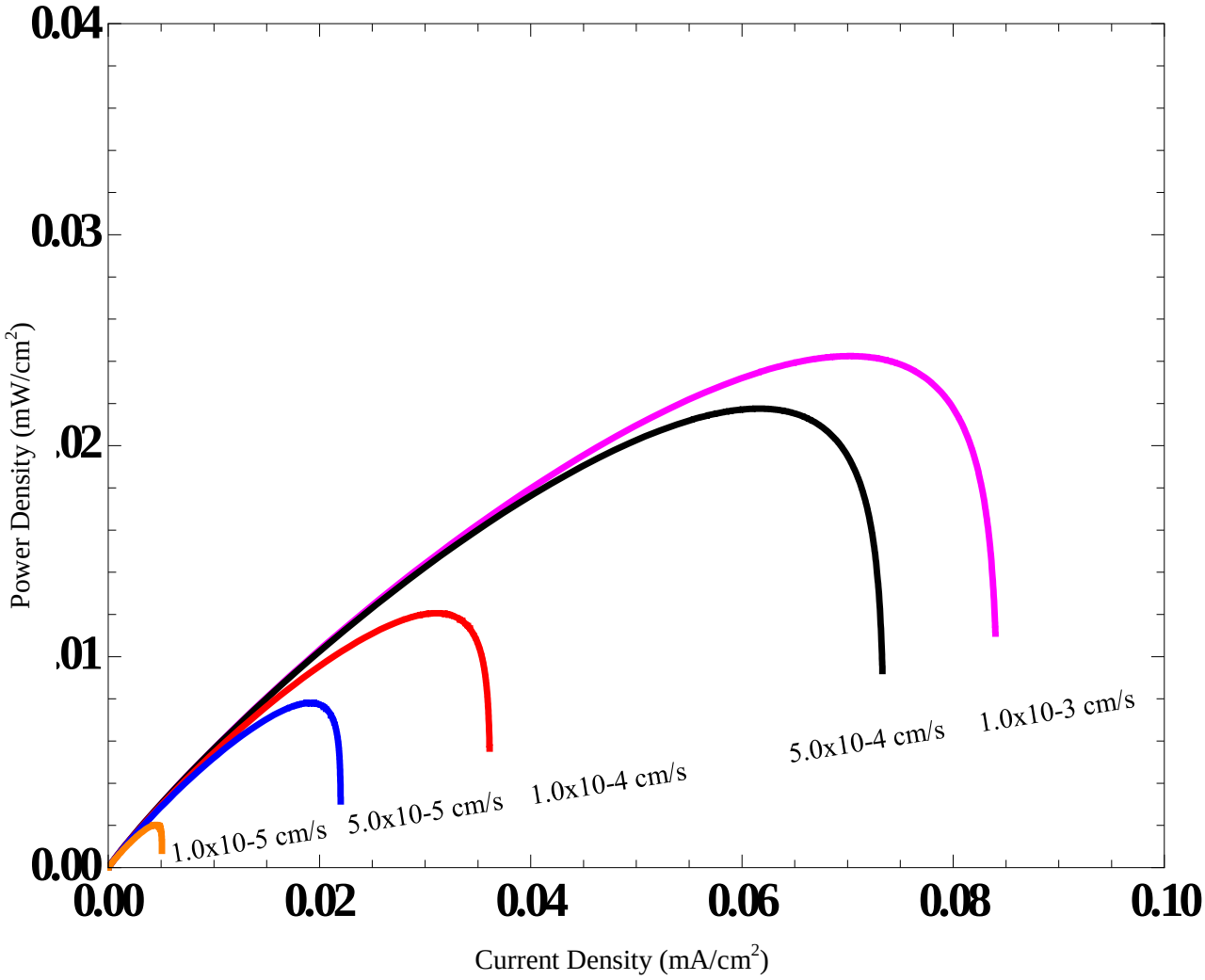

Figure 43: Mass Transfer Coefficient Variable in PDMFC Power Graph (303K, 1.0M)

The next prediction that was taken was the variation of the bulk methanol concentration at the interface of the MEA on the anode. This model predicts performance based on the idea that as more methanol is accumulated on the anode as water is produced, the concentration of the methanol can affect how the cell performs. As more methanol vapor is absorbed in the produced water from the methanol oxidation reaction, subsequently the concentration available for permeation onto the anode catalyst increases. Figures 44 and 45 show the polarization and power curves, respectively, and reinforce the notion that increased concentration results in better performance.

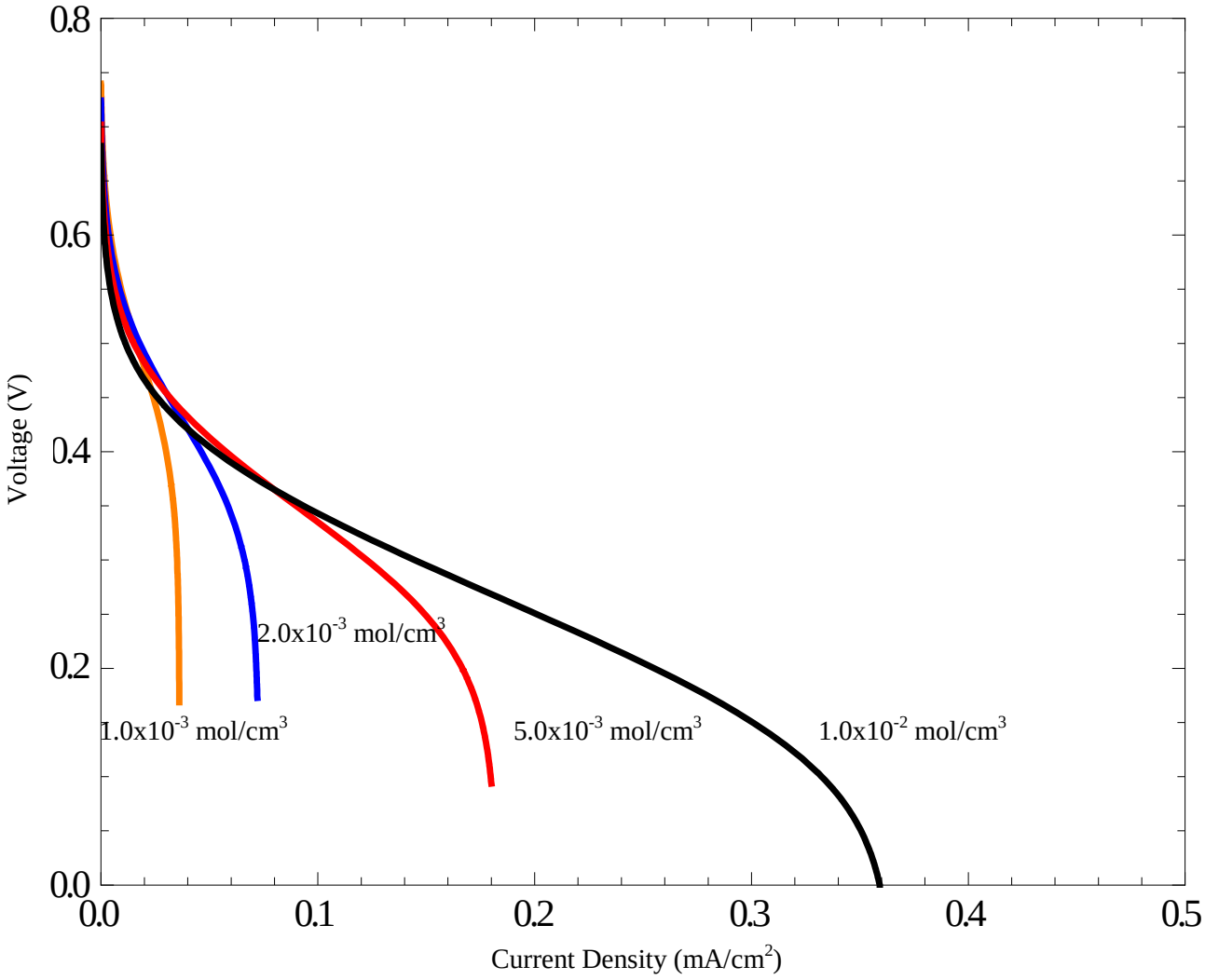

Figure 44: MeOH Bulk Concentration in PDMFC Model Polarization (303K, MT Coef: 1.0×10^{-4})

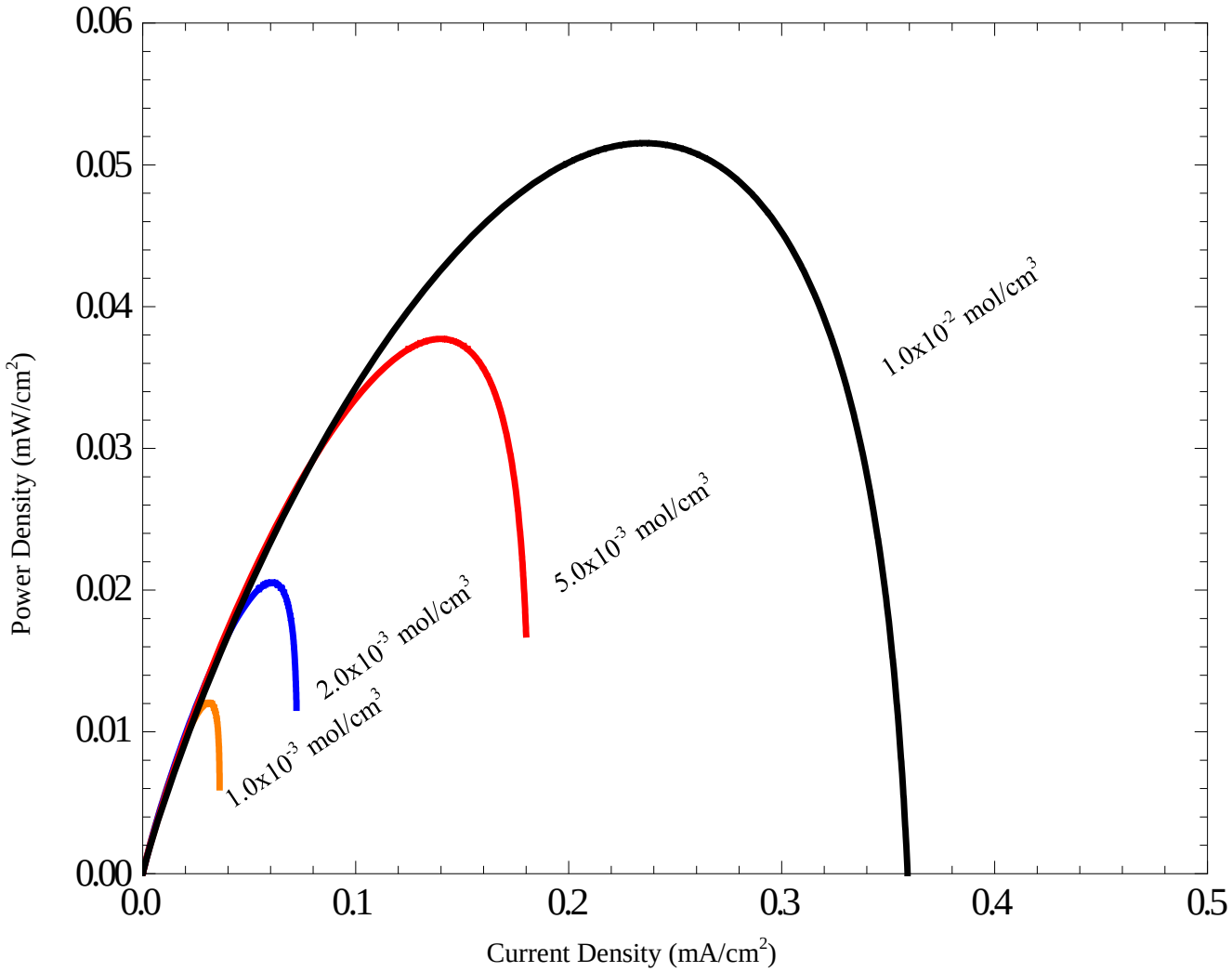

Figure 45:MeOH Bulk Concentration in PDMFC Model Power Graph (303K, MT Coef: 1.0x10^{-4})

CHAPTER 6: CONCLUSIONS

6.1 Final Remarks

There were many tests conducted on the cell both before and after the finalized stack design was completed. These tests were conducted to determine the best performance based on the configuration of the available hardware for the fuel cell stack. The parts changed on the cell ranged from the current collectors, to removing the GDLs, changing the fuel type and arrangement, and types of screws used.

The first tests run were to compare different current collectors to determine which served best with the type of fuel used; in this case the fuel was MeOH gel. The test results showed that the best type of current collectors, with the materials and resources available, were the porous stainless steel current collectors for the cathode. The best available anode current collector was a perforated stainless steel current collector, since the porous stainless steel current collector on the anode allowed diffusion of oxygen from the ambient into the anode chamber.

The next problem that was explored in the stack was the leakage out of and into the anode chamber. While using porous current collectors as the cathode, the leakage in the cell increased. The reason for the leakage increasing was the way tightening the screws would warp the current collector. This problem reduced the performance of the cell; therefore, the solution of adding reinforcement to the cathode was explored. The same current collectors that were being used as the anode were suitable to be added as reinforcement. Once the cathodes were reinforced with the perforated current collectors, the overall performance of the cell improved.

Next tests were conducted to determine if having a GDL on the MEAs would make a difference in performance or not. The tests were conducted with no GDLs, GDLs on both sides of the MEA, and then the GDLs were left on either the anode or the cathode to test for a difference.

The test results showed that the best performance, while using MeOH gel, was having a GDL on the anode side but no GDL on the cathode side.

The cell stack design that was finalized in the project was optimized to be used with methanol gel. Changes would have to be made if the cell was to be run with neat methanol or other types of fuel. These changes would have mostly involved changing the MEA layers by adding a GDL on the cathode side or removing the GDL on the anode side, as well as picking the current collectors that best is suited for the fuel being used.

The final cell stack design in this project was a 12 MEA stack connected in series, with a perforated anode current collector, a GDL on the anode side, no GDL on the cathode side, a porous steel cathode current collector with a perforated current collector used as reinforcement. This arrangement provided the best results for the methanol gel. The advantages of using MeOH gel are that it is very portable as compared to liquids or gases, and is readily available, as well that it provides good diffusion making it easier for the cell to operate.

While using results from experiments to describe the performance of the PDFMC, the model was used to evaluate theoretical values for how the PDMFC should be performing. The results obtained from the cell experimentation and those obtained from the model are close as expected. However, while the model described and applied in the project approximates results for PDMFC performance well, there are aspects that can be improved. One of these aspects would be to better understand the behavior of how methanol behaves as the current and temperature are varied. This model was also adjusted to be used with PDMFC, instead of DMFC that used an active set up. The main difference between the two models is the mass transfer.

The model also only predicted performance for a single cell PDFMC. For future work it should be considered to have the model describe accurately the performance of a multiple cell set up.

When calculating limiting current density, it is important to consider internal resistance of the cell, such as that caused by Nafion® thickness, weak connection points, etc. This was shown by Chiu et al [36]. One last thing to consider was the thickness of the GDL. The final stack set up used in this project had no GDLs in place, however for future modeling it would be highly recommended to take into consideration the thickness of the GDL as well, or the lack thereof.

In the future, this model can be refined to produce more accurate results. This model will be able to describe the performance of a PDMFC set up, as well as take the place of one when there is a lack of equipment to test on.

6.2 Recommendations

For future work with this cell stack, it would be interesting to do more experiments with different current collectors and different GDLs of different hydrophobicity. Exploring different conductive materials that provide good diffusion, as well as being more cost efficient would be useful. At the same time finding new screws for the stack will be very beneficial to the construction of the cell. New screws of a non-conduction material would provide better sealing of the cell without the chance of short circuiting the cell.

Another aspect to continue investigation is to find different MEAs that could be more effective for a PDMFC. It would be useful to determine if better performance could be obtained by using a membrane other than Nafion® 117. In addition to testing new MEAs, it would be useful to determine the need for a GDL and look more into an explanation for this.

Towards the end of this project, other stack designs were designed as discussed below. Future work could also include getting these stacks manufactured and conducting experiments on them. When doing this, it is suggested to use the finalized stack set up of the current collectors and MEAs discussed above to compare positioning of cells when using MeOH gel.

6.3 Alternate Stack Design

The stack that was used in this project was an initial design that was optimized to run with MeOH gel. This, however, left the opportunity to design new stack configurations that would take more advantage of the diffusion properties of MeOH gel. With the current stack design, the MEAs were placed on the side vertically in relation to the fuel. Because of location of the rows of cells on the top and one on the bottom, the fuel was delivered in an uneven manner; the top row generally receiving more methanol vapor. The stack was also not optimized for portability and was prone to leakage.

The stacks proposed are designed with the flaws of the current cell stack in mind. The spaces where the MEAs are placed are thought to take advantage of the delivery of the MeOH gel. With the stack having a top and a bottom open to MEAs, that stack would have no directional preference and could be used for more portable purposes. There are also other advantages to the proposed stacks, including the design of a possible cartridge that would be filled with MeOH gel. This would make this design very useful for applications as well as very easy to operate. The first proposed stack (Figure 46 and Figure 47) utilizes (6) 50cm² active area MEAs, while the second one (Figure 48 and Figure 49) utilizes (8) 25cm² MEAs

These proposed designs are shaped like a notebook to be more portable. The flat design would use MeOH gel with a larger surface area. This stack could be used to charge laptop computers, tablets, or other portable electronic devices. A stack is also designed to be used in a competition style remote control car for the American Institute of Chemical Engineers. The design easily adapts to that needed to be mounted to the vehicle and be used in a long term experiment.

The variation in the cell size and number allows the voltage and current capabilities to be varied. To increase the overall voltage of a stack, the number of MEAs is increased regardless of size.

Increasing the active area also increases the possible current from the individual cells. This is why most calculations and results are displayed in terms of unit area, to allow for sizing up and comparison between cells of similar material and make, but different active areas.

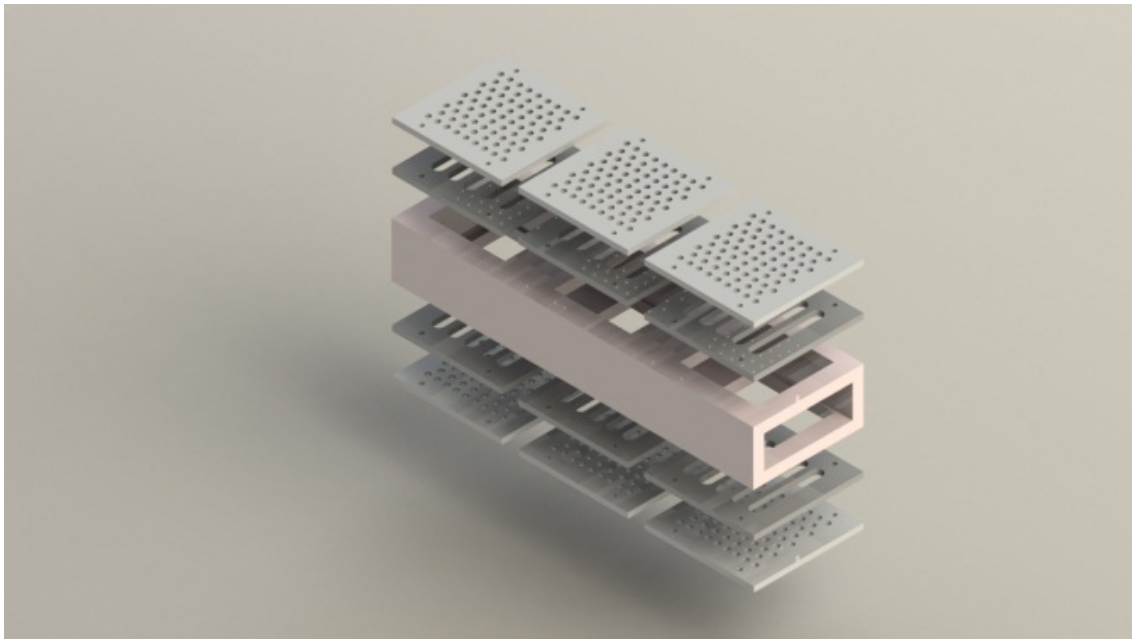

Figure 46: 50cm^2 Active Area Stack Exploded

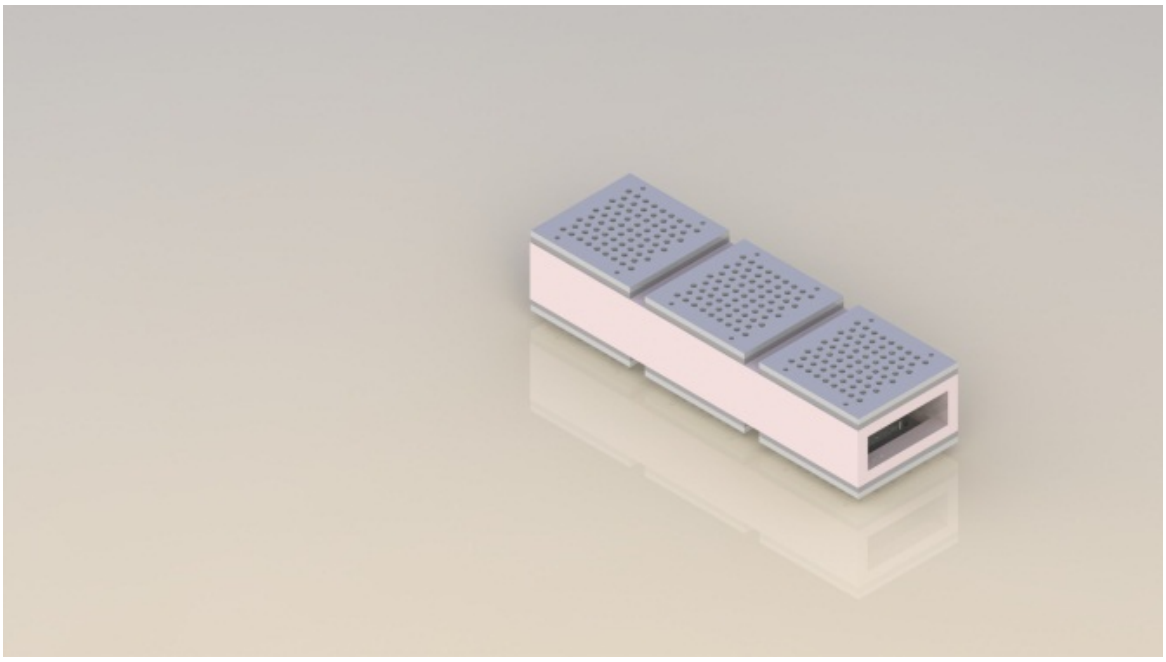

Figure 47: 50cm^2 Active Area Stack

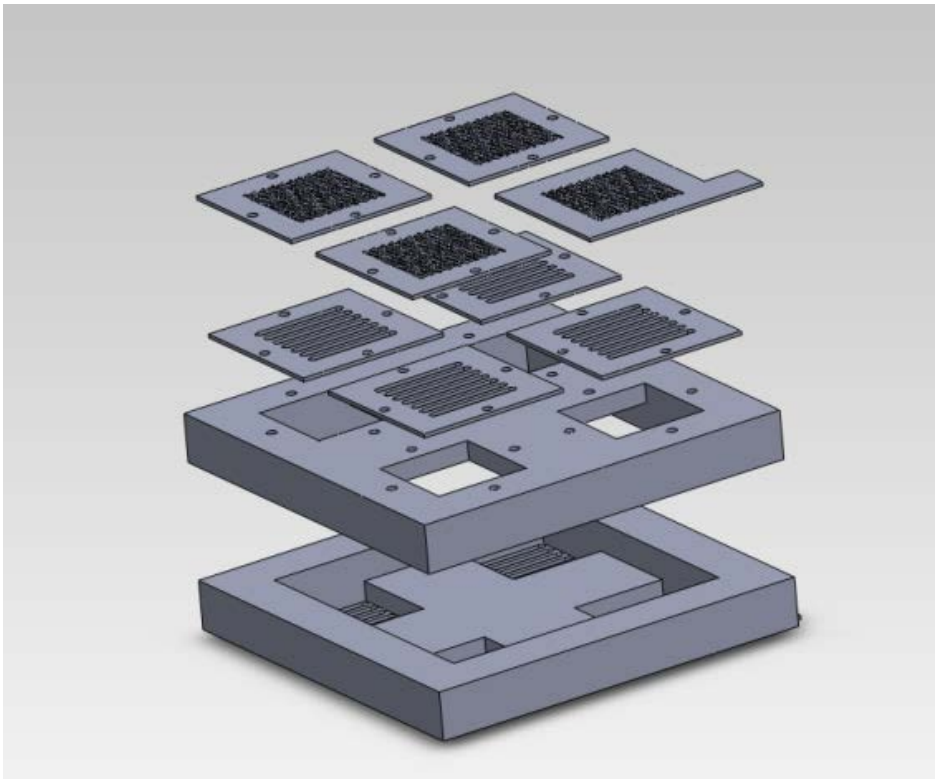

Figure 48: 25cm^2 Stack Exploded

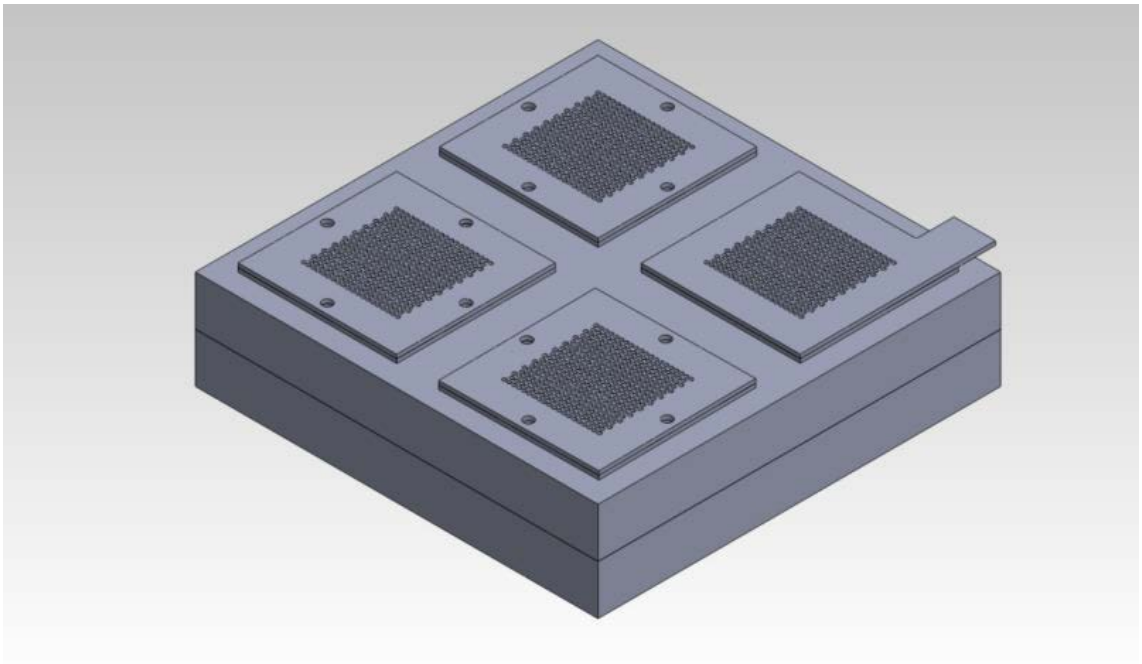

Figure 49: 25cm^2 Stack

APPENDIX 1: REFERENCES

[1] Shimizu, T. (2004). Design and fabrication of pumpless small direct methanol fuel cells for portable applications. Journal of Power Sources, 137(2), 277-283. doi:10.1016/j.jpowsour.2004.06.008

[2] "REN21 - Renewables 2010 Global Status Report." REN21. Web. 21 Feb. 2012. <http://www.ren21.net/Portals/97/documents/GSR/REN21_GSR_2010_full_revised%20Sept2010.pdf>.

[3] "Fuel Cell." *Wikipedia*. Wikimedia Foundation, 20 Feb. 2012. Web. 21 Feb. 2012. <http://en.wikipedia.org/wiki/Fuel_cell>.

[4] "CED Engineering - Continuing Education Course Online - Engineering Courses - Online PDH Courses." CED Engineering. Web. 21 Feb. 2012. <http://www.cedengineering.com>.

[5] "Types of Fuel Cells." *FCT Fuel Cells:*. Web. Nov.-Dec. 2011. <http://www1.eere.energy.gov/hydrogenandfuelcells/fuelcells/fc_types.html>

[6] Kho, B. K., Bae, B., Scibioh, M. A., Lee, J., & Ha, H. Y. (2005). On the consequences of methanol crossover in passive air-breathing direct methanol fuel cells. Journal of Power Sources, 142(1-2), 50-55. doi:10.1016/j.jpowsour.2004.10.027

[7] Chen, R., & Zhao, T. S. (2005). Mathematical modeling of a passive-feed DMFC with heat transfer effect. Journal of Power Sources, 152, 122-130. doi:10.1016/j.jpowsour.2005.02.088

[8] "DTI Energy Inc." DMFC, Direct Methanol Fuel Cell, Technology --. Web. 21 Feb. 2012. <http://www.dtienergy.com/>

[9] Lai, Q.-Z., Yin, G.-P., Wang, Z.-B., Du, C.-Y., Zuo, P.-J., & Cheng, X.-Q. (2008). Influence of Methanol Crossover on the Fuel Utilization of Passive Direct Methanol Fuel Cell. Fuel Cells, 8(6), 399-403. doi:10.1002/fuce.200700066

[10] Rosenthal, Neal, Vilekar Saurabh , and Ravindra Datta. "A Comprehensive yet Comprehensible Analytical Model for the Direct Methanol Fuel Cell." *Fuel Cell Center, Department of Chemical Engineering, Worcester Polytechnic Institute*. (2012): 1-62. Print.

[11] Kim, W.-J., Choi, H.-G., Lee, Y.-K., Nam, J.-D., Cho, S. M., & Chung, C.-H. (2006). Suppression of the methanol crossover by hydrogels in passively operated flat-pack type DMFCs and its application for the power source of cellular phone. Journal of Power Sources, 163(1), 98-102. doi:10.1016/j.jpowsour.2006.05.048

[12] Guo, Z. (2008). Development of a 1 W passive DMFC☆. International Communications in Heat and Mass Transfer, 35(3), 225-239. doi:10.1016/j.icheatmasstransfer.2007.07.008

[13] Ali Abdelkareem, M., & Nakagawa, N. (2006). DMFC employing a porous plate for an efficient operation at high methanol concentrations. Journal of Power Sources, 162(1), 114-123. doi:10.1016/j.jpowsour.2006.07.012

[14] Chen, R, & Zhao, T. (2007). Porous current collectors for passive direct methanol fuel cells. Electrochimica Acta, 52(13), 4317-4324. doi:10.1016/j.electacta.2006.12.015

[15] Chen, R., & Zhao, T. S. (2007). Performance characterization of passive direct methanol fuel cells. Journal of Power Sources, 167(2), 455-460. doi:10.1016/j.jpowsour.2007.02.083

[16] Rosenthal, Neal. "An Exploration of the Promises and Limitations of Passive Direct Methanol Fuel Cells."*Fuel Cell Center, Department of Chemical Engineering, Worcester Polytechnic Institute*. (2011): 1-117. Print.

[17] Y.-J. Chiu, Int. J. Hydrogen Energy. 35 (2010) 6418-6430.][Y.-J. Chiu, T. L. Yu, and Y.-C. Chung, J. Power Sources. 196 (2011) 5053-5063.]

[18] Chu, D., & Jiang, R. (2006). Effect of operating conditions on energy efficiency for a small passive direct methanol fuel cell. Electrochimica Acta, 51(26), 5829-5835. doi:10.1016/j.electacta.2006.03.017

[19] Yao, S.-C., Tang, X., Hsieh, C.-C., Alyousef, Y., Vladimer, M., Fedder, G. K., & Amon, C. H. (2006). Micro-electro-mechanical systems (MEMS)-based micro-scale direct methanol fuel cell development. Energy, 31(5), 636-649. doi:10.1016/j.energy.2005.10.016

[20] Xu, C., Zhao, T. S., & Ye, Q. (2006). Effect of anode backing layer on the cell performance of a direct methanol fuel cell. Electrochimica Acta, 51, 5524-5531. doi:10.1016/j.electacta.2006.02.030

[21] Nakagawa, N., Abdelkareem, M. A., & Sekimoto, K. (2006). Control of methanol transport and separation in a DMFC with a porous support. Journal of Power Sources, 160(1), 105-115. doi:10.1016/j.jpowsour.2006.01.066

[22] Oedegaard, a, Hebling, C., Schmitz, a, Møller-Holst, S., & Tunold, R. (2004). Influence of diffusion layer properties on low temperature DMFC. Journal of Power Sources, 127(1-2), 187-196. doi:10.1016/j.jpowsour.2003.09.015

[23] Park, Y.-C., Lee, S.-H., Kim, S.-K., Lim, S., Jung, D.-H., Lee, D.-Y., Choi, S.-Y., et al. (2010). Performance and long-term stability of Ti metal and stainless steels as a metal bipolar plate for a direct methanol fuel cell. International Journal of Hydrogen Energy, 35(9), 4320-4328. Elsevier Ltd. doi:10.1016/j.ijhydene.2010.02.010

[24] Kim, Y.-J., Bae, B., Scibioh, M. A., Cho, E., & Ha, H. Y. (2006). Behavioral pattern of a monopolar passive direct methanol fuel cell stack. Journal of Power Sources, 157(1), 253-259. doi:10.1016/j.jpowsour.2005.06.037

[25] Lai, Q.-zhi, Ã, G.-ping Y., & Wang, Z.-bo. (2009). Effect of anode current collector on the performance of passive direct methanol fuel cells. International Journal of Energy Research, (November 2008). doi:10.1002/er

[26] Guo, Zhen, & Faghri, A. (2006). Development of planar air breathing direct methanol fuel cell stacks. Journal of Power Sources, 160(2), 1183-1194. doi:10.1016/j.jpowsour.2006.03.045

[27] Jewett, G., Guo, Z., & Faghri, A. (2007). Water and air management systems for a passive direct methanol fuel cell. Journal of Power Sources, 168(2), 434-446. doi:10.1016/j.jpowsour.2007.03.052

APPENDIX 2: MATHEMATICA ® MODELING FILES

Active DMFC Input [36]

Adapted from Rosenthal, et al.

```
F = 96487; αA=1/2;
αC=1/2;νA=+1 (* for anode
this agrees with Gojkovic et
al., 2003*);νC=-2; R=8.314;
iA0,ref=2.0× 10^-8 (*fitted*);
iC0,ref=1.0× 10^-10; LB=178 ×10^-4;
LD=260 ×10^-4;LE=260 ×10^-4;εD
=0.65;εE =0.65; RI=0;Tref=298;
EA=65000(*Desai and Neurock
(2003) provide a barrier of
60 kJ for CO.S+OH.S=CO2 + H^+
+ e-*); EC=67000;pO,ref=1;
cMe,ref=1×10^-3; cW=55.5×10^
-3(*mol/cm^3*); ξ=2.9 (*X.Ren
and
S.Gottesfeld,J.Electrochem.So
c.,148,A87-A93,2001*);
DO,W=2.5 10^-5 (*assumed*);
κO=0.144;κMe,D=1.0;κMe,B=0.4(
*Ren, Zawo, 2000, Fig
11*);φI=0.75; ρPt=21.45;
ρRu=12.3;EμΩ=14000;δ=1.65(*fitted to
conductivity data for DMFC of Ren, Zawo,
2000, Fig 8*); νmax=1.255 (*max
voltage*); RI=0;
 cMe,in=1.0×10^-3 (*mol/cm^3*);
 a=3.5 3.5; (*du Pont MEAs
area*)
 h=0.1; l=45; n=1; (*Flow
channel height, length, and
number of parallel channels*)
 mMA=4.0 10^-3; mMC=2.0 10^-3;
ωRu=0.5; dMA=2.7 10^-7; dMC=2.7
10^-7 (* These catalysts are C
supported frm du Pont.
Hogarth and Ralph give
Subscript[γ, MA]/Subscript[m,
MA]=39m2/g for black
catalyst*);
QA=5/60;QC=150/60;(*Volumetric
anode and cathode flow rates,
cm3/s*)
 pW=Exp[11.676-3816.44/(T-
46.13)];(*vapor pressure of
water in cell*)
 pO,in=xO,in(pc-pW);
 pC=1.0;xO,in=0.21;
 cMe,b=cMe,in -(a (y))/(12 F
QA);(*Current should actually
also include crossover
current*)
 λ=20; (*Taken from Ren,
Zawo, 2000. For liquid
methanol feed. For vapor
feed, this would be lower.
Further, due to compression,
actual λ may be lower than
this value indicated by
sorption isotherm??*)
 cO,ref=pO,ref /(82 T);

cO,in=pO,in /(82 T);
 cO,b=cO,in -(a y)/(8 F QC);
 cMe,0=κMe,D cMe,b;
 xMe,b=cMe,b/cW;
 vO=1.214 - 1.4 10^-4 (T-
298)+(R T)/(6 F)
Log[(cMe,in/cW) pO,in];
 DO,E = 0.357(T/352)^1.823
(*Reid*);
 DMe,W=2.1 10^-5 Exp[-
(20460/R)(1/T-1/313)] (*This,
along with (
 SubsuperscriptBox[ ϵ , B ,
1.5 \ ]\
 SubscriptBox[ D , Me, W ]
), agrees very well with Fig
9 of Ren, Zawo, 2000, for
effective methanol
diffusivity in Nafion*);
 εB=λ/(537/18+λ);
 χ=1.8/(537/18+1.8);
 cH0=1/(18 λ);
```

```
K_A=6.2Exp[-((-52300)/R)(1/T-1/298)];

β=((λ+1)-√((λ+1)^2-4λ(1-1/K_A)))/(2(1-1/K_A));
T=303;
σB=(Subscript[ϵ, B]-χ)^1.5 (349.8/(1+δ))Exp[-(E_μ/R)(1/T-1/298)] c_H0 β
0.0804085
k_+1=1.41 10^5 Exp[-(0/(R T))];(*Vilkar and Datta, 2007*)
k_-1=1.0 10^13 Exp[-(130000/(R T))];(*Vilkar and Datta, 2007*)
K=k_+1/k_-1;
ρMA=(1-ωRu) ρPt+ωRu ρRu;
γMA=φI m_MA(6/(ρMA d_MA));
γMC=φI m_MC(6/(ρPt d_MC));
θCO=(K c_Me,0)/(1+K c_Me,0);
θCO,ref=(K c_Me,ref)/(1+K c_Me,ref);
i_A0=γMA×(c_Me,0/c_Me,ref)(1-θCO)/(1-θCO,ref) Exp[-(E_A/R)(1/T-1/Tref)] i_A0,ref;
i_C0=γMC×(c_O,b/c_O,ref)Exp[-(E_C/R)(1/T-1/Tref)] i_C0,ref;
τMe=Q_A/(n h^2 l);
k_Me=2.696 D_Me,W/h (1+0.139 h^2/(Subscript[τ, Me] Subscript[D, Me,W]))^0.81;
D_Me,D,e=0.975 Exp[-(30975/(R T))];(*Fitted to limiting current density in Fig 3 of Chiu, 2011. Also preseumably includes the partition coefficient, Subscript[κ, Me,D], although assumed here as unity, and its temperature variation, accounting for the higher activation energy than Subscript[D, Me,W]*)
P_Me,D,e=1/(L_D/(κMe,D D_Me,D,e)+1/k_Me);
τO=Q_C/(n h^2 l);
k_O=2.696 D_O,E/h (1+0.139 h^2/(Subscript[τ, O] Subscript[D, O,E]))^0.81;
q_W=0.5 (*or 0.4*)(*for liquid feed this is high and should be virtually independent of current*)(*For vapor feed, may assume Subscript[q, W]=2.0 y assumed proportional to water flux or current*);
P_O,E,e=1/(L_E/(κO ϵ_E^1.5 (1-Subscript[q, W])^1.5 D_O,E)+1/k_O);
i_AL=6F P_Me,D,e c_Me,b ;
i_CL=4F P_O,E,e c_O,b;
i_X,Me,L=κMe,B (6F)/L_B (ϵ_B^1.5 D_Me,W) c_Me,b;
P_O,D,e=ϵ_D^1.5 /L_D D_O,W κO;
i_X,O=4F c_O,b(P_O,D,e+ϵ_B^1.5 /L_B D_O,W κO);
i_X,Me=((i_X,Me,L+3 (κMe,B/κMe,D) x_Me,b ξ y)(1-y/i_AL))/(1+1/i_AL (i_X,Me,L+3 (κMe,B/κMe,D) x_Me,b ξ y));
ηA=(R T)/(αA νA F) ArcSinh[(y+i_X,O)/(2 i_A0)/(1-(y+i_X,O)/i_AL)(1+1/i_AL (i_X,Me,L+3 (κMe,B/κMe,D) x_Me,b ξ y))];
ηC=(R T)/(αC νC F) ArcSinh[(y+i_X,Me)/(2 i_C0)/(1-(y+i_X,Me)/i_CL)];
ηB=y (L_B/σB);ηI=y R_I;
Ψ=v_0+ηC;
V=v_0-ηA+ηC-ηB-ηI;
P=V y;
q=(y+i_X,Me+i_X,O) v_ma-P;
Ξ=P (1/v_ma)(1/(y+i_X,Me+i_X,O))100;
    T=303;
```

Passive DMFC Input [36]

Adapted from Rosenthal, et al.

```
F = 96487; αA=1/2;
αC=1/2;νA=+1 (* for anode
this agrees with Gojkovic et
al., 2003*);νC=-2; R=8.314;
iA0,ref=2.0× 10^-8 (*fitted*);
ic0,ref=1.0× 10^-10; LB=178 ×10^-4;
LD=260 ×10^-4;LE=260 ×10^-4;εD
=0.65;εE =0.65; RI=0;Tref=298;
EA=65000(*Desai and Neurock
(2003) provide a barrier of
60 kJ for CO.S+OH.S=CO2 + H^+
+ e-*); EC=67000;po,ref=1;
cMe,ref=1×10^-3; cW=55.5×10^
-3(*mol/cm^3*); ξ=2.9 (*X.Ren
and
S.Gottesfeld,J.Electrochem.So
c.,148,A87-A93,2001*);
Do,W=2.5 10^-5 (*assumed*);
κO=0.144;κMe,D=1.0;κMe,B=0.4(
*Ren, Zawo, 2000, Fig
11*);φI=0.75; ρPt=21.45;
ρRu=12.3;Eμ=14000;δ=1.65 (*fitted to
conductivity data for DMFC of Ren, Zawo,
2000, Fig 8*); νmax=1.255 (*max
voltage*); RI=0;
 T=303;
 mMA=4.0 10^-3; mMC=2.0 10^-3;
ωRu=0.5; dMA=2.7 10^-7; dMC=2.7
10^-7 (* These catalysts are C
supported frm du Pont.
Hogarth and Ralph give
Subscript[γ, MA]/Subscript[m,
MA]=39m2/g for black
catalyst*);
 pW=Exp[11.676-3816.44/(T-
46.13)];(*vapor pressure of
water in cell*)
 po,in=xo,in(pc-pW);
 pc=1.0;xo,in=0.21;
 λ=20; (*Taken from Ren,
Zawo, 2000. For liquid
methanol feed. For vapor
feed, this would be lower.
Further, due to compression,
actual λ may be lower than
this value indicated by
sorption isotherm??*)
 co,ref=po,ref /(82 T);
 co,in=po,in /(82 T);
 co,b=co,in ;
 cMe,0=κMe,D cMe,b;
 xMe,b=cMe,b/cW;
 v0=1.214 - 1.4 10^-4 (T-
298)+(R T)/(6 F) Log[(cMe,b/cW)
po,in];
 Do,E = 0.357(T/352)^1.823
(*Reid*);
 DMe,W=2.1 10^-5 Exp[-
(20460/R)(1/T-1/313)] (*This,
along with (
 SubsuperscriptBox[ ϵ , B ,
1.5 \ ]\
 SubscriptBox[ D , Me, W ]
), agrees very well with Fig
9 of Ren, Zawo, 2000, for
effective methanol
diffusivity in Nafion*);
 εB=λ/(537/18+λ);
 χ=1.8/(537/18+1.8);
 cH0=1/(18 λ);
 KA=6.2Exp[-((-52300)/R)(1/T-
1/298)];
 β=((λ+1)-
√((λ+1)^2 - 4 λ (1 - 1/KA))
)/(2(1-1/KA));
 σB=(Subscript[ϵ, B]-χ)^1.5
(349.8/(1+δ))Exp[-(Eμ/R)(1/T-
1/298)] cH0β;
 k+1=1.41 10^5 Exp[-(0/(R T))];
(*Vilkar and Datta, 2007*)
 k-1=1.0 10^13 Exp[-(130000/(R
T))];(*Vilkar and Datta,
2007*)
 K=k+1/k-1;
 ρMA=(1-ωRu) ρPt+ωRu ρRu;
 γMA=φI mMA(6/(ρMA dMA));
 γMC=φI mMC(6/(ρPt dMC));
 θCO=(K cMe,0)/(1+ K cMe,0);
```

```
θCO,ref=(K cMe,ref)/(1+ K cMe,ref);
iA0=γMA×(cMe,0/cMe,ref) (1-θCO)/(1-θCO,ref) Exp[-(EA/R)(1/T-1/Tref)] iA0,ref;
iC0=γMC×(cO,b/cO,ref)Exp[-(EC/R)(1/T-1/Tref)] iC0,ref;
DMe,D,e=0.975 Exp[-(30975/(R T))];(*Fitted to limiting current density in Fig 3 of Chiu, 2011. Also preseumably includes the partition coefficient, Subscript[κ, Me,D], although assumed here as unity, and its temperature variation, accounting for the higher activation energy than Subscript[D, Me,W]*)
PMe,D,e=1/(LD/(κMe,D DMe,D,e)+1/kMe);
hC=0.3; (*Oxygen diffusion film thickness - assumed simply to estimate the gas-phase MT coeff - alternatively different values of MT coeff may be assumed*)
kO=2.696 DO,E/hC;
qW=0.5 (*or 0.4*)(*for liquid feed this is high and should be virtually independent of current*)(*For vapor feed, may assume Subscript[q, W]=2.0 y assumed proportional to water flux or current*);
PO,E,e=1/(LE/(κO ϵE^1.5 (1-Subscript[q, W])^1.5 DO,E)+1/kO);
iAL=6F PMe,D,e cMe,b ;
iCL=4F PO,E,e cO,b;
iX,Me,L=κMe,B (6F)/LB (ϵB^1.5 DMe,W) cMe,b;
PO,D,e=ϵD^1.5 /LD DO,W κO;
iX,O=4F cO,b(PO,D,e+ϵB^1.5 /LB DO,W κO);
iX,Me=((iX,Me,L+3 (κMe,B/κMe,D) xMe,bξ y)(1-y/iAL))/(1+1/iAL (iX,Me,L+3 (κMe,B/κMe,D) xMe,bξ y));
ηA=(R T)/(αA νA F) ArcSinh[(y+iX,O)/(2 iA0)/(1-(y+iX,O)/iAL)(1+1/iAL (iX,Me,L+3 (κMe,B/κMe,D) xMe,bξ y))];
ηC=(R T)/(αC νC F) ArcSinh[(y+iX,Me)/(2 iC0)/(1-(y+iX,Me)/iCL)];
ηB=y (LB/σB);ηI=y RI;
Ψ=v0+ηC;
V=v0-ηA+ηC-ηB-ηI;
P=V y;
q=(y+iX,Me+iX,O) vma-P;
Ξ=P (1/vma)(1/(y+iX,Me+iX,O))100;
kMe=1×10^-4;(*cm/s*)
cMe,b=1.0×10^-3;(*mol/cm^3*)(*assumed methanol concentration in the liquid phase at the anode GDL, the vapor phase methanol concentration is different and depends upon VLE and mass balance*);
```

APPENDIX 3: MSDS SAFETY SHEETS

MATERIAL SAFETY DATA SHEET

GEL HEAT™ BLUE GEL METHANOL CHAFING DISH FUEL

HOLLOWICK® INC.

24 hour emergency assistance: CHEMTREC 1-800-424-9300 day or night. Outside the continental United States, call CHEMTREC at 1-703-527-3887 (collect calls accepted).

Hollowick urges the customer receiving the Material Safety Data Sheet (MSDS) to study it carefully to become aware of hazards, if any, of the product involved. In the interest of safety, you should (1) notify your employees, agents and contractors of the information on this sheet, and (2) furnish a copy to each of your customers to inform their employees as well.

SECTION I – PRODUCT INFORMATION

TRADE NAME:	GHBLUE, **GEL HEAT™ BLUE**
PACKAGE:	Cans (72 per case)
SYNONYMS:	Gel (or jelled) Methanol (Consumer Commodity)
PRODUCT IS:	Mixture, CAS number not applicable
CHEMICAL FAMILY:	Not applicable
GENERAL INFORMATION:	A gel alcohol fuel for warming food in chafing dishes only. The fuel is methanol in a colloidal gel.
DATE PREPARED:	December 1, 2005

SECTION II – HAZARDOUS INGREDIENTS/IDENTITY INFORMATION

COMPOSITION	*CAS RN.*	*WT/WT%*	*TLV (UNITS)*
Methanol	67-56-1	74.8	200 ppm
Acetone	67-64-1	0.4	1000 ppm
Denatonium Benzoate	3734-33-6	Trace	----------

SECTION III – PHYSICAL/CHEMICAL CHARACTERISTICS

APPEARANCE AND ODOR:	Blue gel with alcohol odor
SPECIFIC GRAVITY (H_2O=1) at 80° F:	Not applicable
% VOLATILE BY VOLUME:	98%
SOLUBILITY IN WATER:	Slightly soluble
pH:	Not applicable

SECTION IV – FIRE AND EXPLOSION HAZARDS

FLASH POINT:	Tag Closed Cup 54° F (12.2° C)
IGNITION TEMPERATURE:	410° F
EXTINGUISHING MEDIA:	Carbon dioxide, dry chemical, water mist or fog
SPECIAL FIREFIGHTING PROCEDURES:	Do not use high-pressure stream of water to extinguish burning material
UNUSUAL FIRE OR EXPLOSION HAZARD:	Closed can exposed to flame and heat may erupt scattering burning fragments.

SECTION V – REACTIVITY DATA

STABILTY:	Stable
CONDITIONS AND MATERIALS TO AVOID:	Heat, open flame, strong oxidizers
HAZARDOUS DECOMPOSITION PRODUCTS:	None known
HAZARDOUS POLYMERIZATION:	Will not occur

Page 1 of 2

SECTION VI – HEALTH/HAZARD DATA

EYES:	Can cause moderate irritation, redness, tearing
SKIN:	Prolonged or repeated contact can cause moderate irritation, defatting and dermatitis
BREATHING:	Excessive inhalation of vapors can cause nasal and respiratory irritation
SWALLOWING:	Can cause gastrointestinal irritation, nausea, vomiting and diarrhea

SECTION VII – EMERGENCY FIRST AID PROCEDURE

IF ON SKIN:	Thoroughly wash exposed area with soap and water. Remove contaminated clothing. Launder contaminated clothing before re-use.
IF IN EYES:	Flush with large amounts of water, lifting upper and lower lids occasionally. GET MEDICAL ATTENTION.
IF SWALLOWED:	If victim is conscious, give two glasses of water, induce vomiting immediately by sticking finger down throat. Call a physician. Never give anything by mouth to an unconscious person.
IF INHALED:	Move individual to fresh air.

SECTION VIII – OCCUPATIONAL EXPOSURE LIMITS

THRESHOLD LIMIT VALUE: Not established

SECTION IX – EMPLOYEE PROTECTION

RESPIRATORY PROTECTION:	Not required under normal conditions of use
VENTILATION:	Not required under normal conditions of use

SECTION X – ENVIRONMENTAL PROTECTION

ENVIRONMENTAL PRECAUTIONS:

Keep away from fire and other ignition sources. Avoid spills and leaking of this material. Absorb spilled material using paper, floor absorbents or other absorbent material. Ventilate the area.

SECTION XI – REGULATORY CONTROLS

DEPARTMENT OF TRANSPORTATION (DOT):

DOT CLASSIFICATION:	ORM-D
DOT PROPER SHIPPING NAME:	Consumer Commodity ORM-D
DOT EMERGENCY GUIDE NUMBER:	Not applicable

SECTION XII – SARA TITLE III

Components present in this product at a level which could require reporting under the statute (Section 313) are:

Chemical	CAS #	Concentration
Methanol	67-56-1	74.8%
Acetone	67-64-1	1.4%

The information contained herein is furnished without warranty of any kind. Employers should use this information only as a supplement to other information gathered by them and must conduct testing and/or make independent determinations of suitability and completeness of information from all sources to assure proper use of these materials and the safety and health of employees.